A Novel Perylene Polymer Based on the 1,3,5-Triazines

Meltem Dinleyici

Submitted to the
Institute of Graduate Studies and Research
in partial fulfillment of the requirements for the degree of

Master of Science
in
Chemistry

Eastern Mediterranean University
July 2015
Gazimağusa, North Cyprus

Approval of the Institute of Graduate Studies and Research

_____
Acting Prof. Dr. Serhan Çiftçioğlu
Director

I certify that this thesis satisfies the requirements as a thesis for the degree of Master of Science in Chemistry.

_____
Prof. Dr. Mustafa Halilsoy
Chair, Department of Chemistry

We certify that we have read this thesis and that in our opinion it is fully adequate in scope and quality as a thesis for the degree of Master of Science in Chemistry.

_____
Prof. Dr. Huriye İcil
Supervisor

Examining Committee
_____

1. Prof. Dr. Huriye İcil   _____

2. Asst. Prof. Dr. Nur P. Aydınlık   _____

3. Asst. Prof. Dr. Hürmüs Refiker   _____

ABSTRACT

Perylene chromophore containing supramolecular chromogenic polymers represent an important research topic relating to its interesting optoelectronic and redox properties.

In the present study, a novel chromogenic polymer (TAPPI) was synthesized by polycondensation of perylene-3,4,9,10-tetracarboxylic dianhydride (PDA) with hindered aromatic diamine, 2,4-diamino-6-phenyl-1,3,5-triazine in isoquinoline and m-cresol solvents mixture under argon atmosphere. The synthesized product purity was confirmed using elemental analysis, IR and UV-vis spectroscopy.

The product TAPDI is soluble mainly in polar solvents such as pyridine, NMP, DMF, DMSO, m-cresol in purple and TFAc pink colours.

It is important to note that, different absorption and emission properties have been observed due to different intermolecular interactions in various solvents.

The lower fluorescence quantum yield of the TAPPI in NMP, DMF and DMSO solvents (70%, 60% and 30%) could be attributed to conformational changes, torsional movement, or other non-radiative decays.

Overall, the new polymer TAPPI has shown great potential for further photonic technology.

Keywords: Perylene polymers, hindered diamine, photonics, solar cells.

ÖZ

Perilen kromoforları ihtiva eden süpramoleküler ve kromojenik polimerler ilginç optoelektronik ve redoks özellikleri nedeniyle önemle araştırılmaktadırlar.

Bu çalışmada yeni bir perilen polimeri (TAPPI), perilen-3,4,9,10-tetrakarboksilik dianhidrit (PDA) ve engelli aromatik diamin, 2,4-diamino-6-fenil-1,3,5-triazine polikondensasyon reaksiyonu ile isokinolin ve m-kresol çözgenleri karışımında ve argon ortamında sentezlenmiştir. Elde edilen ürünün saflığı elemental analiz, IR ve UV-vis spektroskopileri ile doğrulanmıştır.

TAPPI polimeri özellikle piridin, NMP, DMF, DMSO, m-kresol içerisinde mor ve TFAc'de ise pembe renkte çözünmektedir.

Moleküller arası farklı ilişkilere bağlı olarak gözlemlenen farklı absorpsiyon ve emisyon özellikleri fotonik cihazlarda uygulamalar açısından önemlidir.

NMP, DMF and DMSO çözgenlerinde ölçülen fluoresans kuantum verimlerin düşük olmasının (sırasıyla; 70%, 60% ve 30%) konformasyon değişimleri, torsiyon hareketleri ve diğer ışınımsız geçişlerle bağlı olduğu düşünülmektedir.

Genel itibariyle, sentezlenmiş olan yeni perilen polimerinin fotonik uygulamalar için büyük potansiyele sahip olduğu saptanmıştır.

Anahtar kelimeler: Perilen polimerleri, engelli diamin, fotonik, solar hücreler.

ACKNOWLEDGEMENT

TABLE OF CONTENTS

LIST OF TABLES

LIST OF FIGURES

LIST OF SHEMES

ABBREVIATIONS

Å	Armstrong
A	Absorption
A	Electron acceptor
AU	Arbitrary unit
C	Concentration
CT	Charge Transfer
D	Electron donor
DMF	Dimethylformamide
DMSO	Dimethyl sulfoxide
DSSC	Dye sensitized solar cells
Eqn.	Equation
E_s	Singlet energy
ε	Molar Absorption Coefficient
ε_{max}	Maximum Extinction Coefficient / Molar absorptivity
f	Oscillator Strength
FT–IR	Fourier Transform Infrared Spectroscopy
h	Hour
HOMO	Highest Occupied Molecular Orbital
IR	Infrared Spectrum/Spectroscopy
k_d	Rate Constant of Radiationless Deactivation
k_f	Fluorescence Rate Constant
l	path length
LUMO	Lowest Unoccupied Molecular Orbital

M	Molar concentration
max	Maximum
min	Minimum
mmol	Millimole
mol	Mole
NMP	N-methylpyrrolidinone
Φ_f	Fluorescence quantum yield
OFED	Organic Field Effect Transistor
OLED	Organic Light Emitting Diod
PDA	Perylene 3, 4, 9, 10-tetracarboxylic dianhydride
PDI	Perylene Diimide
Std.	Standard
τ_0	Theoretical Radiative Lifetime
t	Time
TFAc	Trifluoroacetic acid
UV	Ultraviolet
UV-Vis	Ultraviolet visible light absorption
$\bar{v}$	Wavenumber
$\Delta\bar{v}_{1/2}$	Half-width (of the selected absorption)
υ_{max}	Maximum wavenumber
λ	Wavelength
λ_{exc}	Excitation wavelength
λ_{em}	Emission wavelength

Chapter 1

INTRODUCTION

The chemistry of perylene dyes, also known as Perylene diimide derivatives, or PDIs, (Figure 1.1) began with the work of M. Kardos in 1913. He gave definition about the naphthalene-1,8-dicarboximides reaction in liquefied alkali to perylene-3,4,9,10-tetrecarboxylic bisimides. They have been started to be used as lightfast vat dyes [1, 2] and their diversified derivatives are still in production for red dyes and pigments.
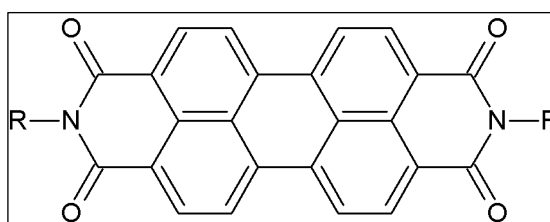
Figure 1.1: A General Structure of Perylene Dyes

Perylene dyes are important chromophores with strong absorption in the UV-visible region of electromagnetic spectrum, high quantum yield of fluorescence (almost one) and thermal, chemical and photochemical stabilities. Their strong π-π stacking interactions make them insoluble in common organic solvents. These potentially fluorescent dyes with excellent fluorescent quantum yields, photo and thermal stabilities were first informed by Geissler and Remy in 1959. The poor solubilities of these photonic dyes limit their several industrial applications. Synthetic progresses in this area have shown that the solubility could be enhanced by using proper bulky and

sterically hindered substituents [3, 4]. Furthermore, the water soluble perylene dyes were reported in the literature [5].

Highly soluble novel perylene derivatives have been reported to be used in photonic technology such as field-effect transistors [6, 7], electrophotographic devices [8], dye lasers [9, 10], organic photovoltaic cells [11, 12], light-emitting diodes [13], liquid crystal displays and fluorescent solar collectors [14].

The intermolecular interactions of organic choromophores such as hydrogen bonding, dipole-dipole, metal complexation and π-π stacking, could change their optical and photochemical properties intensively. Perylene tetracarboxylic diimides have been investigated owing to their excellent properties in DSSCs, OLEDs, OFETs, liquid crystal displays and dye lasers applications [15].

Cyclophane is a molecule that composed from one aromatic ring and an aliphatic chain connecting two carbon atoms of a ring or from two or more aromatic rings bonded by either saturated or unsaturated chains. Cyclophane chemistry begun in 1899, when trans-[2,2]-metacyclophane (Figure 1.2) has been synthesized by Pellegrin [16]. The [*m.n*]paracyclophanes (Figure 1.3) has been synthesized by Cram and Steinberg [17] in order to investigate face-to-face interactions.
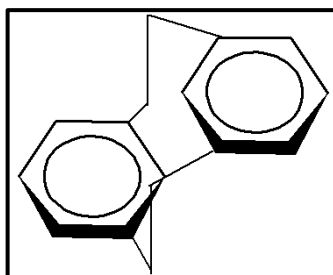
Figure1.2: Structure of Trans-[2,2]-metacyclophane
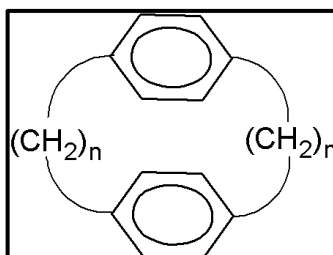
Figure 1.3: Structure of [m.n]Paracyclophanes

Chemistry of cyclophanes is an old and well-established area. In the last century, these cyclic structures have been the topic of intense experimental and theoretical researches [18, 19]. Cram and his co-workers reported π interactions and nonplanarity of cyclophane rings.

Nowadays, cyclophane's applicability in sensors, catalysis, anti-bacterial efficacy, supramolecular chemistry [20], polymer chemistry [21-23] and molecular motors are investigated intensively. The synthesis of novel cyclophanes for applications are still needed for the progress in this area [24].

In this project, we have designed and prepared a novel perylene polymer based on 1,3,5-Triazines named as Perylene-3,4,9,10-tetracarboxylic acid-bis-(N,N'-bis-6-phenyl-1,3,5 triaznylpolyimide). The product was purified and characterized by using several spectroscopic techniques and its optical and photochemical properties were investigated. Other possible product, N,N'–di(2-amino-4-phenyl-1,3,5-triazine)-

3,4,9,10-perylenetetra- carboxydiimide couldn't be characterized due to its limited amount.
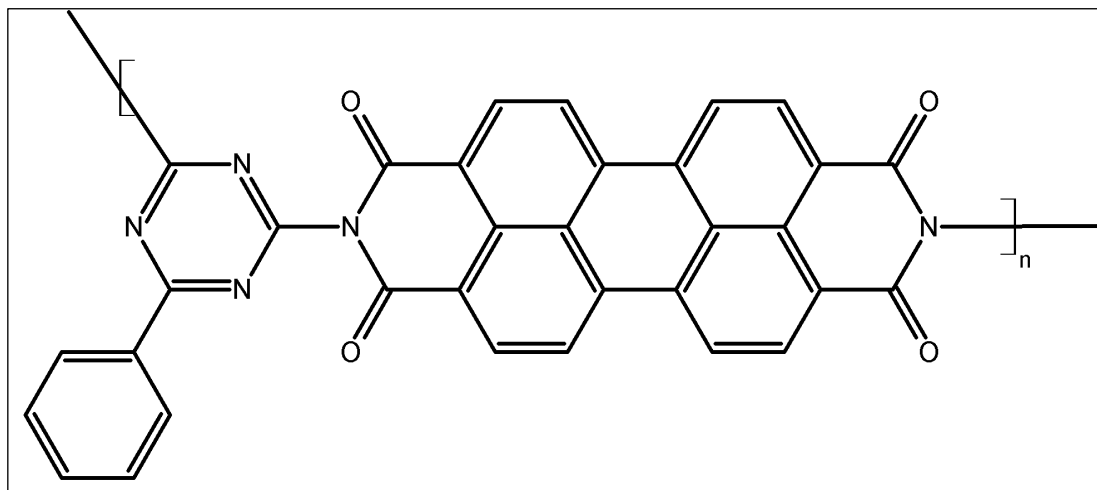
Figure 1.4: Chemical Structure of a Novel Perylene-3,4,9,10-tetracarboxylic acid-bis-(N,N'-bis-6-phenyl-1,3,5 triaznylpolyimide) (TAPPI)
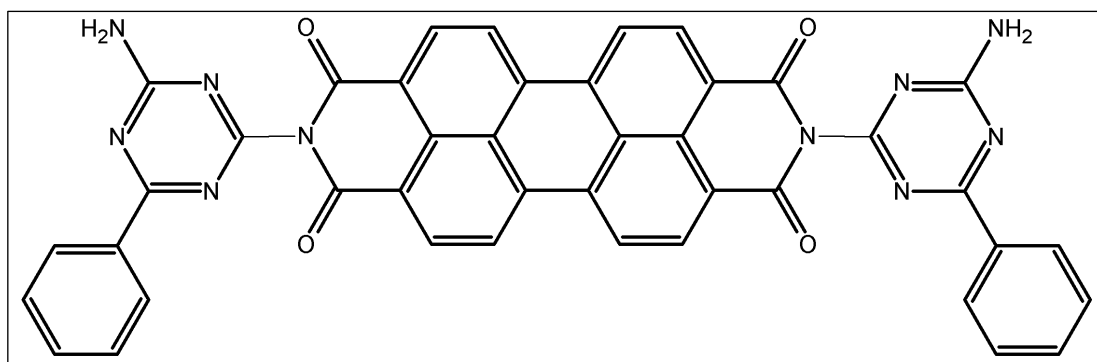
Figure 1.5: Chemical Structure of a N,N'–Di(2-Amino-4-Phenyl-1,3,5-Triazine)-3,4,9,10-Perylenetetra- Carboxydiimide (TAPDI)

Chapter 2

THEORETICAL

2.1 Perylene Dyes in Applications

Perylene dyes, with short optical band gaps (~2.2 eV) [25], low-lying LUMO levels (ca. -3.9 eV) [11], high electron mobilities (> 1 cm^2 V^{-1} s^{-1}) [26], great molecular ordering in thin films[27], high molar absorption coefficients (~ 1 × 10^5 M^{-1} cm^{-1}) [28] and facile chemical substitution at both imide and bay positions, indicate potentially promising electron transport materials or organic acceptor materials in organic electronics, particularly for OFET and OLED applications.
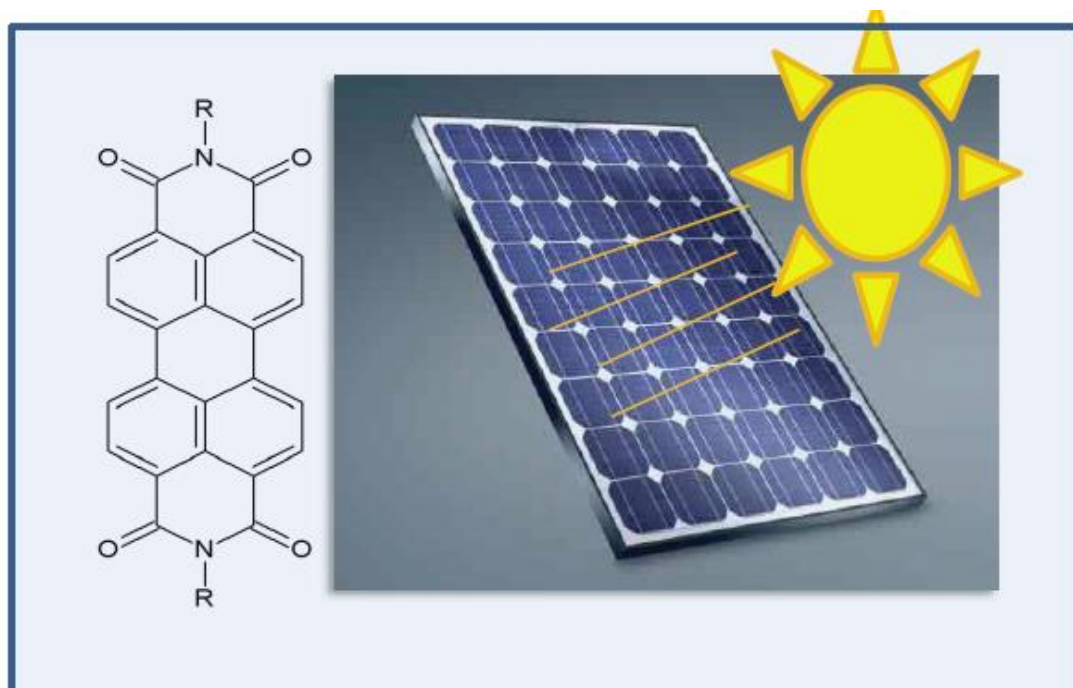
Figure 2.1: Perylene Dyes in Solar Cell Applications

2.1.1 Organic Field-Effect Transistors (OFETs)

OFETs have been produced with the organic semiconducting thin film layer. In general, the Organic Field-Effect Transistors have low values of field effect movement comparing to conventional field-effect transistors based on inorganic materials. It is known that Organic Field-Effect Transistors can present a suitable cheap building block for flexible organic circuits and large field electronic applications like sensors, smart cards and organic-based displays in the future years [29-32].

Perylene dyes are the most promising materials amongst the large number of conjugated polyene systems and due to their properties (photoluminescent, electron accepting stable, etc.), they can be utilized in numerous types of photonic systems. Their properties can be modified synthetically in order to obtain 'clever' products.
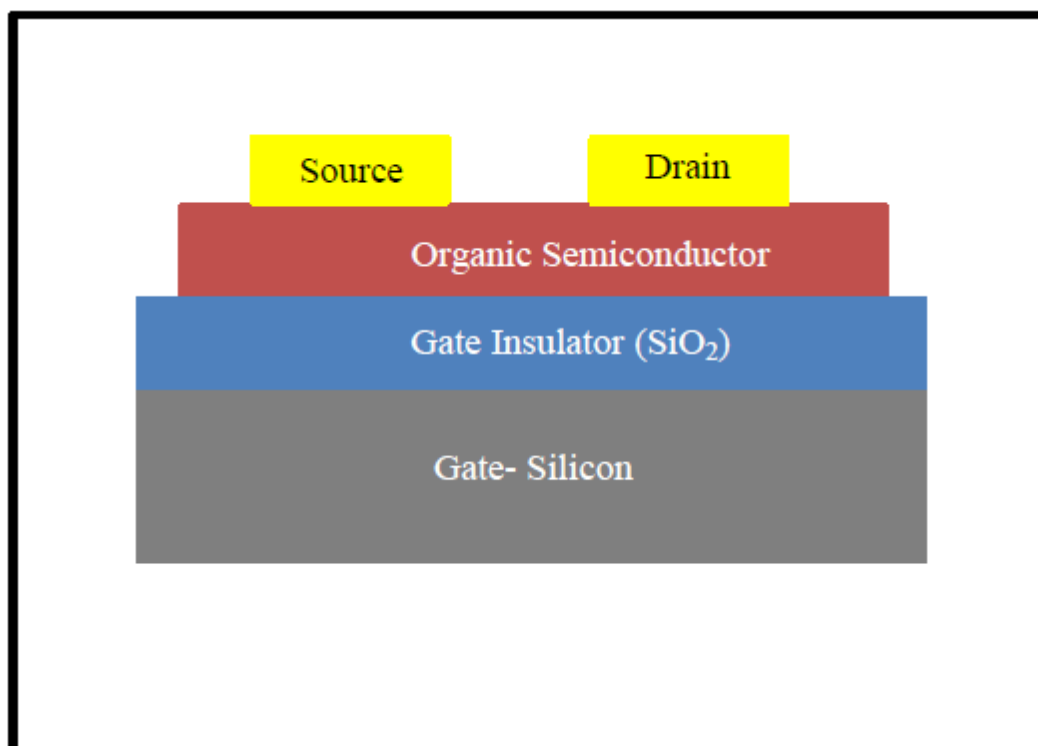
Figure 2.2: The Schematic Structure of a OFED

2.1.2 Organic Light-Emitting Diods (OLEDs)

OLEDs are one of the most attractive subjects owing to their ability to be utilized in new generation flat panel displays and cheap solid state lighting. OLEDs devices were firstly demonstrated in 1980s by Tang. In the last twenty years, important endeavour has been devoted to enhance device efficiency through the design and synthesis of new materials as well as device engineering. For example, Tang suggested a host-guest system, in which charge transport and photoluminescence were separated into two distinct materials, i.e. host and guest respectively in 1989 [33].
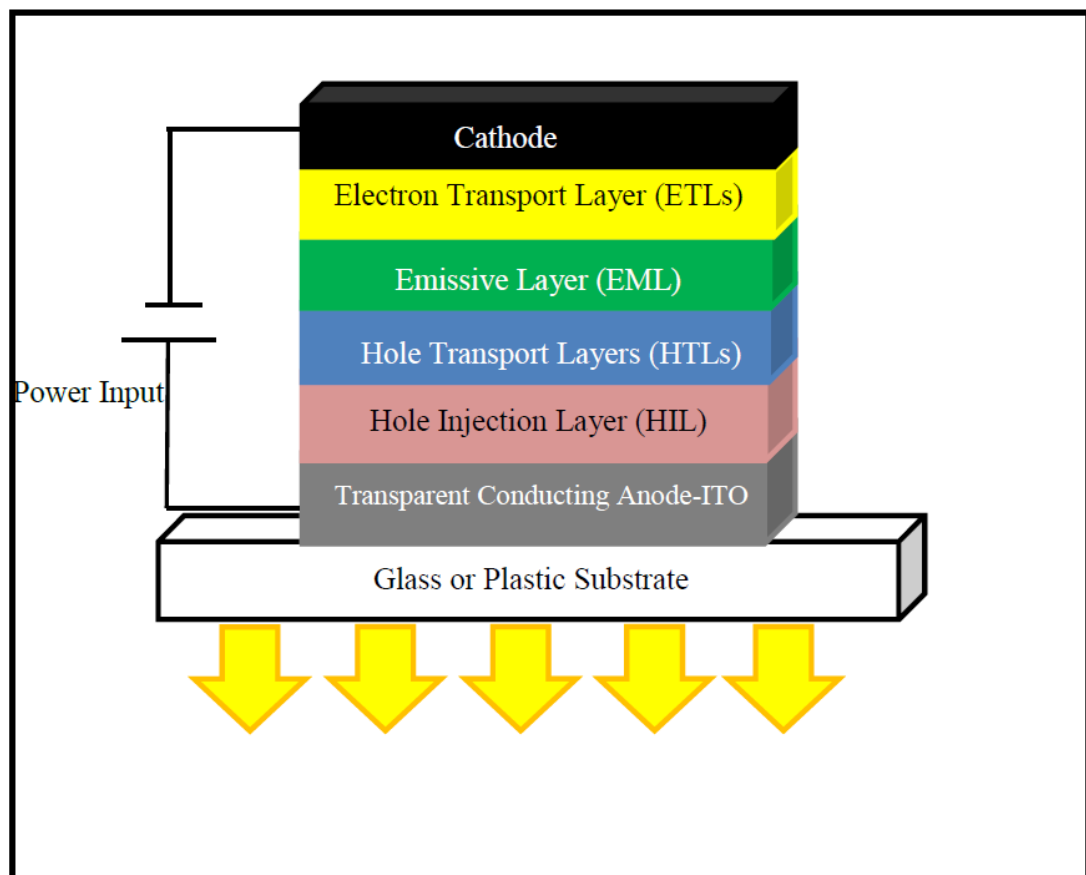
Figure 2.3: The Basic Structure of a Typical OLED

In terms of OLED design, LiF/Al bi-layer cathode is the most commonly utilized cathode in order to inject electrons into the devices. Nearly all of the OLEDs device designs and optimizations were based upon Indium tin oxide (ITO). For instance, numerous hole injection layers were recommended to inject sufficient holes from the ITO to raise the device performances.

2.2 Energy Transfer

Resonance energy transfer (RET) or simply energy transfer is the emission of molecule in an electronically excited state (donor) which is absorbed by another ground state chromophore (acceptor). Finally, the excited donor will be decayed and acceptor excited.

Resonance energy transfer is occurring via two dissimilar mechanisms; radiative or radiationless mechanisms. Radiative energy transfer is known as trivial, because of its simplicity. This transfer takes place emission of photon of light by the donor molecule in the electronically excited state and is followed via absorption of the emitted quantum by an acceptor molecule.

$$A^* \longrightarrow A + h\nu'$$

$$B + h\nu' \longrightarrow B^*$$
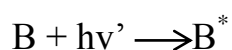
Hamiltonian, H^{en} gave description that non-radiative energy transition can occur from an electron donating molecule (D) in the electronically excited level to an electron accepting molecule (A) when there are in dipole-dipole noncovalent interactions. The transfer rate constant of energy can be estimated from the Fermi Golden Rule [34].

$$K_{en} \ = \ (4\pi/h) \ (H^{en})^2 \ FC^{en} \qquad\qquad \textbf{(Eqn. 2.1)}$$

FC^{en} is the Frank Condon factor and H^{en} is the electronic coupling between the HOMO and the LUMO of the acceptor and donor molecules in the resonance energy transfer.

The electronic coupling (H^{en}) between the two species in excited state can be divided into two distinct terms, an exchange ("Dexter-type") and a Coulombic (''Förster'', ''resonance'' or ''dipole-dipole'') mechanisms which are dependent on the different parameters such as the systems and probable experimental conditions. The orbital for the two referred electronic energy transfer mechanisms are illustrated in Figure 2.4.
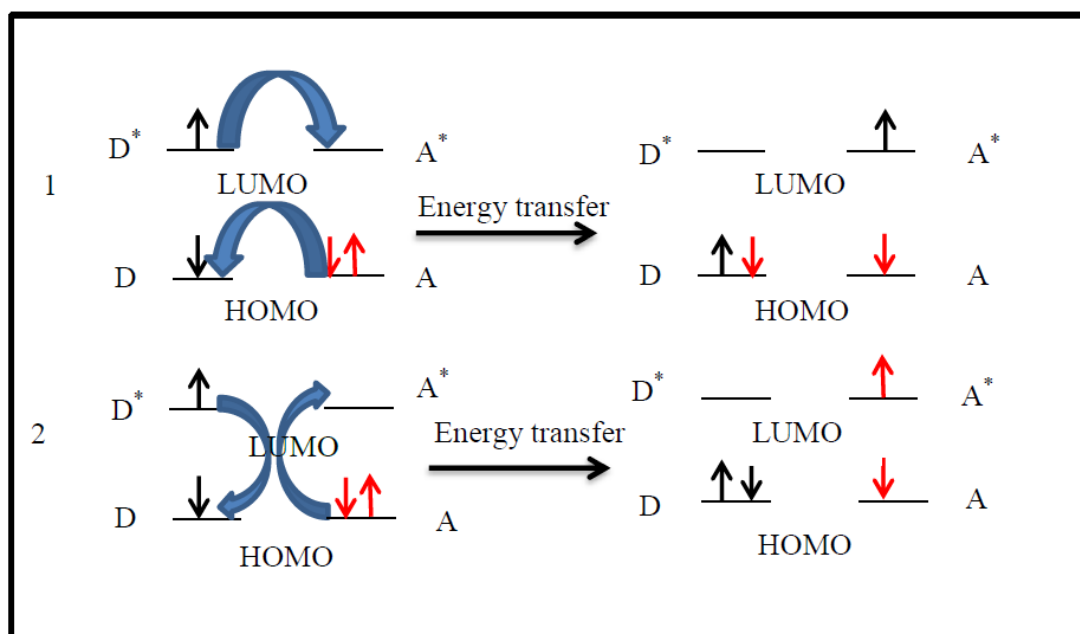
Figure 2.4: Schematic Illustration of Exchange (1) and Coulombic (2) Mechanisms of Energy Transfer.

2.3 Electron Transfer

Electron transfer is of critical significance in numerous processes including photosensitized catalysis, converting of solar energy and molecular signaling. Electron transfer is able to consist of the electron donor molecule (D) to the electron acceptor molecule (A), resulting in the constitution of a charge separated level from which charge recombination can come about to bring the system back to the lowest energy level.

Generally, the thermodynamics and kinetics of the photoinduced electron transfer reaction mechanisms have been comprehensively researched and many of these properties have been defined via the Rehm-Weller equation [35], the changing in Gibbs function for the charge separation and by Marcus theory for the [36-39] electron transfer rate constant.

The Rehm-Weller equation displays a calculation for the change in driving force (ΔG_{CS}) for the photoinduced charge separation process in molecular donor-acceptor systems, by summing three terms describing the thermal energy of excited electronic state redox reaction, the Coloumb term for the limited distance between positive and negative charges.

$$\Delta G_{CT} = e\left[E^{1/2}_{(D/D^{+\cdot})} - E^{1/2}_{(A^{-\cdot}/A)}\right] - E_{(0,0)} - E_{coul} \qquad \textbf{(Eqn. 2.2)}$$

In the above equation $E^{1/2}_{(D/D^{+\cdot})}$, $E^{1/2}_{(A^{-\cdot}/A)}$, $E_{(0,0)}$, and E_{coul} are electrochemical oxidation half-wave potential in the electron donating group, electrochemical reduction half-wave potential in the electron accepting group, the energy of the

relaxed first singlet electronically excited level and the Coulombic stabilization energy, respectively.

k_{CS}, rate constant of electron transfer mechanism and ΔG^{++}, barrier of the free energy can be calculated according to following equation which is presented by the Marcus theory [36-39]. In given equation, V is the electronic coupling between electronic donating and electronic accepting groups in the electronically excited state and λ is also the reorganization energy.

$$k_{CS} \ = \ [4\pi^3 \ / \ (h^2 \, \lambda \, k_B \, T)]^{1/2} \ V^2 \exp[-\Delta G^{++} / \ (k_B \, T)] \qquad \textbf{(Eqn. 2.3)}$$

Marcus illustrated that the barrier of the free energy (ΔG^{++}) is defined via the change in free energy of the charge separation (ΔG_{CS}) and the reorganization energy (λ) by:

$$\Delta G^{++} \ = \ (\Delta G_{CS} \ + \ \lambda)^2/4\lambda \qquad \textbf{(Eqn. 2.4)}$$

His theory represents that the barrier of the activation energy is diminished and $-\Delta G_{CS}$, the change in free energy for charge separation rises and correspondingly, till λ, the reorganization energy equals the driving force for electron transfer (where $\lambda=-\Delta G_{CS}$) k_{CS}, rate constant of electron transfer increases. Herein, the maximum value for the electron transfer reaction rate constant can be obtained. On the other hand, a further rise in the free energy change results in a raise in the activation energy and hence, rate of electron transfer reaction is become slower. The inverted region, $-\Delta G_{CS} > \lambda$, where the reorganization energy for the electron transfer is less than the change in free energy, the optimal region, $-\Delta G_{CS} = \lambda$, the normal region, $-\Delta G_{CS} = <\lambda$, where the reorganization energy is larger than the change in free energy are three regions for the electron transfer.

2.4 Supramolecular Systems

Supramolecular chemistry is one of the new branches of chemistry and spreading rapidly. The area of the chemistry has defined as 'chemistry beyond molecule' by Lehn and forms the systems that hold together via reversible non-covalent interactions [40].

Supramolecular chemistry is extremely a multidisciplinary field of science. The chemistry of supramolecular arrays is useful for both organic and inorganic chemistry to synthesize molecules. Physical chemistry is also used for explanation features of supramolecular organic and inorganic structures. Moreover, supramolecular chemistry is attractive for biological sciences for mimic natural materials such as enzymes [41, 42].

The branch of chemistry is attracting attention owing to various applications such as material technology, catalysis, medicine, analytical detection and sensing. It has been used for non-covalent synthesis and catalysis [43, 44] beside characteristic organic synthesis. It is also significant for molecular identification by using photoluminescence and electrochemistry [45, 46]. Furthermore, another topic of supramolecular system is about molecular devices. Solar cells, light harvesting systems [47, 48] and logic gates [49, 50] and surface studies [51, 52] are related applications. At the end, chemistry of supramolecular systems makes likely artificial biological agents such as enzymes, curative agents for determinations diseases.

Supramolecular chemistry is composed of two fundamental groups; host-guest chemistry and self-assembly [53]. The classification is made by taking into consideration the size and shape of molecules. In description of host-guest chemistry,

one of the molecules which is much larger than the other molecule is called 'host'. The other molecule that is smaller and encircled via host is called 'guest'. There are many instances for host-guest systems in biology and chemistry. In biological sciences, enzymes and their substrates can be given as example for host-guest chemistry. Moreover, in coordination chemistry, huge ligands are hosts and metals are guests and interaction between them is electrostatic interaction. Self-assembly is other main group in the supramolecular chemistry. In self-assembly system, the sizes of structure of host and guest are close to each other. These systems can contain two or more components and formation of the supramolecular structures mostly spontaneous and reversible processes.

Chemistry of supramolecular systems focuses on the weaker and reversible noncovalent interactions between molecules. These interactions are Van der Waals forces, hydrogen-bonding, hydrophobic forces, π interactions and electrostatic interactions. Classical chemistry emphasizes the covalent bond.

Electrostatic interactions involve three classes which are dipole-dipole interactions, ion-dipole interactions and ion-ion interactions. The Coulombic attractions which are between negative and positive charges play role in the electrostatic interactions. Hydrogen bonding is a dipole-dipole interaction but distinct from other dipole-dipole interactions aspects of high strength and directionality. Because of these features, hydrogen bonding is the most versatile non-covalent interaction in the supramolecular systems. Hydrogen bond occurs between a donor and acceptor moieties. For proton donor, hydrogen atom has to be bound to oxygen, nitrogen or fluor to generate positively charged hydrogen atom. There must be again oxygen, nitrogen or fluor atoms as acceptor groups. π interactions contain two sorts which are π-π interactions

[54] and cation-π interactions. Cation-π interactions form between cation and aromatic ring. Another kind of non-covalent π interactions is π-π interactions which are consisted via intermolecular overlapping of p-orbitals. These interactions are divided into two groups those are face-to-face and edge-to-face. The other type of non-covalent interactions is Van der Waals interactions formed between induced-dipole and induced-dipole. These interactions cannot be exerted for designing of supramolecular structures. Van der Waals interactions are much dependent on distance and speedily decreasing by rising of distance. Hydrophobic effects are significant in supramolecular chemistry; binding of organic structure to cavity of cyclodextrins in water is example for this effect.

2.5 Perylene Dyes in Organic Solar Cells

Photovoltaic science and technology is related to the processes of converting solar energy into electrical power. Solar energy is expected to become one of the sources without pollutant and renewable alternative energy resources to fossil fuels in the near future of energy.

Organic photovoltaic cells (OPVs) are solar cells that exert organic materials either small molecules or macromolecules like polymers, to absorb energy and manufacture free electrons. Attention in organic photovoltaics started when photoinduced charge transfer between organic small molecules and polymers was indicated in the 1990s by Sariciftci. In recent years, OPVs are seriously being studied owing to their great potential that is making them an economically viable resource of energy. Besides, organic macromolecules can be solved in numerous solvents and deposited on substrates utilizing spin coating or roll to roll methods solution printing. Owing to solution processing, possibility of cheap production can be increased in large-scale.

Polymer-polymer, polymer-fullerene and hybrid solar cells can be shown as three primary classes of organic solar cells. Hybrid organic photovoltaic cells incorporate inorganic nanoparticles into the organic effective material. In organic solar cells, generally, polymers show the electron accepting and donating features, however fullerenes indicate as highly effective electron donating features.

The most important distinction between inorganic and organic solar cells is that absorption of light in organic solar cells cannot generate free charge carriers, directly.

The other distinction between inorganic and organic solar cells is highlighted based on exciton dissociation: charge carrier fabrication and separation are identical mechanisms in organic solar cells. The electron and its hole diffuse to opposite ends of the solar cell after the exciton dissociates at the electron donating and accepting groups. Buffer layer in normal and inverse organic solar cells provides that charge carriers travel to the correct electrode.

Chapter 3

EXPERIMENTAL

3.1 Materials

All the commercial solvents and reagents were used as received. On the other hand, some of the solvents were distilled when needed according to the standard literature procedures given in literature [55]. Spectroscopic grade solvents were directly used in high purity for all spectroscopic measurements.

Perylene-3,4,9,10-tetracarboxylic dianhydride, 2,4–Diamino-6-phenyl-1,3,5-triazine, isoquinoline, *m*-cresol, zinc acetate were purchased from Aldrich.

3.2 Instrumentations

JASCO FT-IR spectrophotometer was used to record IR spectrum of TAPPI through KBr discs.

Carlo Erba-1106 C, H, and N analyzer was used to obtained elemental analysis data.

Varian-Cary 100 spectrophotometer was used to measure all the Ultraviolet Absorption Spectra (UV) of the TAPPI in different solvents.

Varian Cary Eclipse Spectrophotometer was used to obtain all the emission and excitation spectra of TAPPI in different solvents.

3.3 Methods of Synthesis

In this section, the synthesis of TAPPI was described.

The TAPPI was synthesized by the polycondensation of the perylene-3,4,9,10-tetracarboxylic dianhydride (PDA) with the 2,4–Diamino-6-phenyl-1,3,5-triazine in m-cresol / isoquinoline solvent mixture as shown below. (Scheme 3.1)
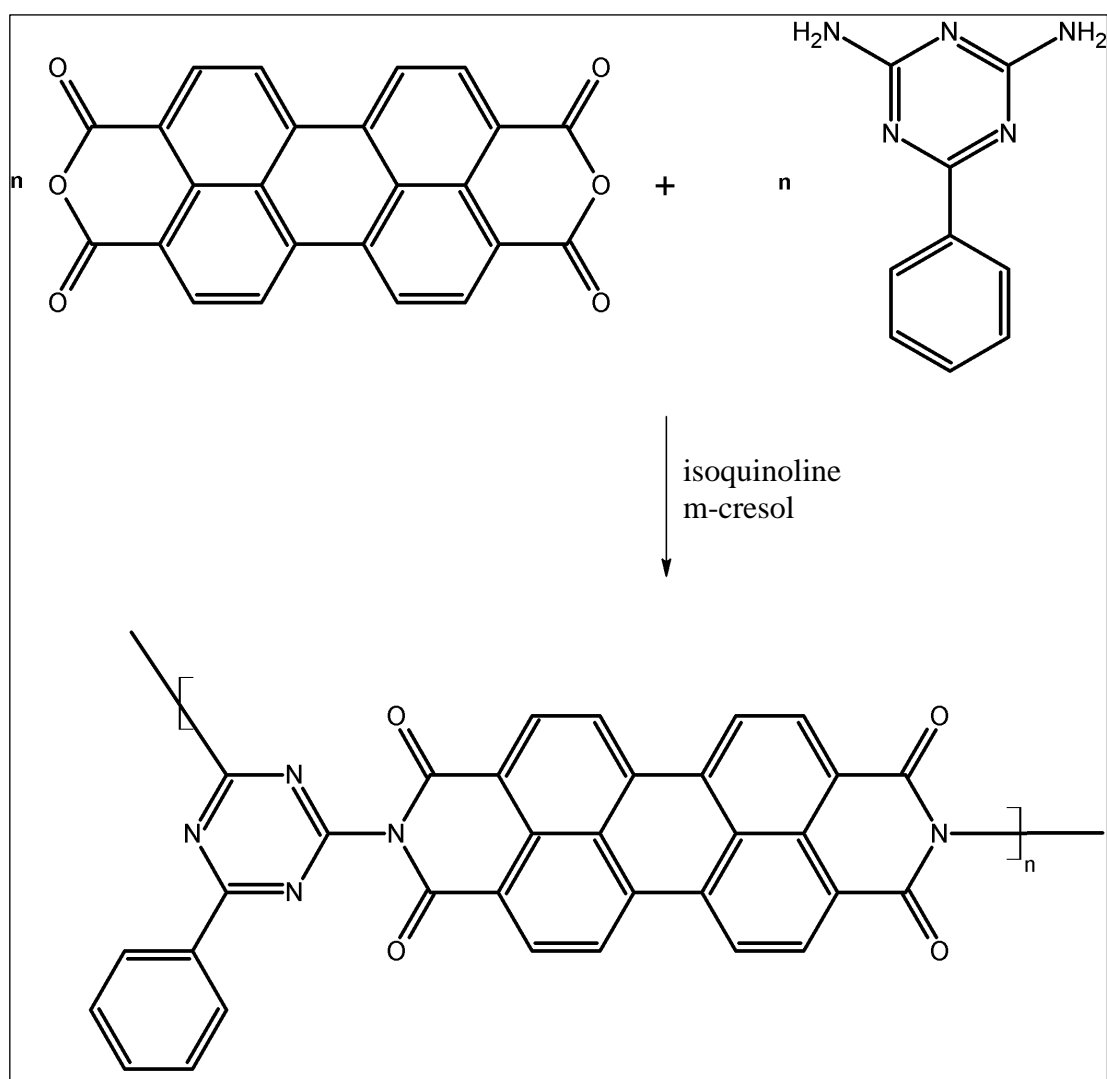
Scheme 3.1: Synthesis of TAPPI

3.4 Synthesis of TAPPI
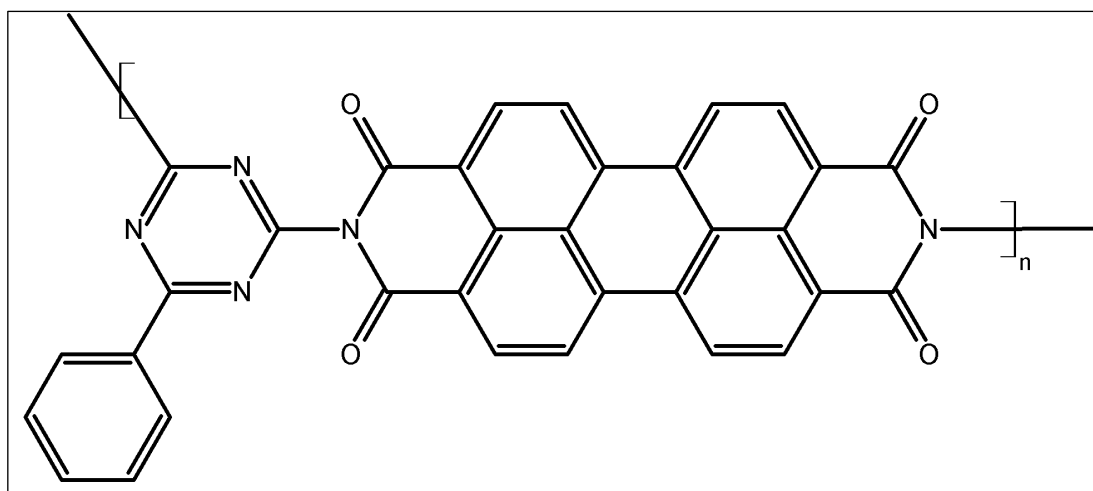
1.003g (2.55 mmol) of perylene- 3,4,9,10-tetracarboxylic dianhydride (PDA), 0.474 g (2.55 mol) of 2,4–Diamino-6-phenyl-1,3,5-triazine, 0.571g (2.55 mmol) of $Zn(OAc)_2.2H_2O$ and 40 ml of dry isoquinoline / m-cresol mixture added into a three-necked flask under the argon atmosphere. The mixture was heated for 5h at 100 ^{o}C, for 2h at 120 ^{o}C, for 8h at 160°C and finally for 4h at 200°C. The warm reaction mixture was poured into 200 mL of methanol. The resulting precipitate was filtered by suction filtration. Then, the crude product was dried under vacuum at 100 ^{o}C. The synthesized crude product was purified in a Soxhlet apparatus with chloroform (1 day) and acetone (1 day). Finally, the pure product was dried by vacuum oven.

Yield: %50

FT-IR (KBr, cm^{-1}): 3385, 3160, 3049, 2927, 2853, 1682, 1676, 1592, 1517, 1434, 1396, 1360, 1277, 1106, 887, 812, 662

UV-vis (NMP) (λ_{max} / nm): 458, 487, 523

Fluorescence (CHCl$_3$) (λ_{max} / nm): 535, 574, 623 $\Phi_f = 0.70$

Anal. Calcd. for C$_{132}$H$_{54}$N$_{20}$O$_{16}$, Mw, 2175,966: C, 72.86; H, 2.50; N, 12.87; Found: C, 72.14; H, 2.43; N,12.36

3.6 General Synthetic Mechanism

STEP 3

STEP 4

21
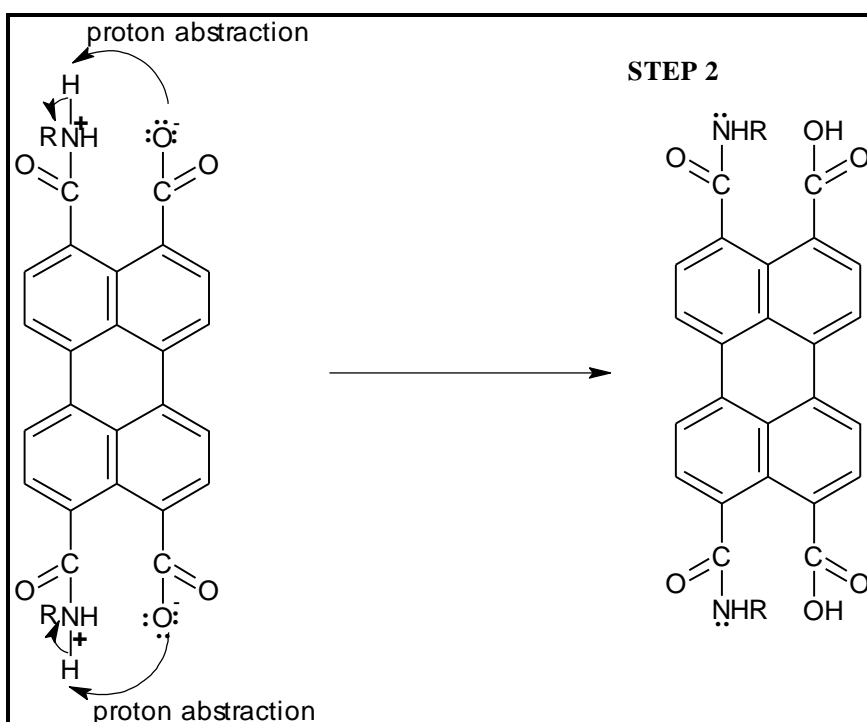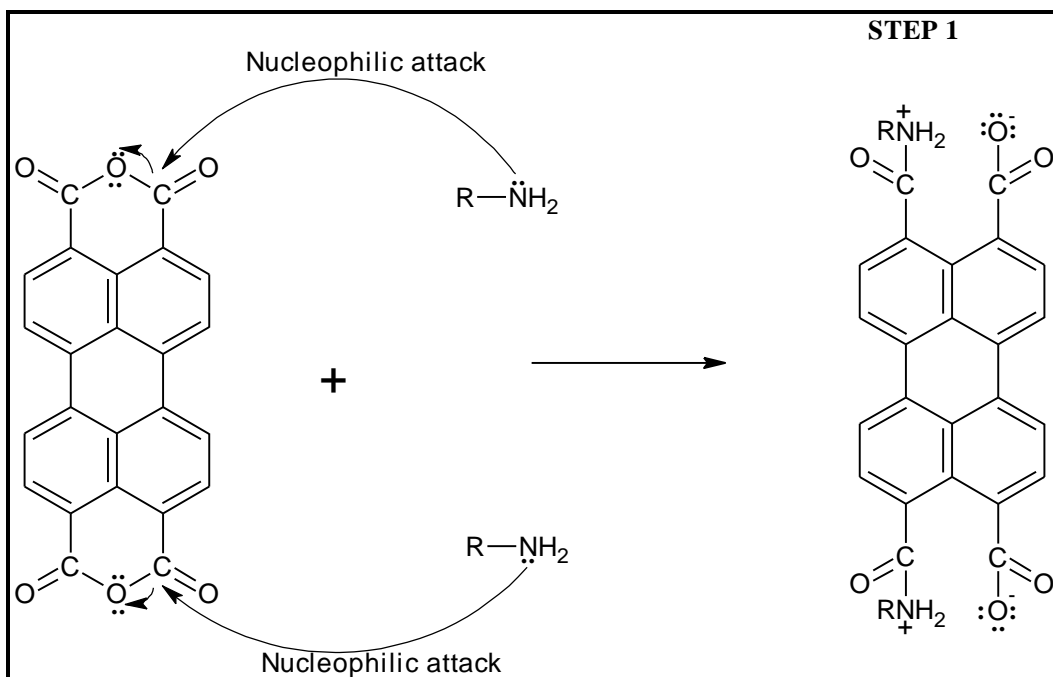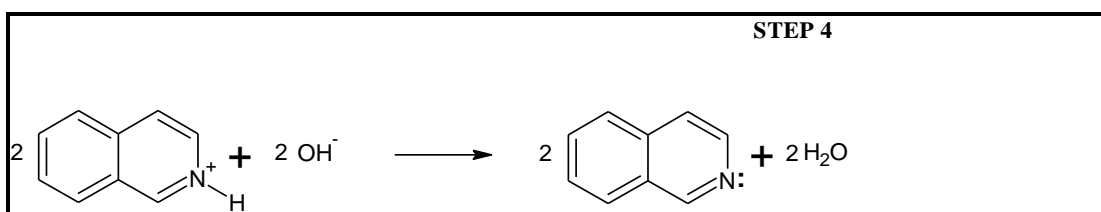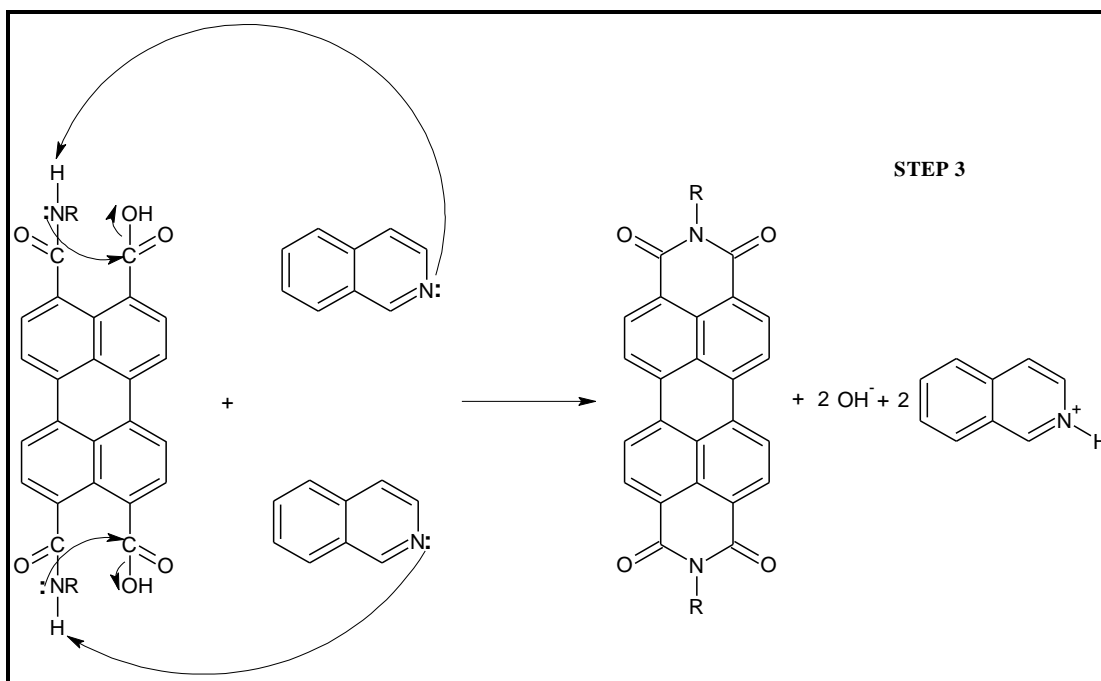
Chapter 4

DATA AND CALCULATIONS

4.1 Photochemical and Photophysical Properties

4.1.1 Extinction Coefficient

According to the Beer-Lambert's law, the molar extinction coefficient (ε_{max}) was calculated from the absorbance and concentration plot. A minimum of five or more different concentrations of the synthesized compound's solutions has to be prepared and their maximum absorbance respecting to the maximum absorption wavelength were recorded for each concentration. Lastly, the slope calculated from the plot of absorbance vs. concentration yielded the maximum molar extinction coefficient.

Table 4.1: Concentration and the their corresponding absorbances data of TAPPI in NMP

Concentration (mol/L)	λ_{max} (nm)	Absorbance
4.7965×10^{-5}	523	1.53
2.3982×10^{-5}	523	0.77
1.1991×10^{-5}	523	0.38
5.9956×10^{-6}	523	0.21
2.9978×10^{-6}	523	0.12
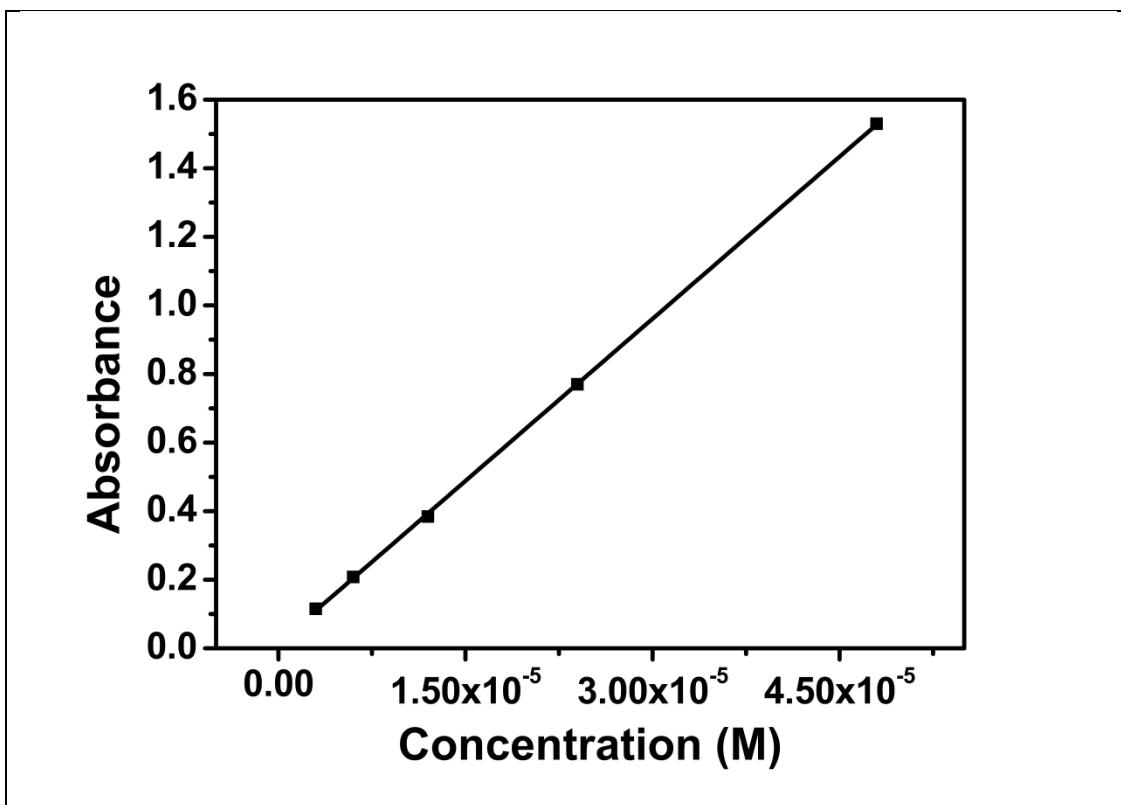
Figure 4.1: Absorption vs. Concentration Plot of TAPPI in NMP

From the plot;

$$Slope = 33000;$$

Therefore;

$$\varepsilon_{max} = 33000 \; L \cdot mol^{-1} \cdot cm^{-1}$$

Table 4.2: Molar extinction coefficient data of TAPPI in different solvents

Solvent	λ_{max} (nm)	ε_{max} $(M^{-1}.cm^{-1})$
NMP	523	33000
DMF	522	24000
DMSO	523	28000

4.1.2 Measurement of Fluorescence Quantum Yield

Basically, the number of photons emitted to the number of photons excited ratio gives the fluorescence quantum yield, Φ_f of a sample. There are several methods for the experimental calculations of fluorescence quantum yields. The most reliable method for experimental Φ_f calculation is called comparative method developed by Williams et. al. [56]. In this method, together with unknown samples a standard sample with known fluorescence quantum yield value is used. Absorption and emission spectra of the unknown and the standard samples were measured under the same conditions. The ratio of integrated fluorescence intensities of unknown and standard solutions gives the experimental Φ_f values of unknown. The Φ_f for the unknown sample was calculated according to following equation Eqn. 4.1.

$$\Phi f\,(U) \;=\; \frac{A_{std}}{A_u} \times \frac{S_u}{S_{std}} \times \left[\frac{n_u}{n_{std}}\right]^2 \times \Phi_{std}$$

Eqn. 4.1

The reference sample of the fluorescence quantum yield calculations is the N,N'-bis(dodecyl)-3,4,9,10-perylenebis(discarboximide) [57, 58]. The fluorescence quantum yield of reference sample in chloroform is equals to 1. Both the unknown and reference samples were excited at 485 nm.

TAPPI Φ_f calculation in NMP:

N,N'-bis(dodecyl)-3,4,9,10-perylenebis(discarboximide) is the reference perylene dye in chloroform.

$\Phi_{std} = 1$

$A_{std} = 0.1082$

$A_u = 0.1045$

$S_u = 39118.2881$

$S_{std} = 68929.00$

$n_{std} = 1.4441$

$n_u = 1.4700$

$$\Phi f\,(U) = \frac{0.1082}{0.1045} \times \frac{39118.2881}{68929.00} \times \left[\frac{1.4700}{1.446}\right]^2 \times 1$$

$\Phi f\,(U) = 0.70$

The fluorescence quantum yield of the TAPPI in the different solvents were estimated with the similar methods and shown in the Table 4.3.

Table 4.3: Calculated fluorescence quantum yield data of TAPPI in different solvents

Solvent	Φf
Pyridine	0.60
NMP	0.70
DMF	0.60
DMSO	0.30
m-Cresol	0.10
TFAc	0.50

4.1.3 Maximum Absorption Half-width

Eqn. 4.2. used to calculate the maximum absorption half-width.

$$\Delta \bar{v}_{1/2} = \bar{v}_1 - \bar{v}_2 \qquad \qquad \textbf{Eqn. 4.2}$$
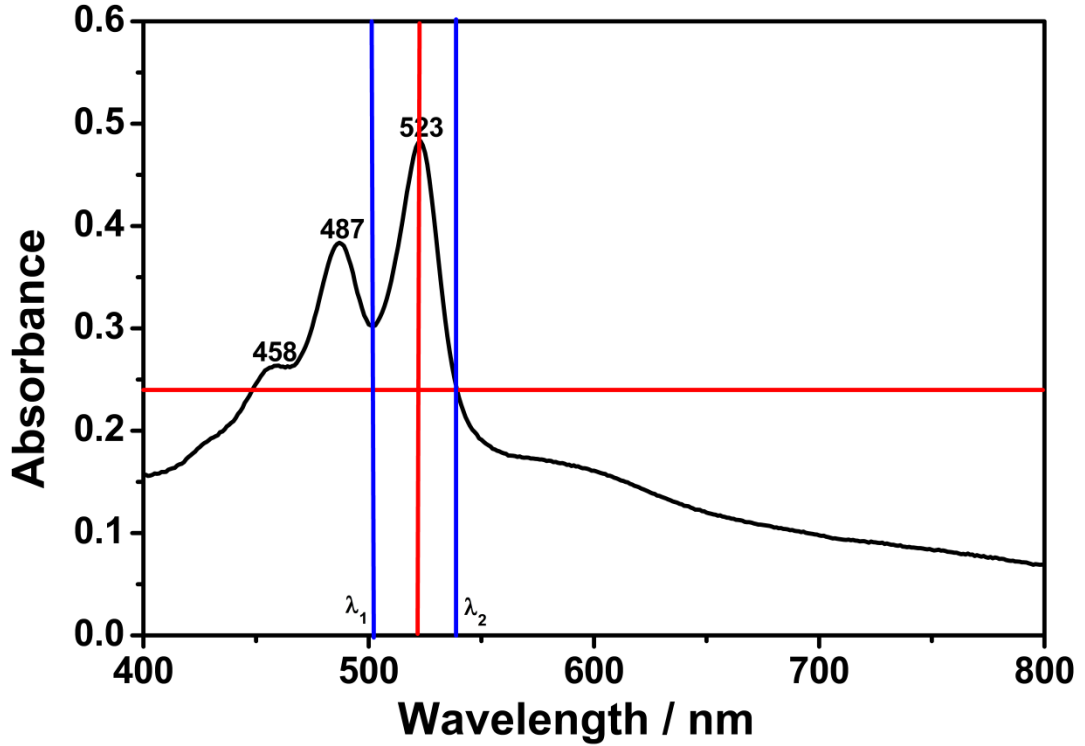
Figure 4.2: Representative Half-Width Plot on the Absorption Spectrum of TAPPI in NMP

As shown in Figure 4.2:

$\lambda_{max} = 523$ nm

Absorption at half-width $= 0.241$

$\lambda_1 = 502.18$

$\lambda_2 = 538.71$

$$\lambda_1 = 502.18 \text{ nm} \times \frac{10^{-9}\text{m}}{1 \text{ nm}} \times \frac{1\text{cm}}{10^{-2}\text{m}} = 5.0218 \times 10^{-5} \text{ cm}$$

$$\bar{v}_1 = \frac{1}{5.0218 \times 10^{-5} \text{ cm}} = 19913.18 \text{ cm}^{-1}$$

$$\lambda_2 = 538.71 \text{ nm} \times \frac{10^{-9}\text{m}}{1 \text{ nm}} \times \frac{1\text{cm}}{10^{-2}\text{m}} = 5.3871 \times 10^{-5} \text{ cm}$$

$$\bar{v}_2 = \frac{1}{5.3871 \times 10^{-5} \text{ cm}} = 18562.86 \text{ cm}^{-1}$$

$$\Delta\bar{v}_{1/2} = \bar{v}_1 - \bar{v}_2 = 19913.18 \text{ cm}^{-1} - 18562.86 \text{ cm}^{-1}$$

$$= 1350.32 \text{ cm}^{-1}$$

The determination of the half-widths of the synthesized compound in different solvents is necessary in order to estimate the theoretical radiative lifetimes of the TAPPI. Similarly, the half-widths of TAPPIs for other solvents were calculated. Table 4.4 summarizes these data.

Table 4.4: Maximum absorption half-widths of the TAPPI in different solvents

Solvent	λ_{max} (nm)	λ_1 (nm)	λ_2 (nm)	$\Delta\bar{v}_{1/2}$ (cm^{-1})
Pyridine	526	505.57	540.44	1276.22
NMP	523	502.18	538.71	1350.32
DMF	522	501.23	537.82	1357.34
DMSO	523	503.77	539.65	1319.80
m-Cresol	549	526.68	567.75	1373.47
TFAc	529	508.09	544.26	1307.98

4.1.4 Theoretical Radiative Lifetimes

Eqn. 4.3 used to calculate the theoretical radiative lifetimes.

$$\tau_0 = \frac{3.5 \times 10^8}{\upsilon_{max}^2 \cdot \varepsilon_{max} \cdot \Delta\bar{\upsilon}_{1/2}}$$

Eqn. 4.3

The TAPPI's theoretical radiative lifetime calculation in NMP:

All the data obtained from Figure 4.1 and 4.2;

$\lambda_{max} = 523$ nm

$\lambda_{max} = 523 \text{ nm} \times \frac{10^{-9}\text{m}}{1 \text{ nm}} \times \frac{1 \text{ cm}}{10^{-2}\text{m}} = 5.23 \times 10^{-5}\text{cm}$

$\upsilon_{max} = \frac{1}{5.23 \times 10^{-5} \text{ cm}} = 19120.46 \text{ cm}^{-1}$

$\upsilon_{max}^2 = (19120.46 \text{ cm}^{-1})^2 = 3.66 \times 10^8 \text{cm}^{-2}$

The theoretical radiative lifetime;

$$\tau_0 = \frac{3.5 \times 10^8}{\upsilon_{max}^2 \cdot \varepsilon_{max} \cdot \Delta\bar{\upsilon}_{1/2}} = \frac{3.5 \times 10^8}{3.66 \times 10^8 \times 33000 \times 1350.32}$$

$\tau_0 = 2.15 \times 10^{-8} s$

$\tau_0 = 21.5 \text{ ns}$

The theoretical radiative lifetime of TAPPI in different solvents were calculated according to same method and all the results were shown in the Table 4.5.

Table 4.5: TAPPI's theoretical radiative lifetimes in different solvents

Solvent	λ_{max} (nm)	ε_{max} $(M^{-1}.cm^{-1})$	ν^2_{max} (cm^{-2})	$\Delta\bar{\nu}_{1/2}$ (cm^{-1})	τ_0 (ns)
NMP	523	33000	3.66×10^8	1350.32	21.5
DMF	522	24000	3.67×10^8	1357.34	29.3
DMSO	523	28000	3.66×10^8	1319.80	25.9

4.1.5 Theoretical Fluorescence Lifetimes

Eqn. 4.4 used to calculate the theoretical fluorescence lifetimes [59].

$$\tau_f = \tau_0 \cdot \Phi_f \qquad \textbf{Eqn. 4.4}$$

The TAPPI's theoretical fluorescence lifetime calculation in NMP:

$\tau_f = \tau_0 \cdot \Phi_f$

$\tau_0 = 21.5$ ns

$\tau_f = \tau_0 \cdot \Phi_f = 21.5 \times 0.70 = 15.05$ ns

The theoretical fluorescence lifetimes of TAPPI in different solvents were calculated according to same method and all the results were shown in the Table 4.6.

Table 4.6: TAPPI's theoretical fluorescence lifetimes in different solvents

Solvent	Φ_f	τ_0 (ns)	τ_f (ns)
NMP	0.70	21.5	15.05
DMF	0.60	29.3	17.58
DMSO	0.30	25.9	7.77

4.1.6 Fluorescence Rate Constants (k_f)

The fluorescence rate constants were calculated according to following Turro's equation.

$$k_f = \frac{1}{\tau_0} \qquad \qquad \textbf{Eqn. 4.5}$$

The TAPPI's fluorescence rate constant calculations in NMP

at $\lambda_{max} = 523$ nm:

$k_f = \dfrac{1}{\tau_0}$

$\tau_0 = 21.5 \text{ ns} = 2.15 \times 10^{-8}\text{s}$

$k_f = \dfrac{1}{2.15 \times 10^{-8}\text{s}} = 4.65 \times 10^7 \text{ s}^{-1}$

The fluorescence rate constant of TAPPI in different solvents were calculated according to same method and shown in the Table 4.7.

Table 4.7: TAPPI's theoretical fluorescence rate constant in different solvents

Solvent	λ_{max} (nm)	τ_0 (s)	k_f (s^{-1})
NMP	523	2.15×10^{-8}	4.65×10^7
DMF	522	2.93×10^{-8}	3.41×10^7
DMSO	523	25.9×10^{-8}	3.86×10^7

4.1.7 Radiationless Deactivation Rate Constants (k_d)

Eqn. 4.6 used to calculate radiationless deactivation rate constants of the compounds.

$$k_d = \left(\frac{k_f}{\Phi_f}\right) - k_f$$

The radiationless deactivation rate constant calculations of TAPPI in NMP:

$$k_d = \left(\frac{k_f}{\Phi_f}\right) - k_f = \left(\frac{4.65 \times 10^7 \text{ s}^{-1}}{0.70}\right) - 4.65 \times 10^7 \text{ s}^{-1} = 1.43 \text{ s}^{-1}$$

The rate constants of radiationless deactivation of TAPPI in different solvents were calculated according to same method and all the results were shown in the Table 4.8.

Table 4.8 Rate constants of radiationless deactivation data of TAPPI in different solvents.

Solvent	Φ_f	k_f (s^{-1})	k_d (s^{-1})
NMP	0.70	4.65×10^7	1.99×10^7
DMF	0.60	3.41×10^7	2.27×10^7
DMSO	0.30	3.86×10^7	9.01×10^7

4.1.8 Oscillator Strengths Calculations

The oscillator strength represents the electronic transition strength. It is a dimensionless quantity. Eqn. 4.7 used to calculate the oscillator strength.

$$f = 4.32 \times 10^{-9} \Delta\bar{v}_{1/2} \, \varepsilon_{max}$$

Eqn. 4.7

The calculation for oscillator strength of TAPPI in NMP at λ_{max}:

$$f = 4.32 \times 10^{-9} \Delta\bar{v}_{1/2} \, \varepsilon_{max} = 4.32 \times 10^{-9} \times 1350.32 \times 33000$$

$$f = 0.19$$

The oscillator strengths of the TAPPI in different solvents were calculated according to same method and all the results were shown in the Table 4.9.

Table 4.9 Oscillator strengths of the TAPPI in different solvents

Solvent	λ_{max} (nm)	$\Delta\bar{v}_{1/2}$ (cm^{-1})	ε_{max} (L.mol^{-1}.cm^{-1})	F
NMP	523	1350.32	33000	0.19
DMF	522	1357.34	24000	0.14
DMSO	523	1319.80	28000	0.16

4.1.9 Singlet Energies Calculations

Eqn. 4.8 used to calculate the singlet energies in the unit of $kcal.mol^{-1}$.

$$E_s = \frac{2.86 \times 10^5}{\lambda_{max}}$$ **Eqn. 4.8**

The singlet energy calculations for TAPPI in NMP

at $\lambda_{max} = 523$ nm:

$$E_s = \frac{2.86 \times 10^5}{\lambda_{max}} = \frac{2.86 \times 10^5}{5230} = 54.68 \, kcal \, mol^{-1}$$

The singlet energies of the TAPPI in different solvents were calculated according to same method and all the results were shown in Table 4.10.

Table 4.10 TAPPI's singlet energies in different solvents

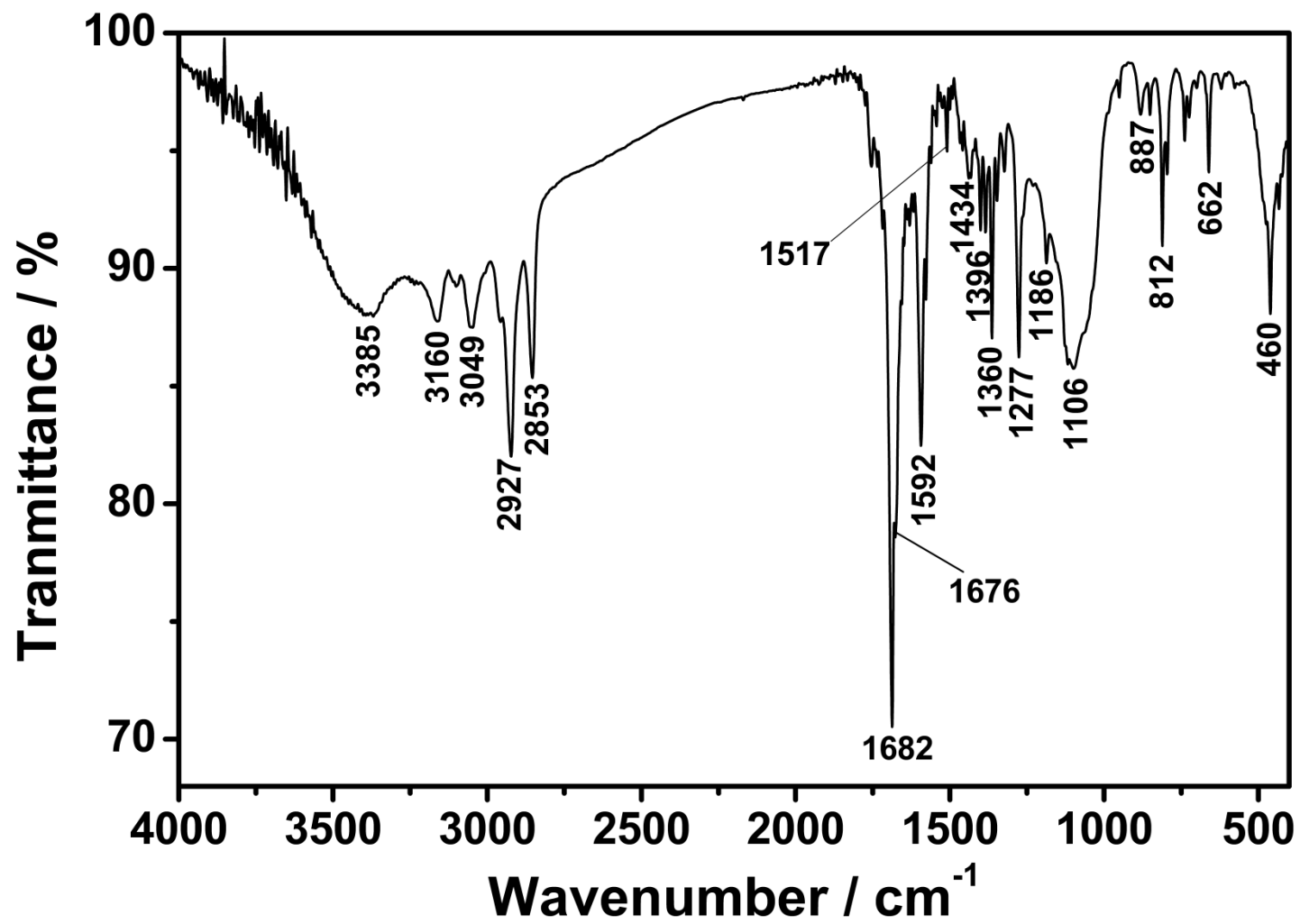| Solvent	λ_{max} (Å)	E_s (kcal mol^{-1})
Pyridine	526	54.37
NMP	523	54.68
DMF	522	54.79
DMSO	523	54.68
m-Cresol	549	52.09
TFAc	529	54.06

Figure 4.3: FT-IR Spectrum of TAPPI

Figure 4.4: UV-Vis Absorption Spectrum of TAPPI in DMSO (C = 1 $\times$ 10^{-5} M)

Figure 4.5: UV-Vis Absorption Spectrum of TAPPI in DMSO (Microfiltered)

Figure 4.6: UV-Vis Absorption Spectrum of TAPPI in DMSO (━━: C = 1 × 10^{-5} M; ━━: Microfiltered)

Figure 4.7: Emission Spectrum of TAPPI in DMSO (C = 1 $\times$ 10^{-5} M; λ_{exc} = 485 nm)

Figure 4.8: Emission Spectrum of TAPPI in DMSO (Microfiltered; λ_{exc} = 485 nm)

Figure 4.9: Emission Spectrum of TAPPI in DMSO (━━ : C = 1 × 10^{-5} M; ━━ : Microfiltered; λ_{exc} = 485 nm)

Figure 4.10: Excitation Spectrum of TAPPI in DMSO ($\blacksquare$: Microfiltered; Inset: C = 1 $\times$ 10^{-5} M; λ_{em} = 650 nm)
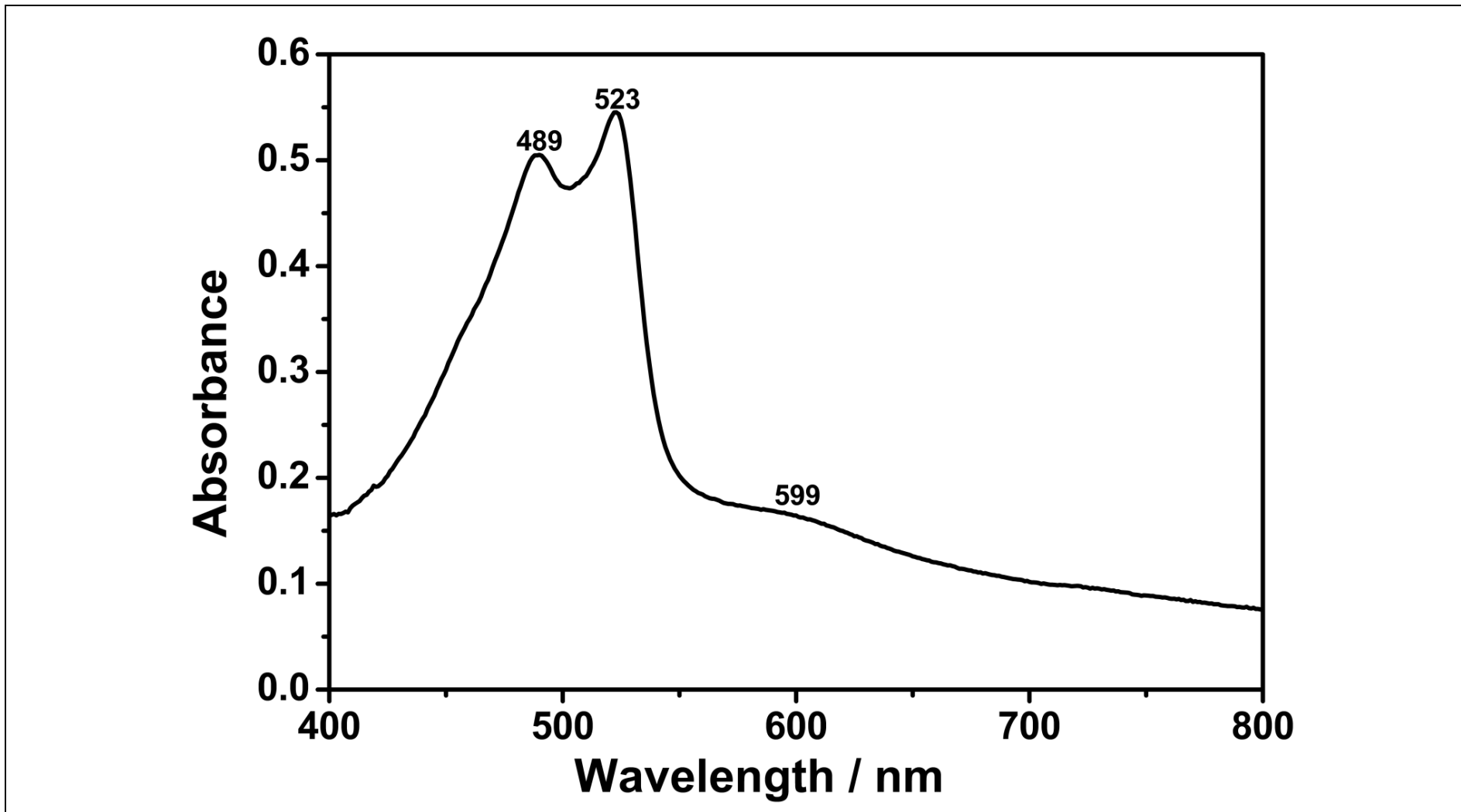
Figure 4.11: UV-Vis Absorption Spectrum of TAPPI in DMF (C = 1 $\times$ 10^{-5} M)
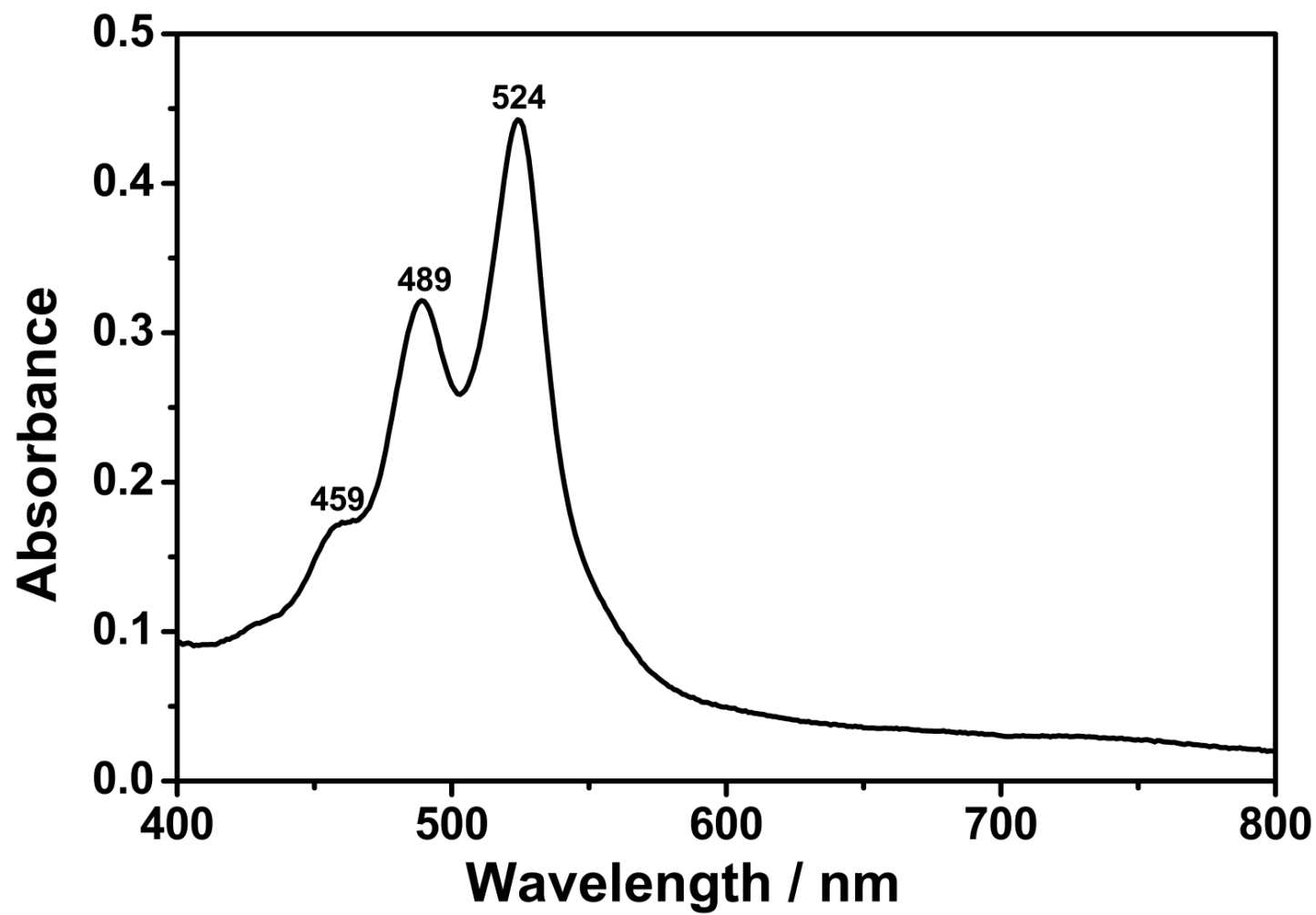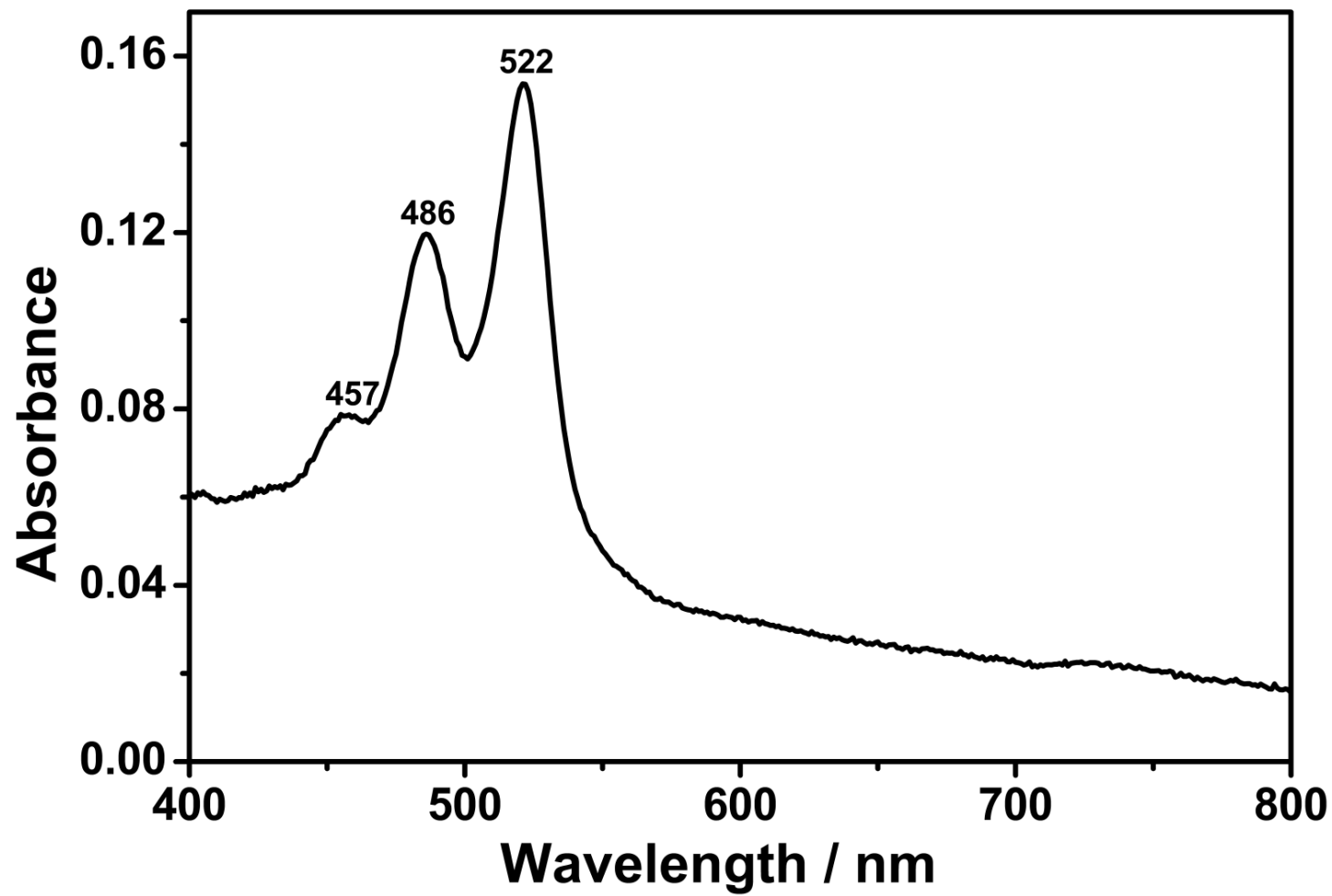
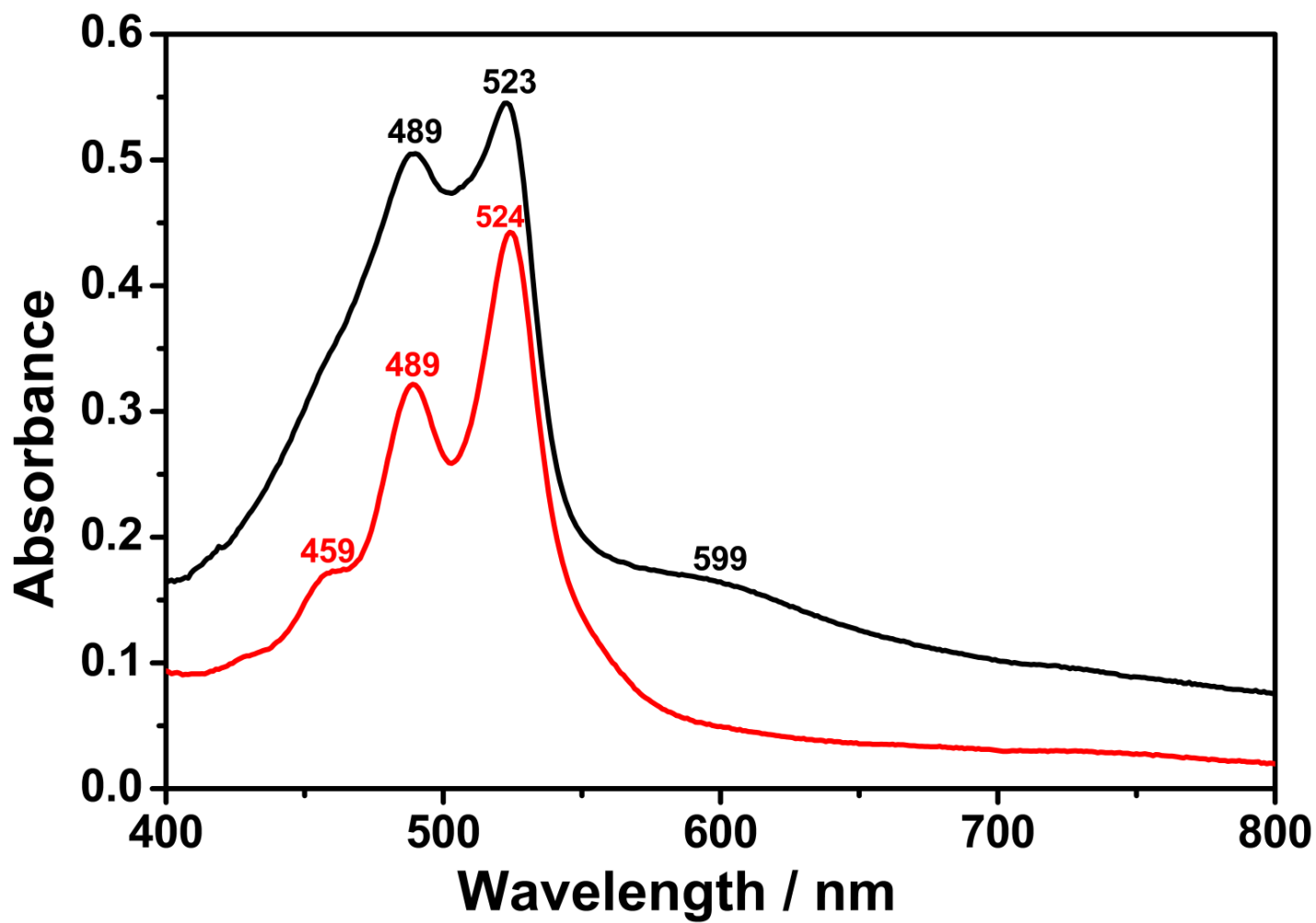Figure 4.12: UV-Vis Absorption Spectrum of TAPPI in DMF (Microfiltered)
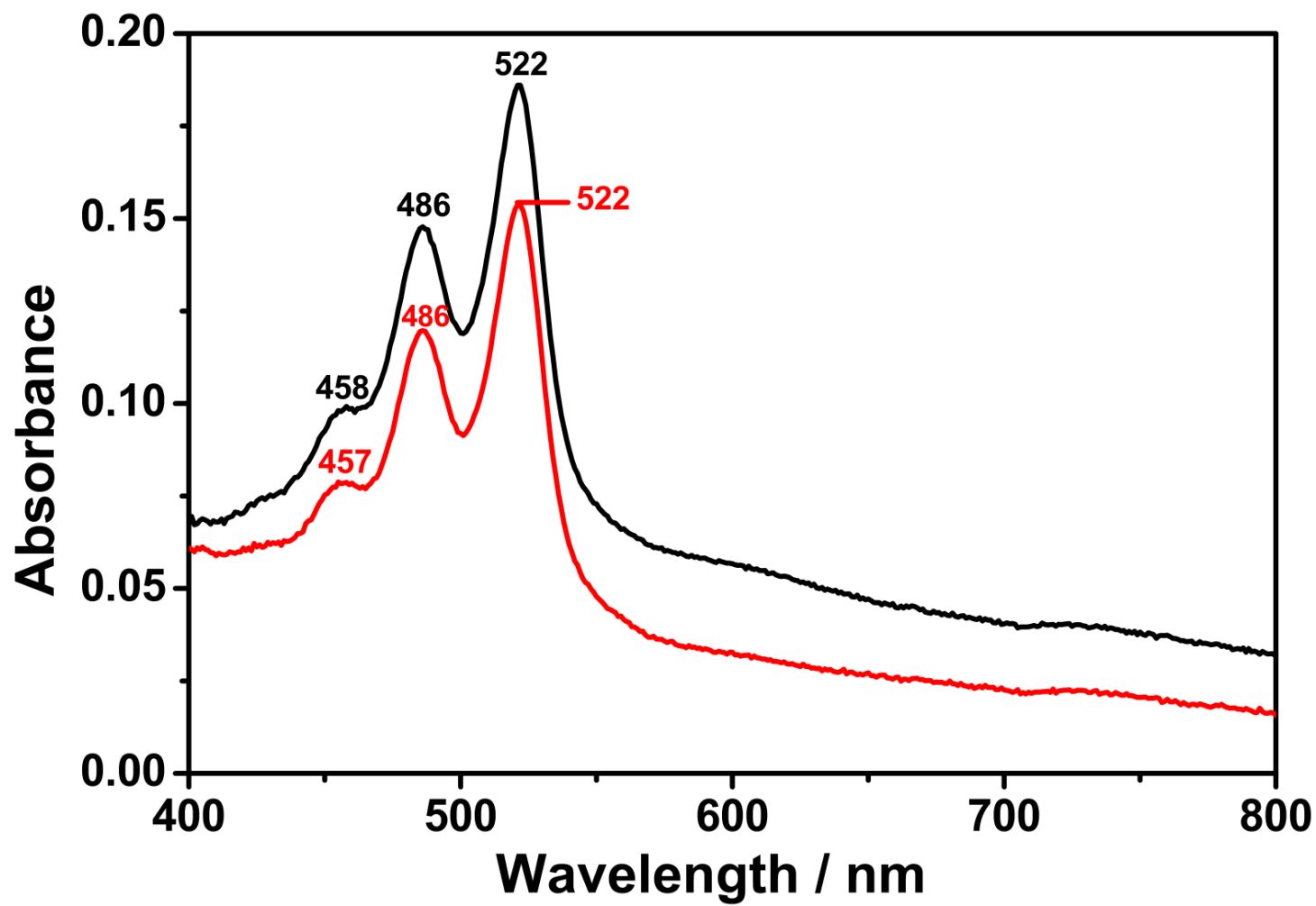
Figure 4.13: UV-Vis Absorption Spectrum of TAPPI in DMF (━━: C = 1 × 10^{-5} M; ━━: Microfiltered)
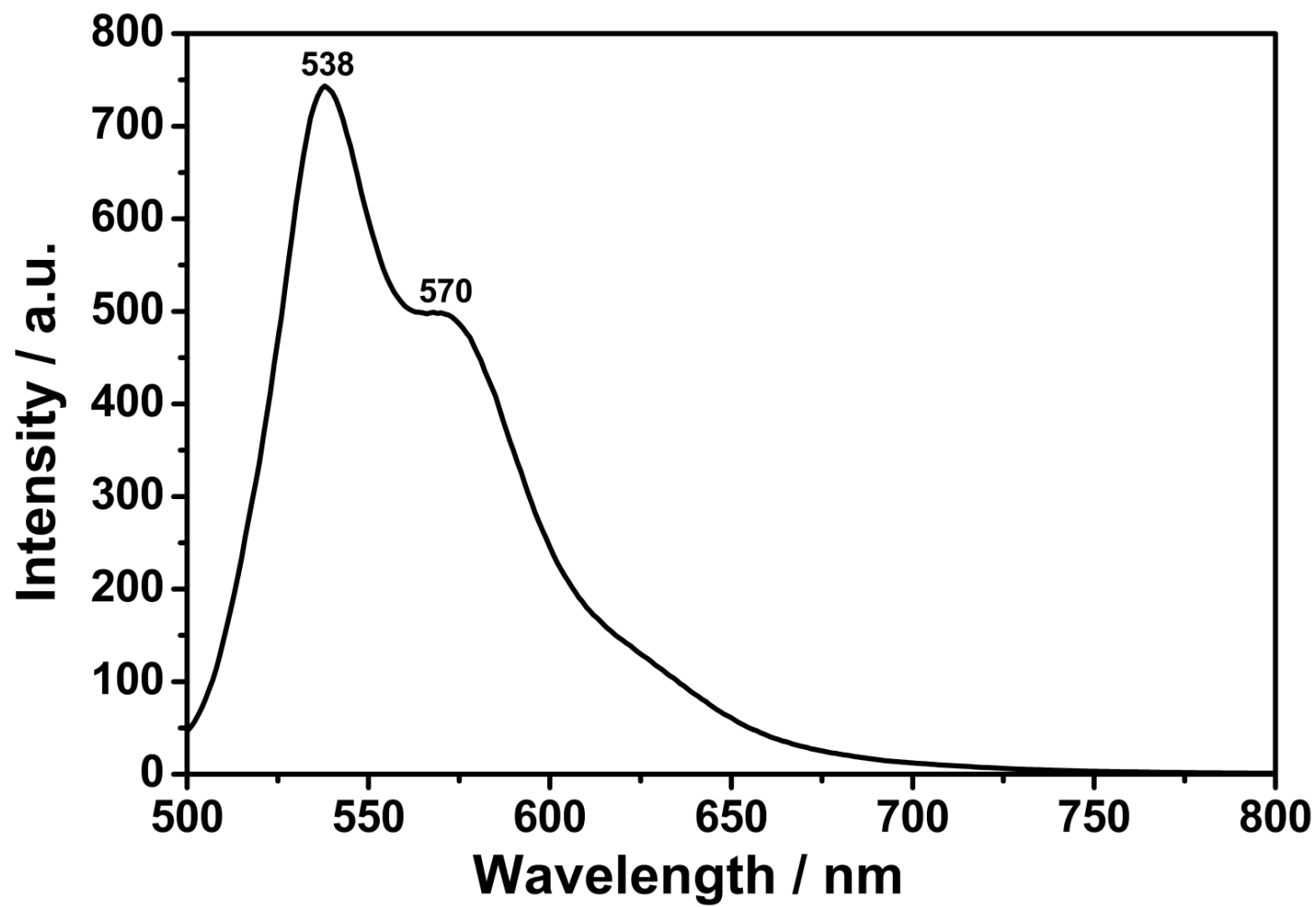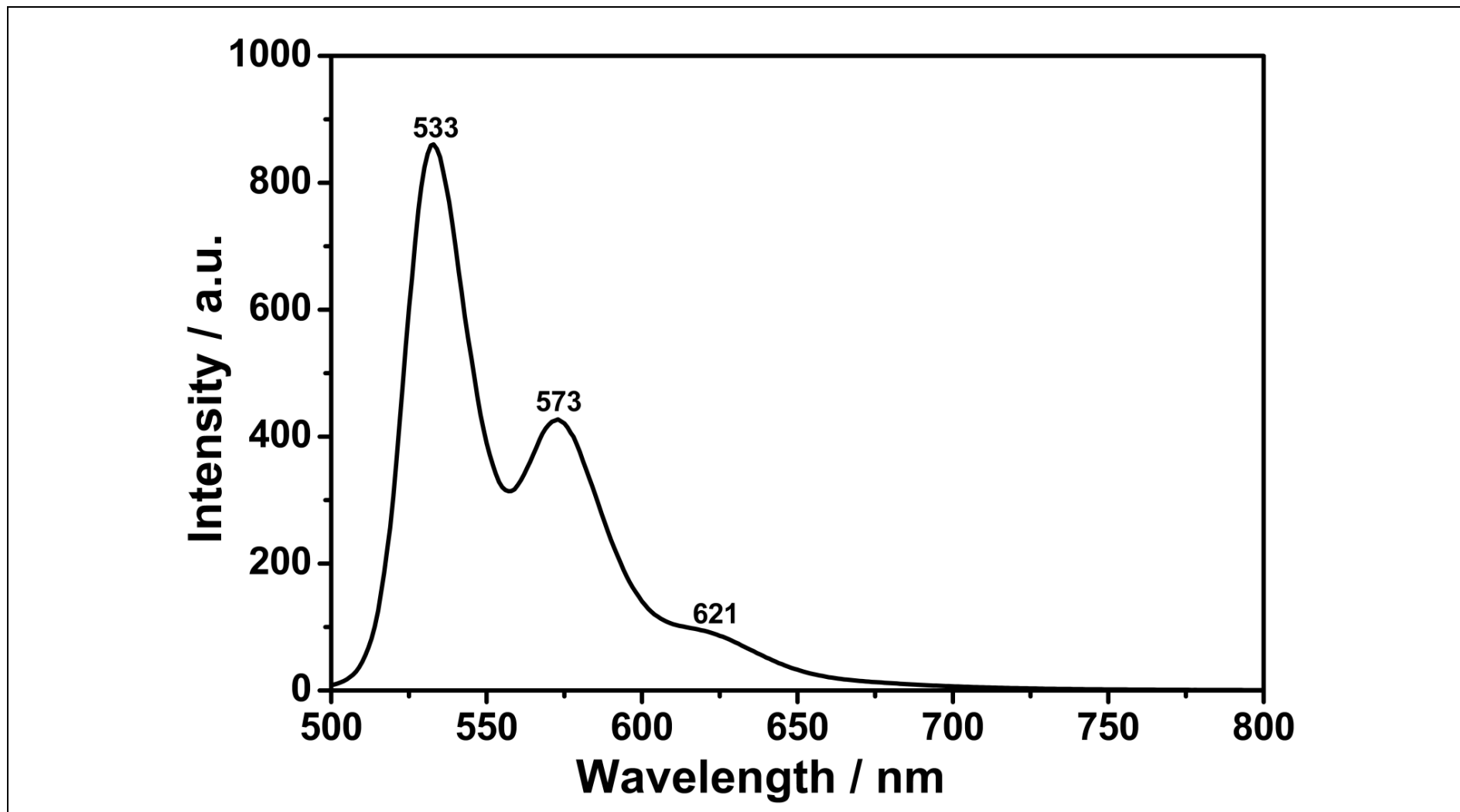
Figure 4.14: Emission Spectrum of TAPPI in DMF (C = 1 $\times$ 10^{-5} M; λ_{exc} = 485 nm)
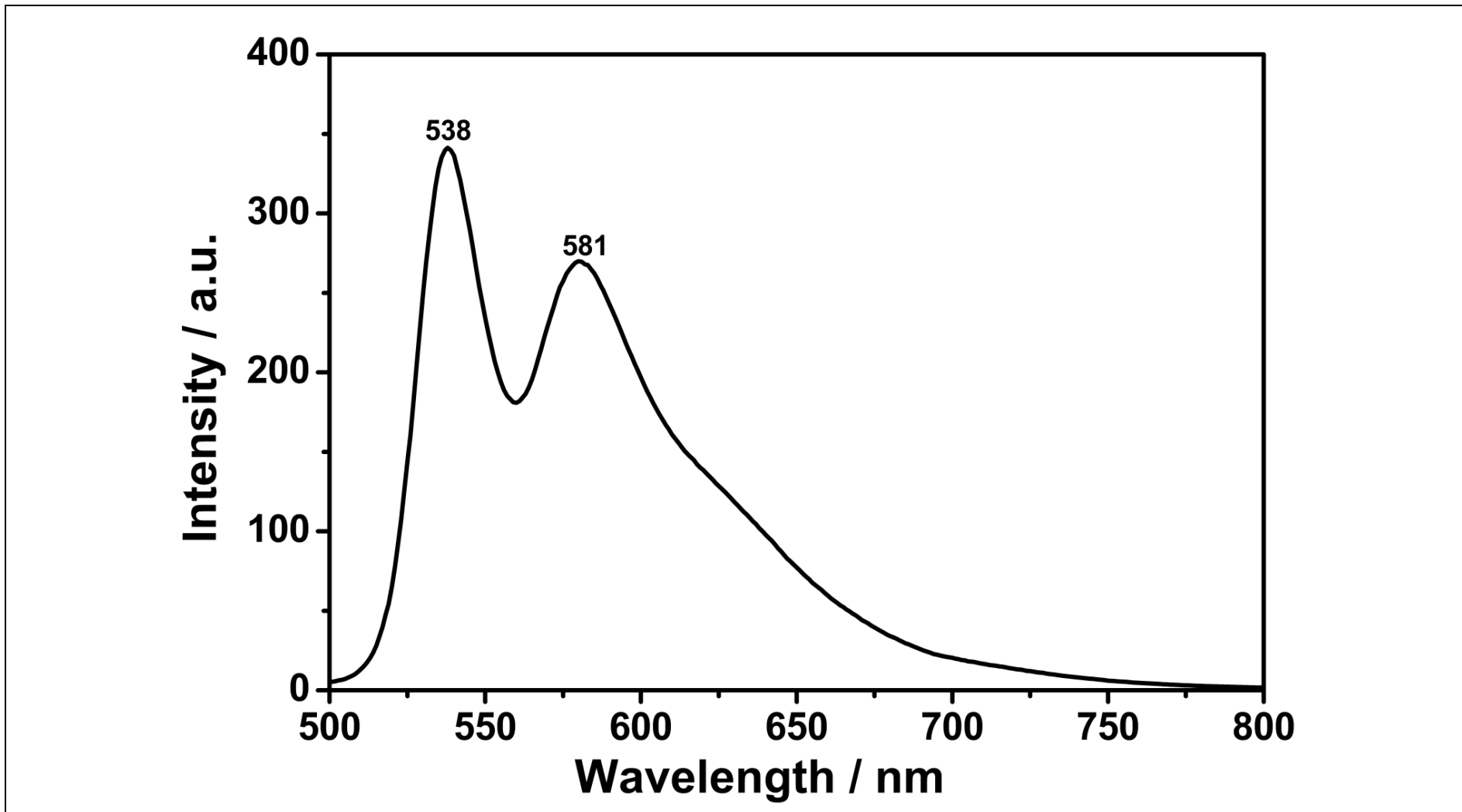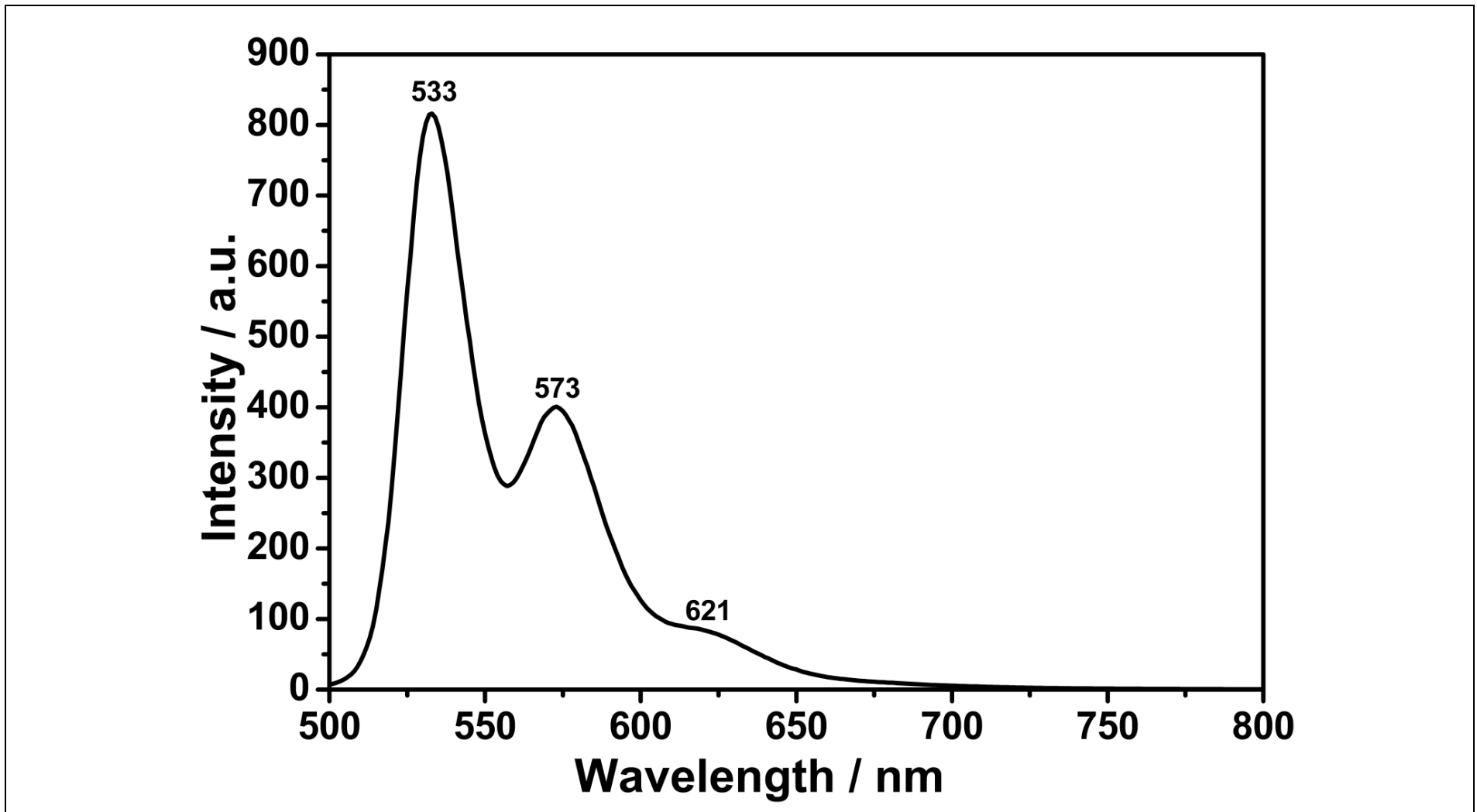
Figure 4.15: Emission Spectrum of TAPPI in DMF (Microfiltered; $\lambda_{exc} = 485$ nm)
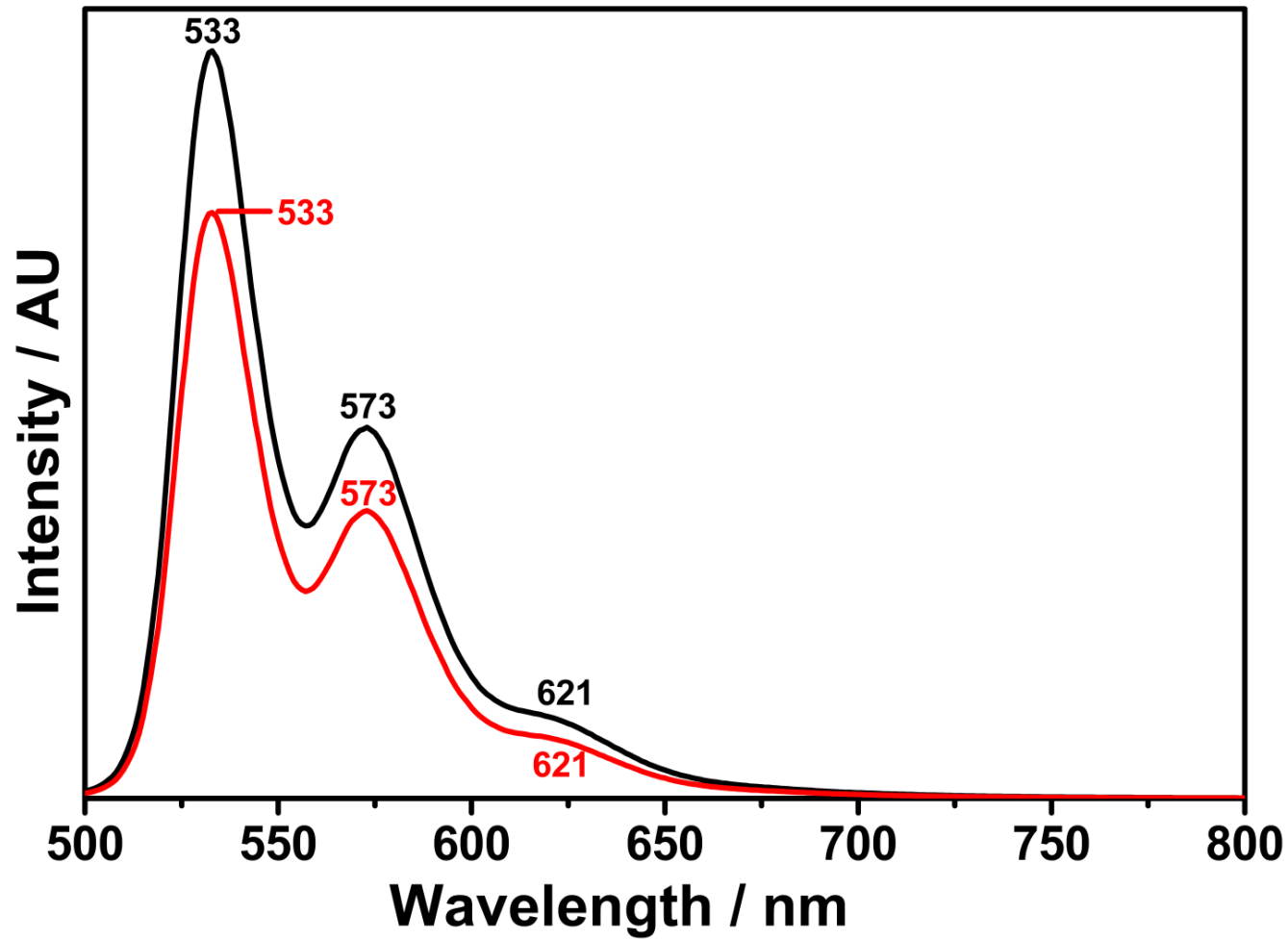
Figure 4.16: Emission Spectrum of TAPPI in DMF (▬▬: C = 1 $\times$ 10^{-5} M; ▬▬: Microfiltered; λ_{exc} = 485 nm)
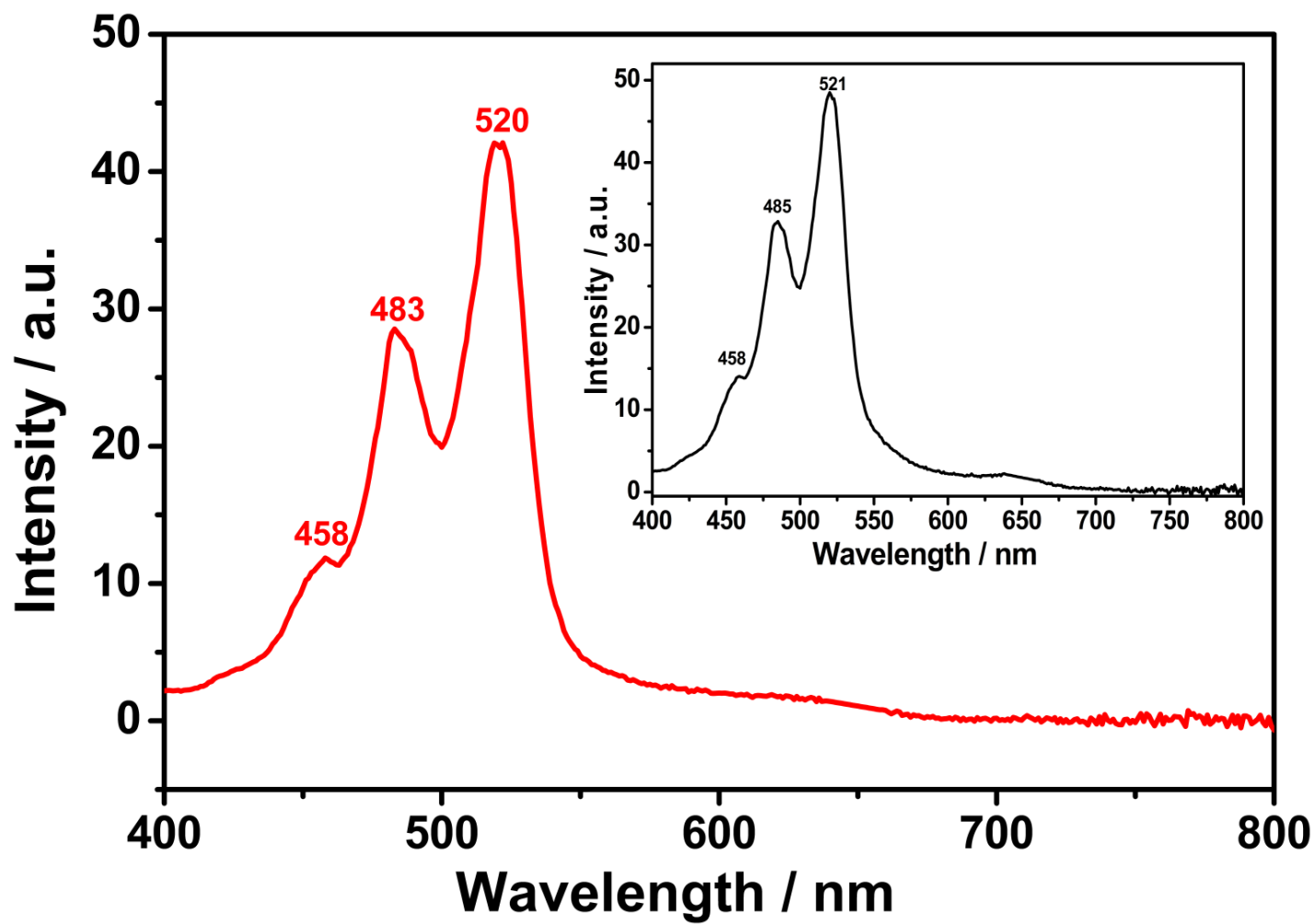
Figure 4.17: Excitation Spectrum of TAPPI in DMF (■■■ : Microfiltered; Inset: C = 1 × 10^{-5} M; λ_{em}= 650 nm)
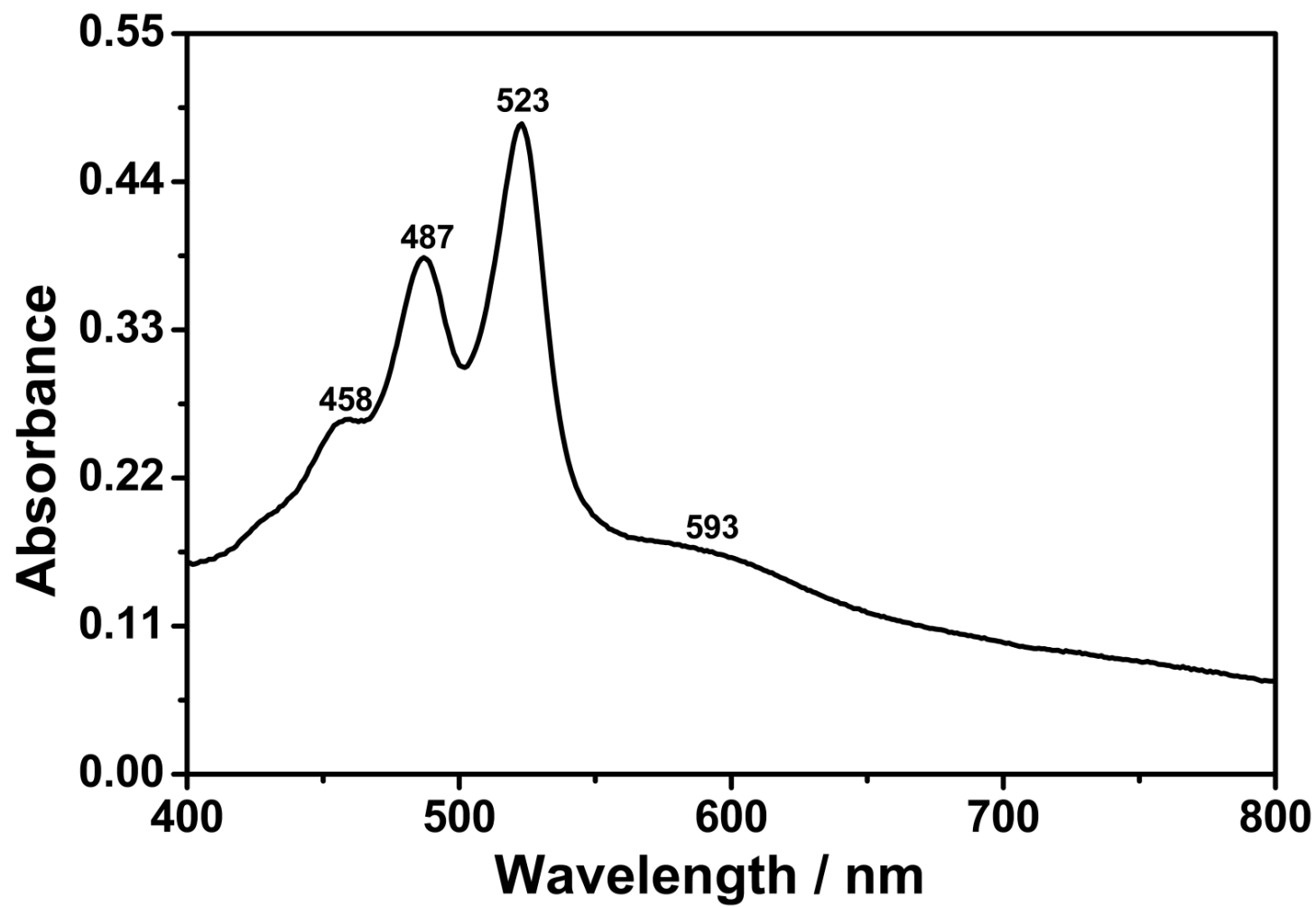
Figure 4.18: UV-Vis Absorption Spectrum of TAPPI in NMP (C = 1 $\times$ 10^{-5} M)
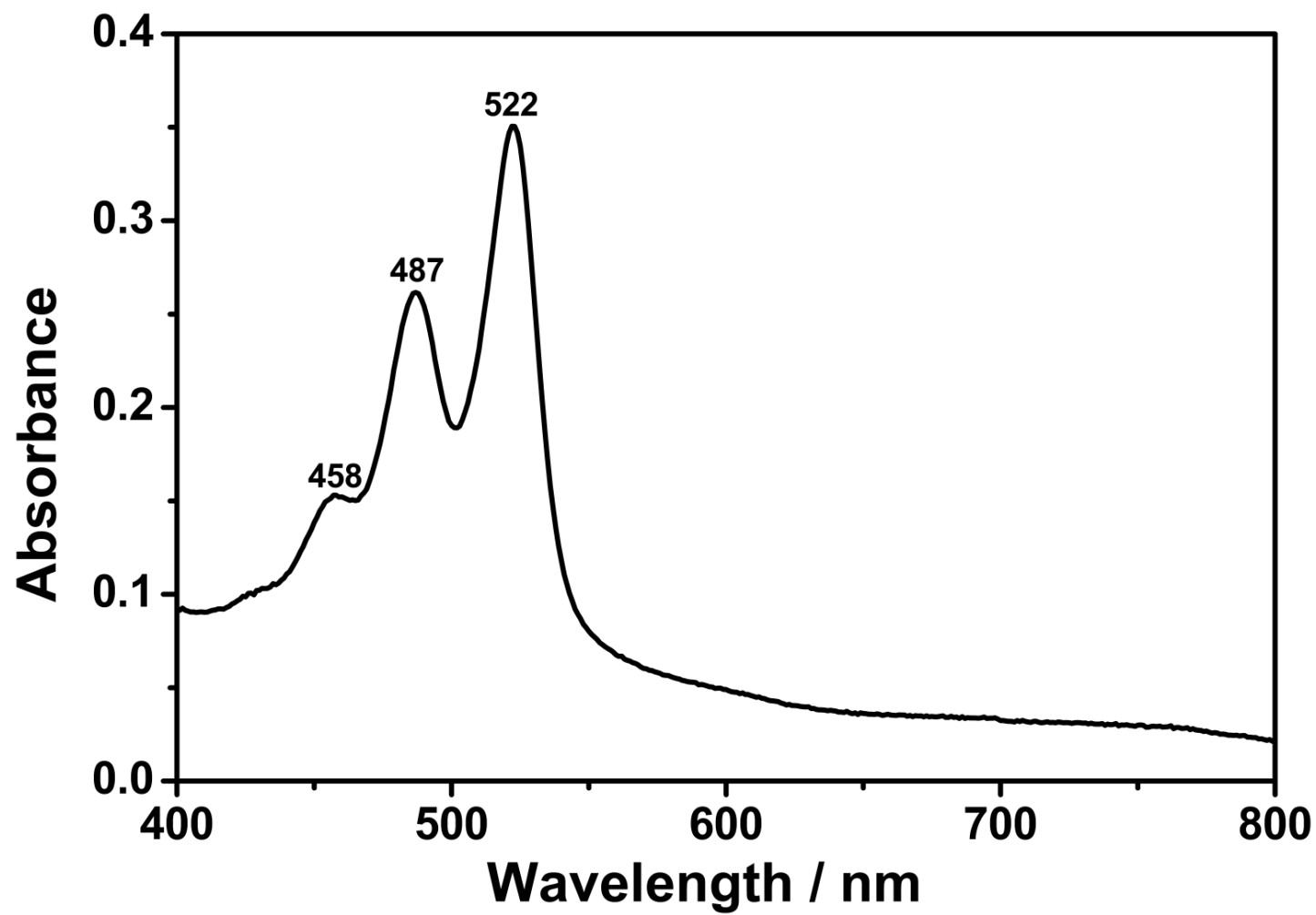
Figure 4.19: UV-Vis Absorption Spectrum of TAPPI in NMP (Microfiltered)
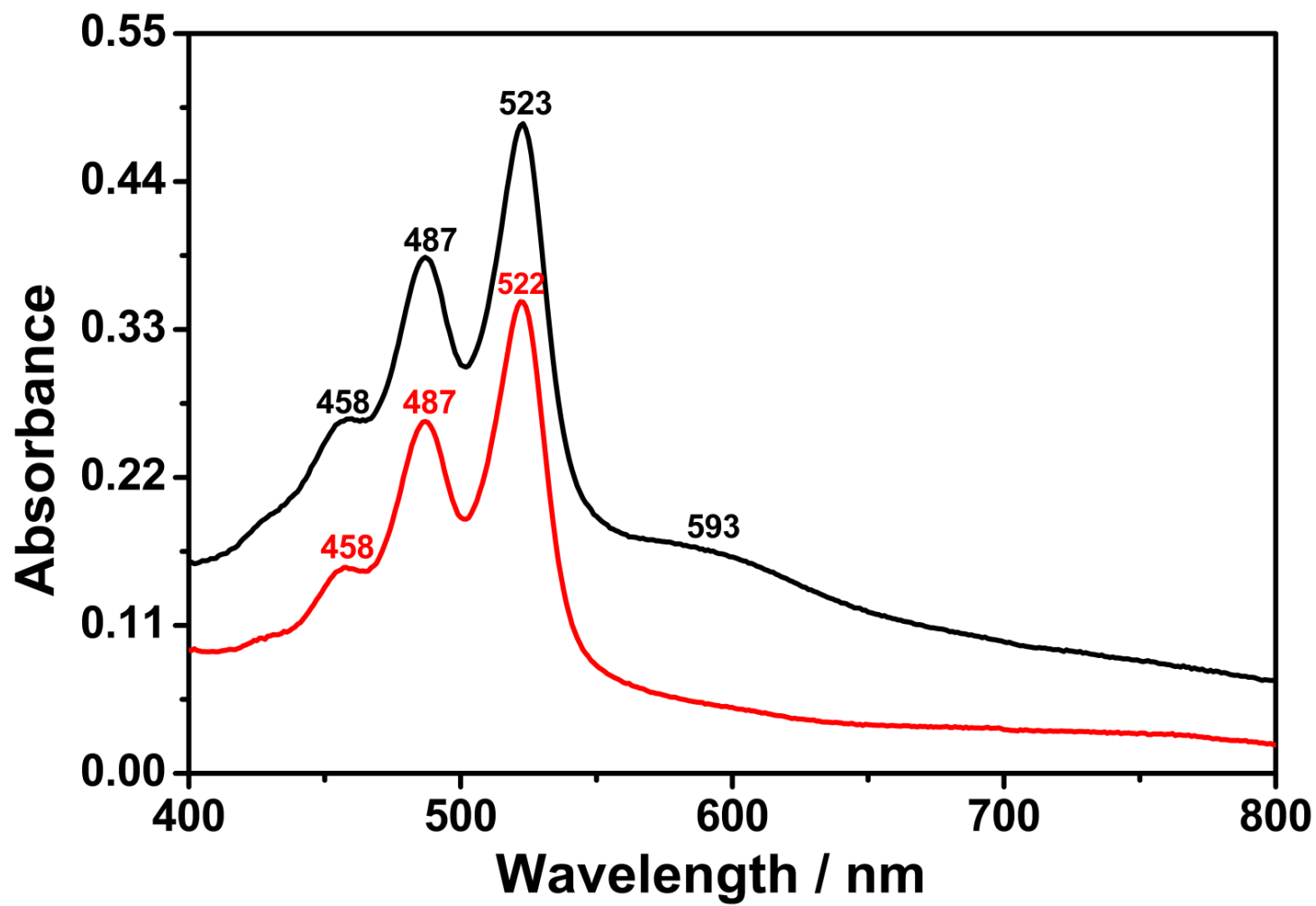
Figure 4.20: UV-Vis Absorption Spectrum of TAPPI in NMP (———: C = 1 × 10^{-5} M; ———: Microfiltered)
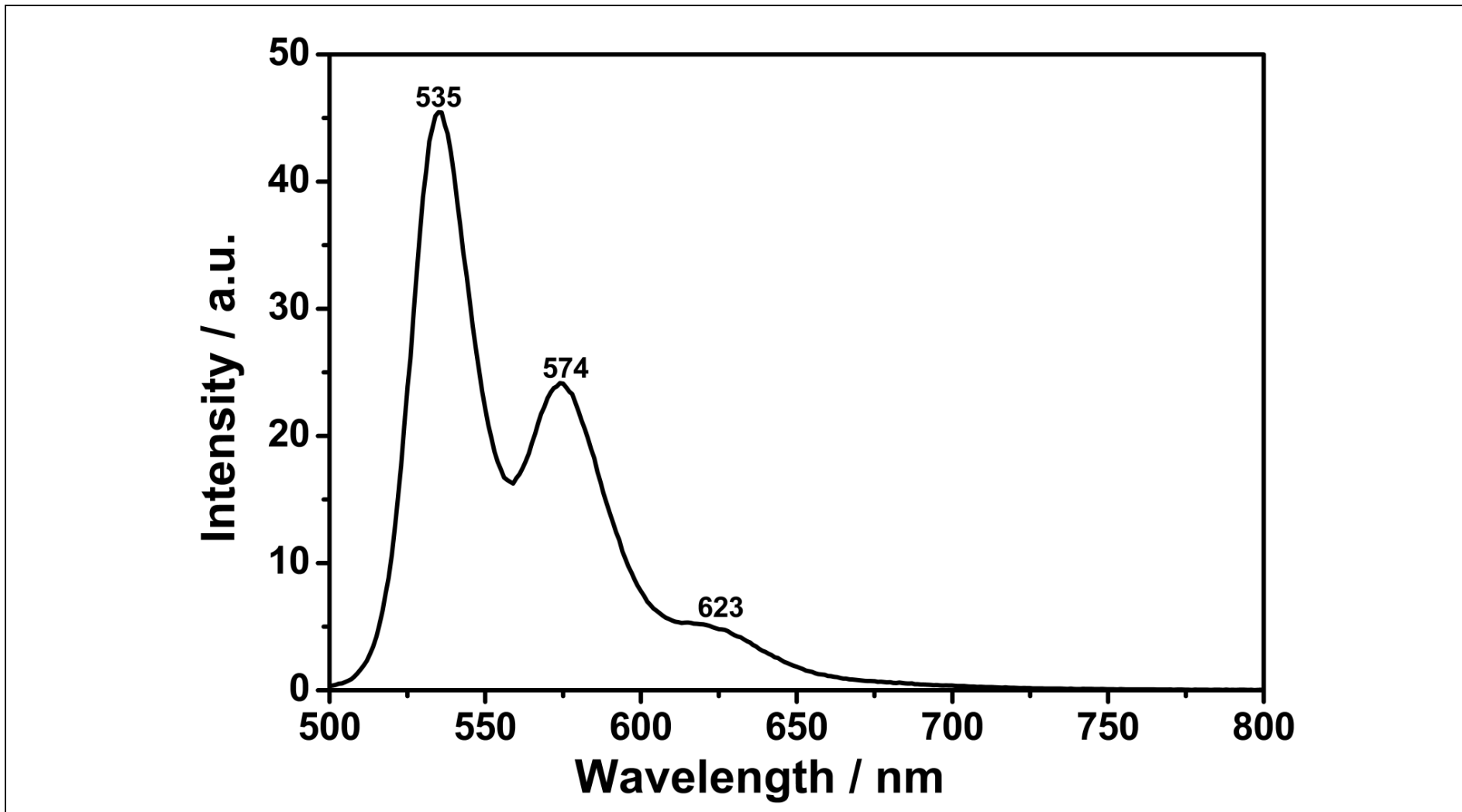
Figure 4.21: Emission Spectrum of TAPPI in NMP (C = 1 $\times$ 10^{-5} M; λ_{exc} = 485 nm)
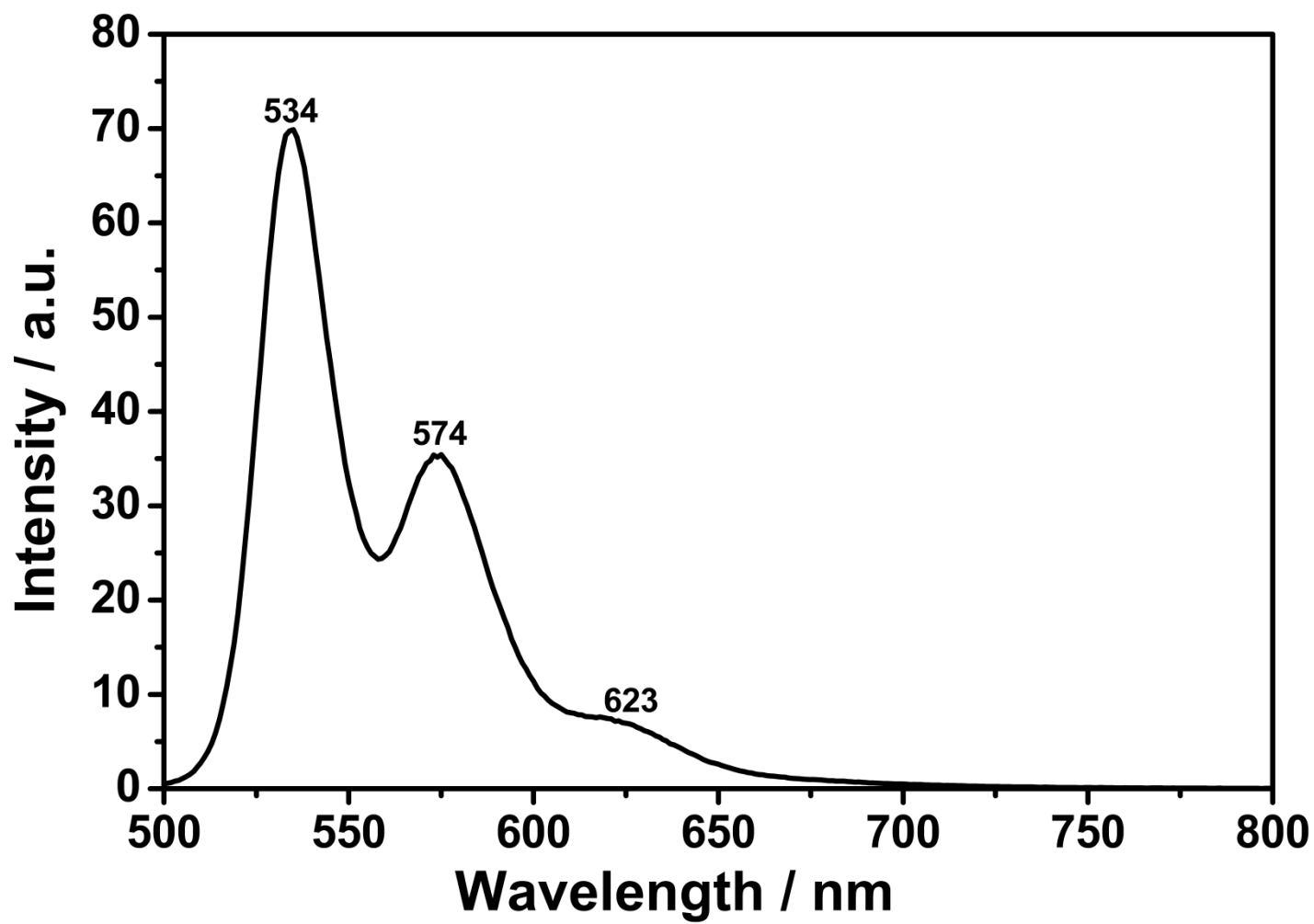
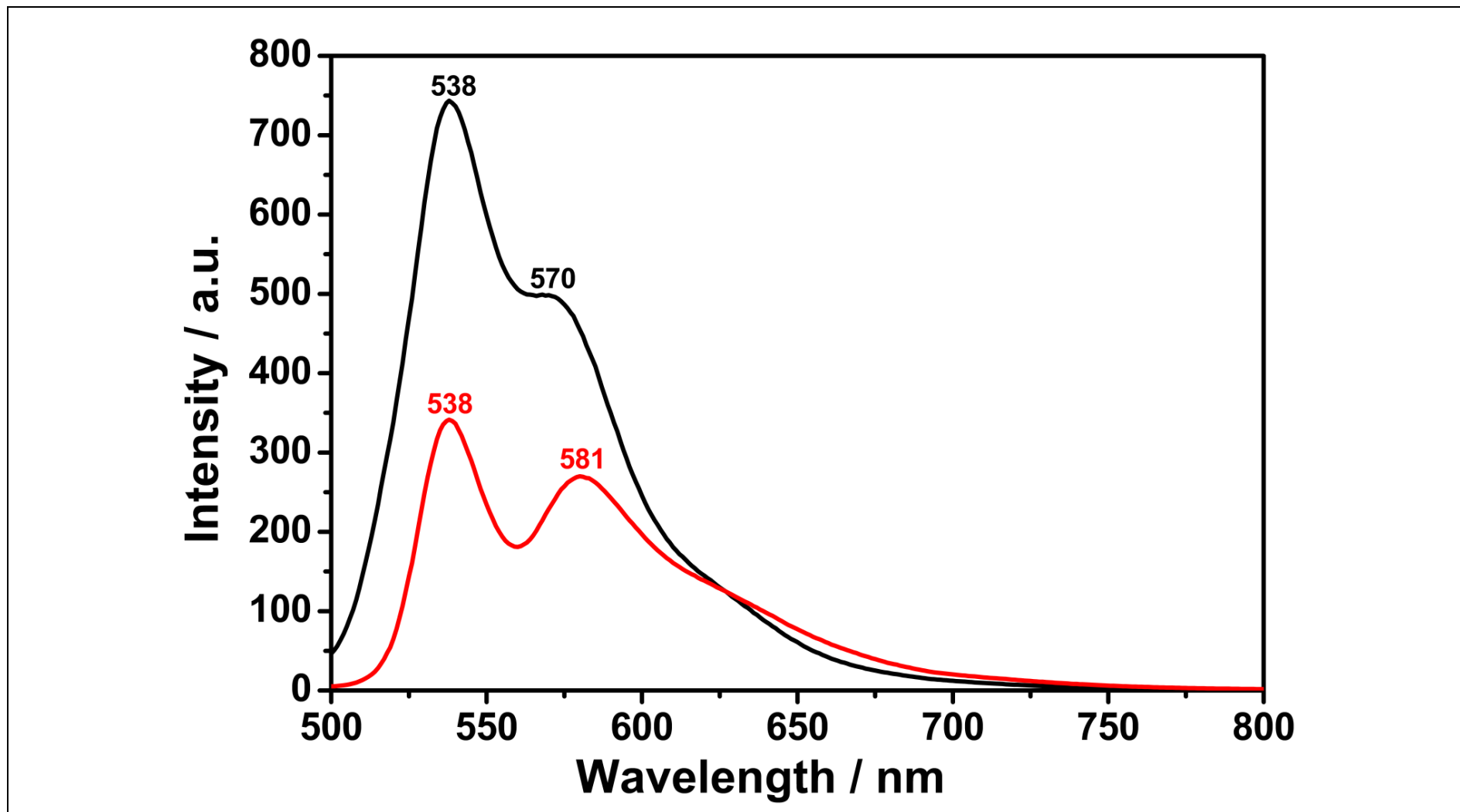Figure 4.22: Emission Spectrum of TAPPI in NMP (Microfiltered; λ_{exc} = 485 nm)

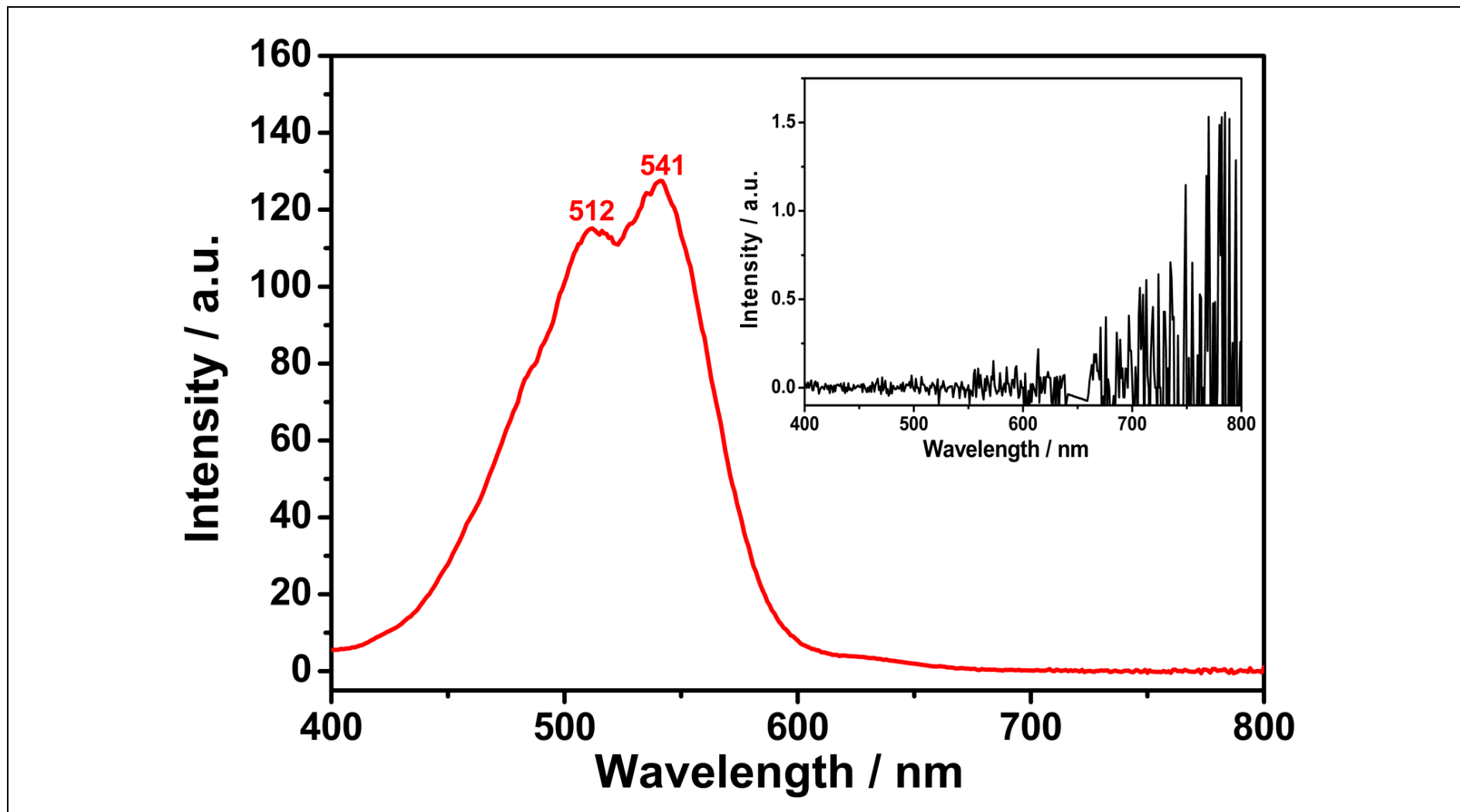Figure 4.23: Emission Spectrum of TAPPI in NMP (━━: C = 1 × 10^{-5} M; ━━: Microfiltered; λ_{exc} = 485 nm)

Figure 4.24: Excitation Spectrum of TAPPI in NMP (━━: Microfiltered; Inset: C = 1 $\times$ 10^{-5} M; λ_{em} = 650 nm)

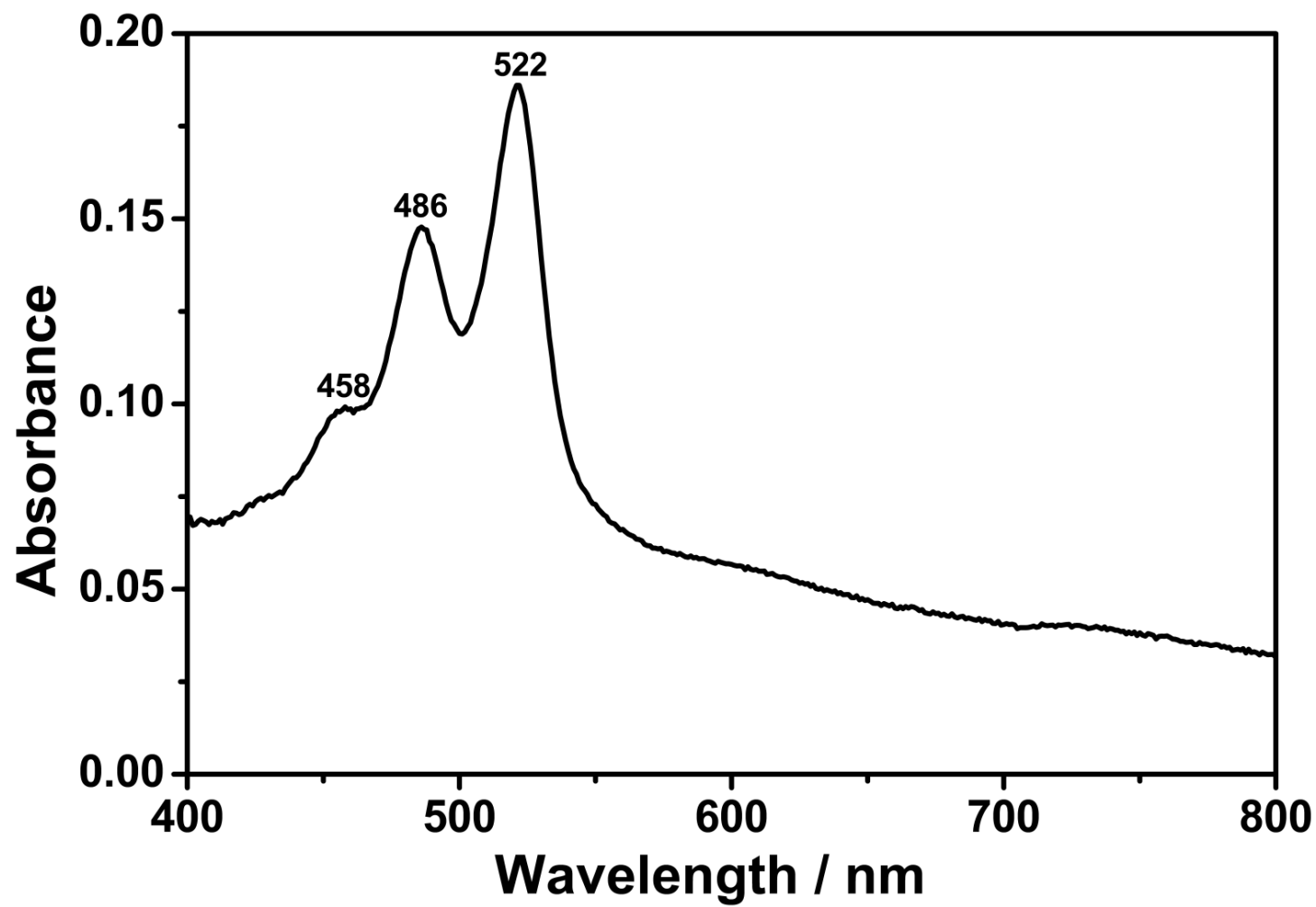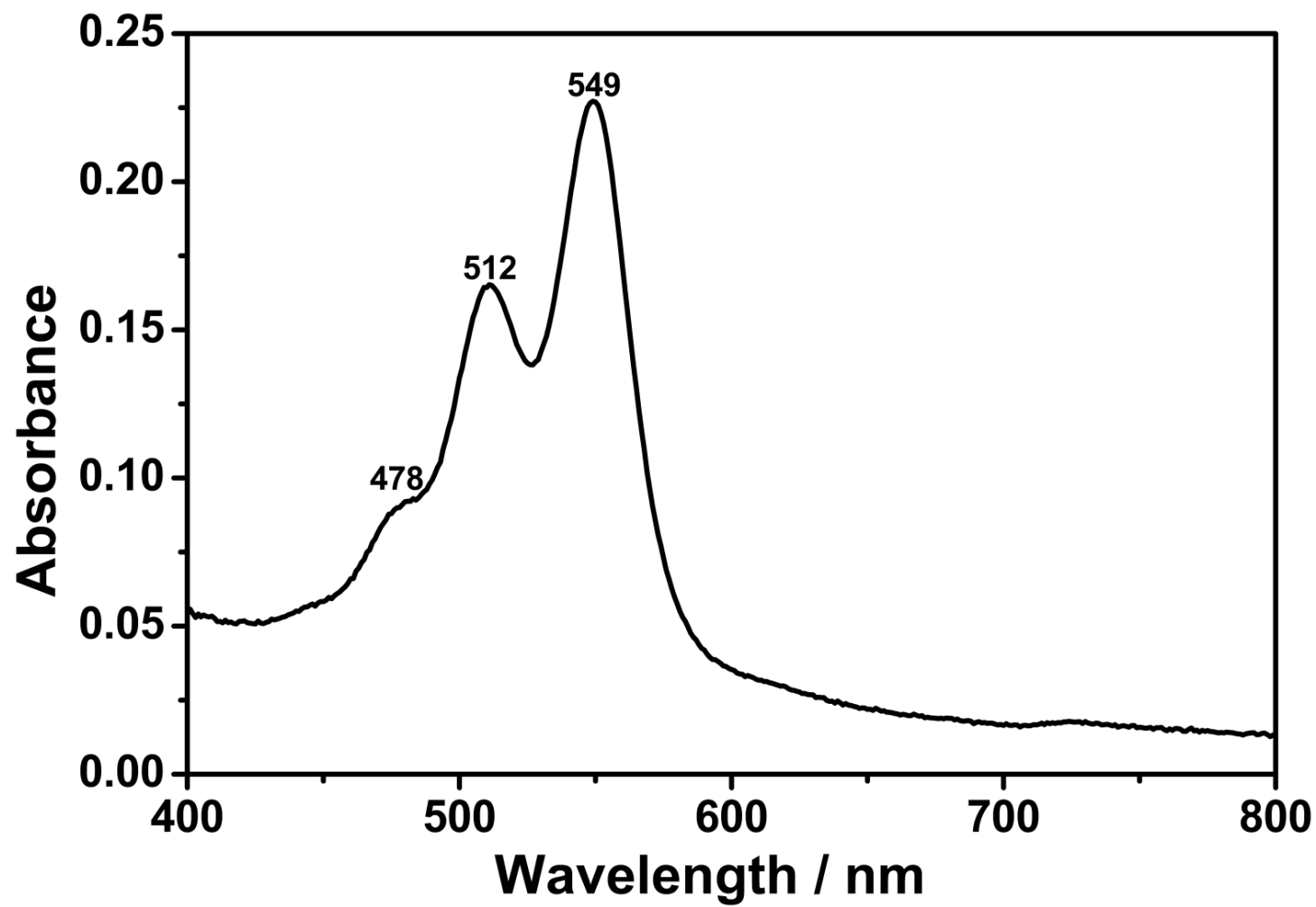Figure 4.25: UV-Vis Absorption Spectrum of TAPPI in m-Cresol (C = 1 $\times$ 10^{-5} M)
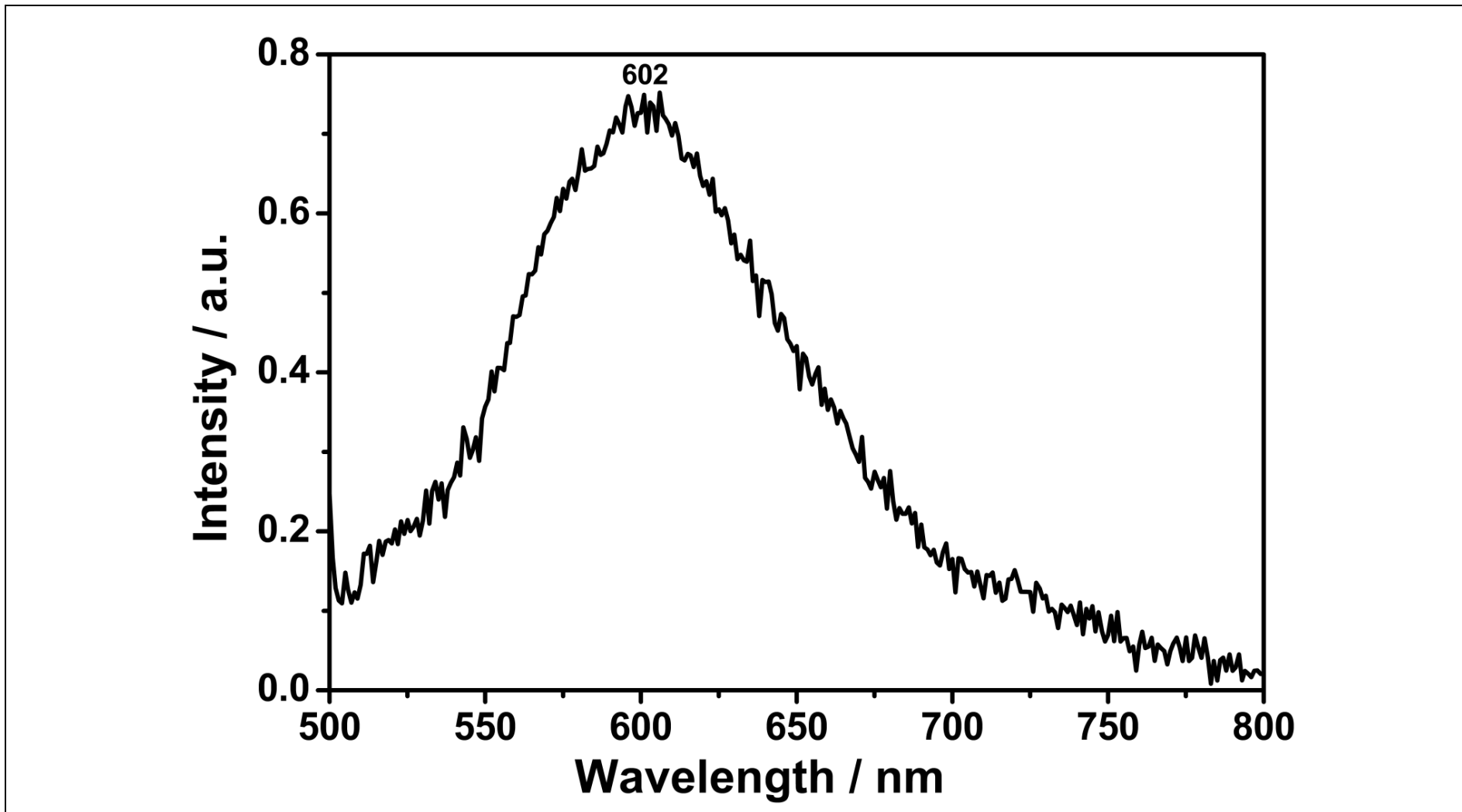
Figure 4.26: Emission Spectrum of TAPPI in m-Cresol (C = 1 $\times$ 10^{-5} M; λ_{exc} = 485 nm)
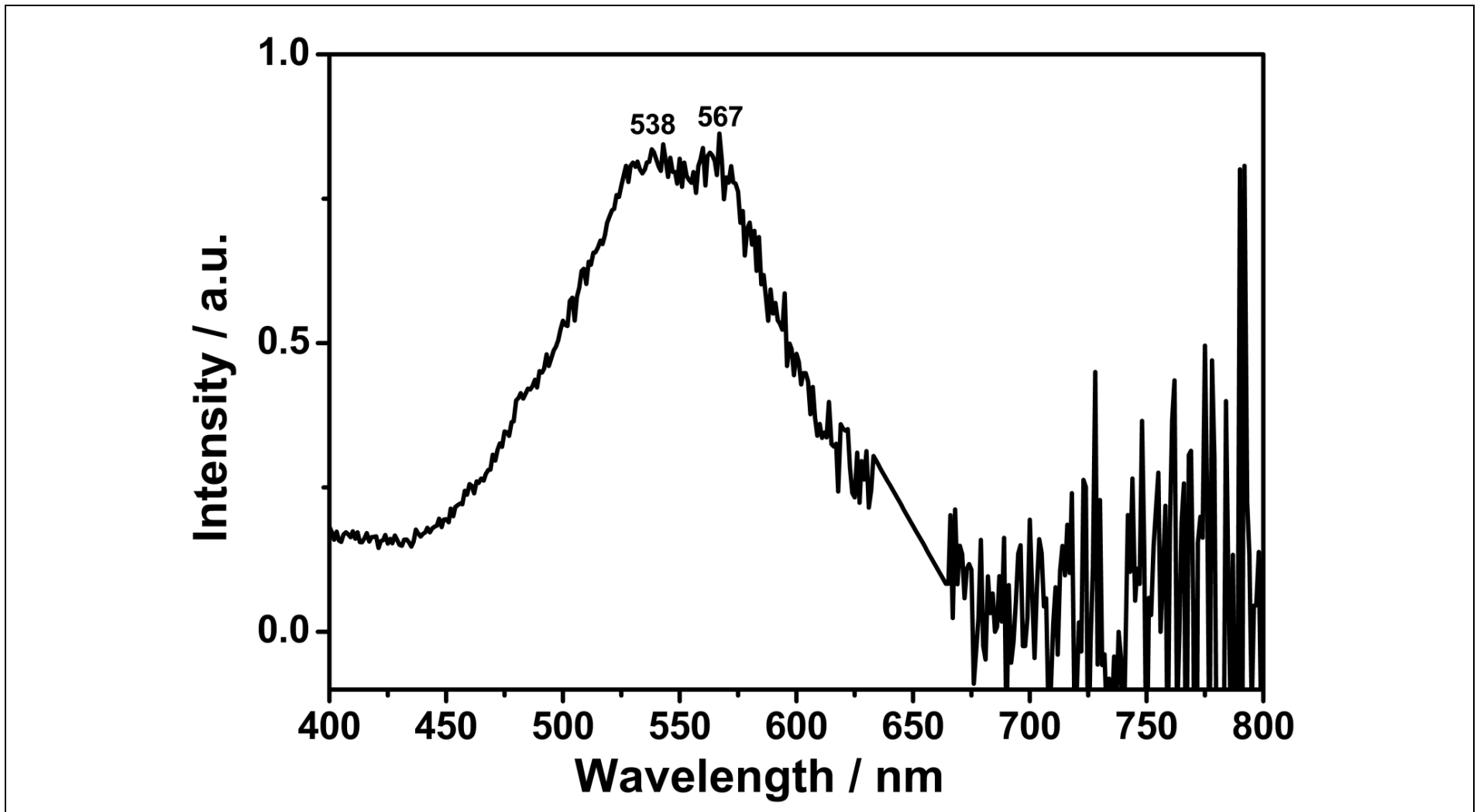
Figure 4.27: Excitation Spectrum of TAPPI in m-Cresol (C = 1 $\times$ 10^{-5} M; λ_{em} = 650 nm)
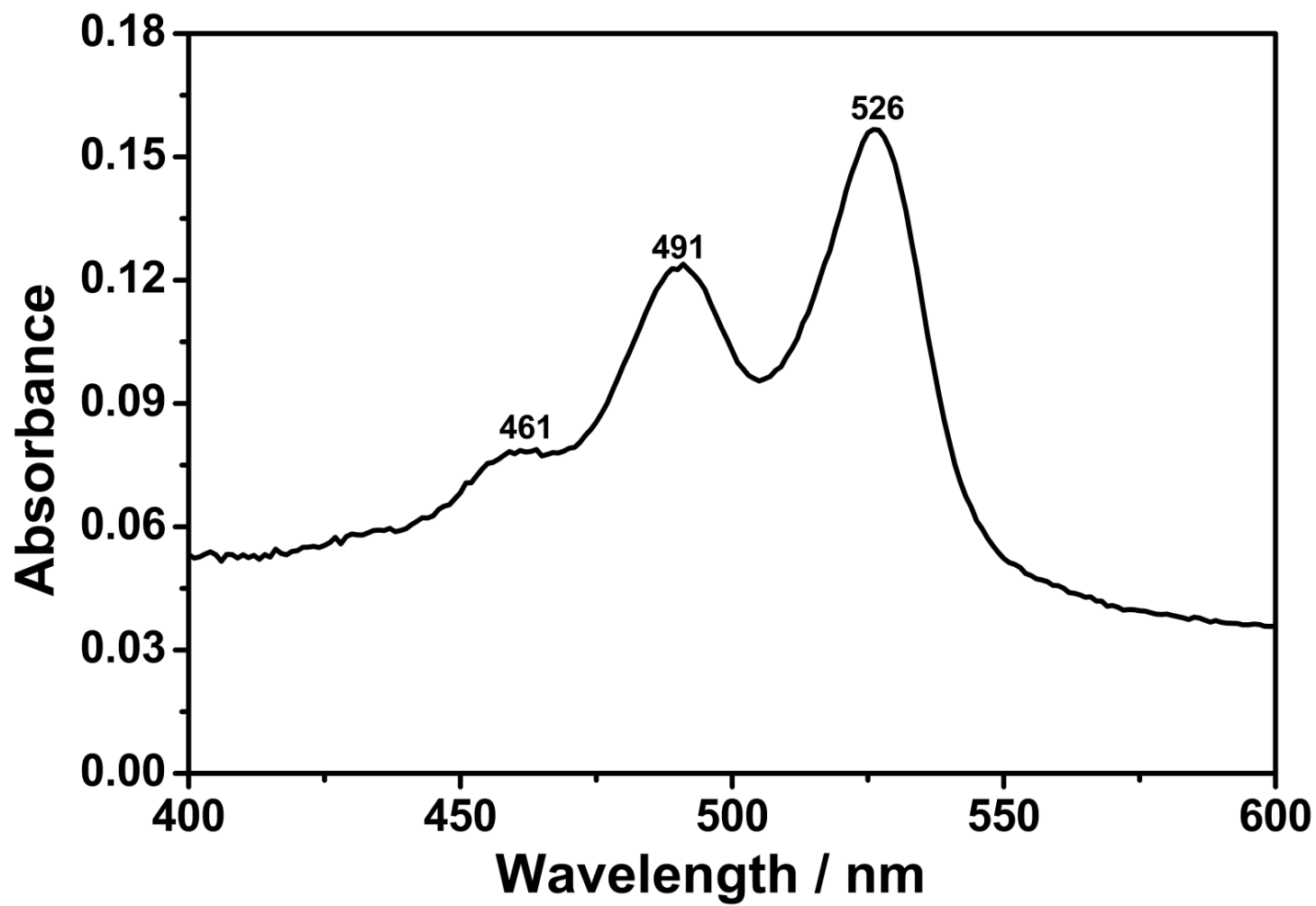
Figure 4.28: UV-Vis Absorption Spectrum of TAPPI in Pyridine (C = 1 $\times$ 10^{-5} M)
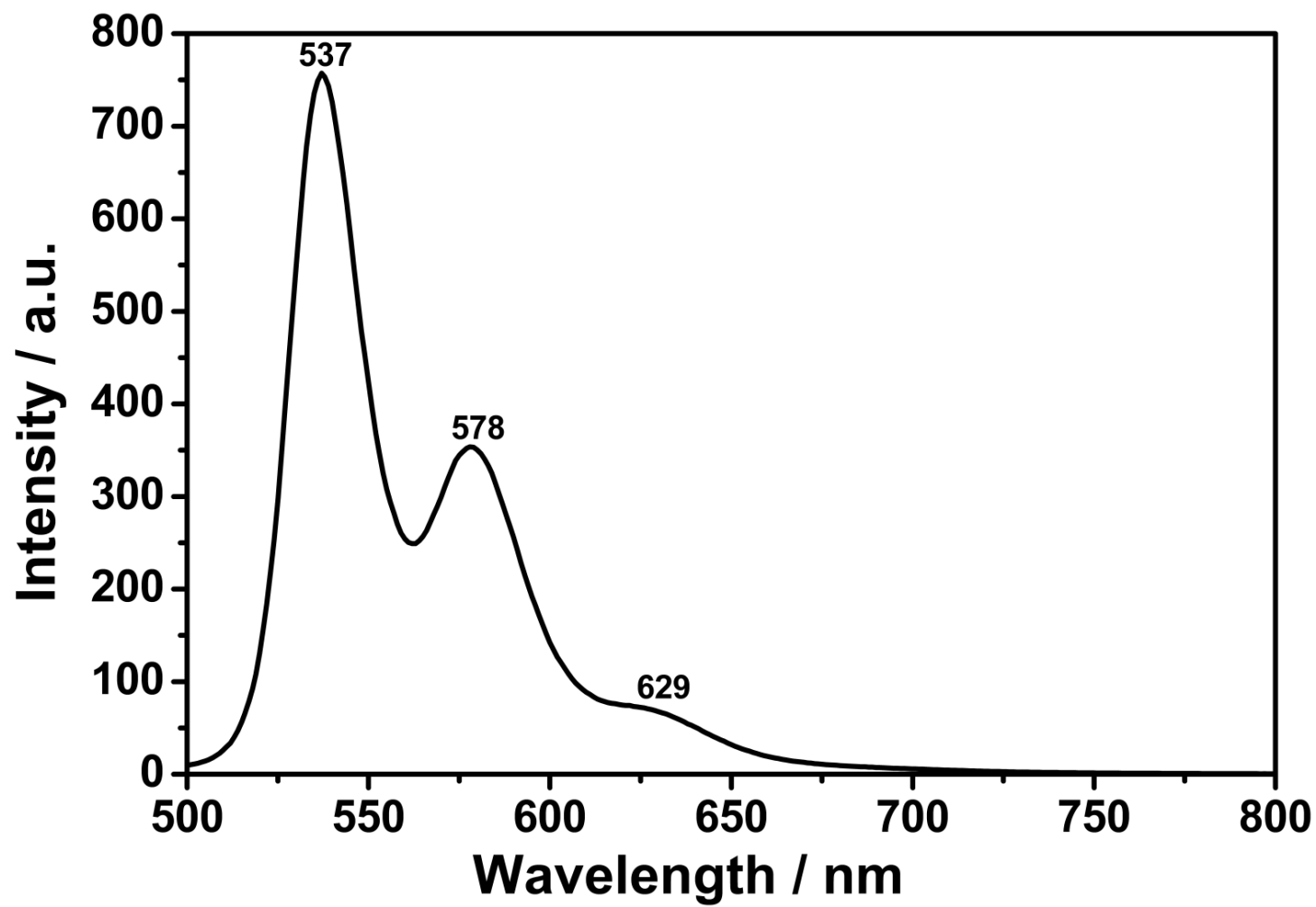
Figure 4.29: Emission Spectrum of TAPPI in m-Pyridine (C = 1 $\times$ 10^{-5} M; λ_{exc} = 485 nm)
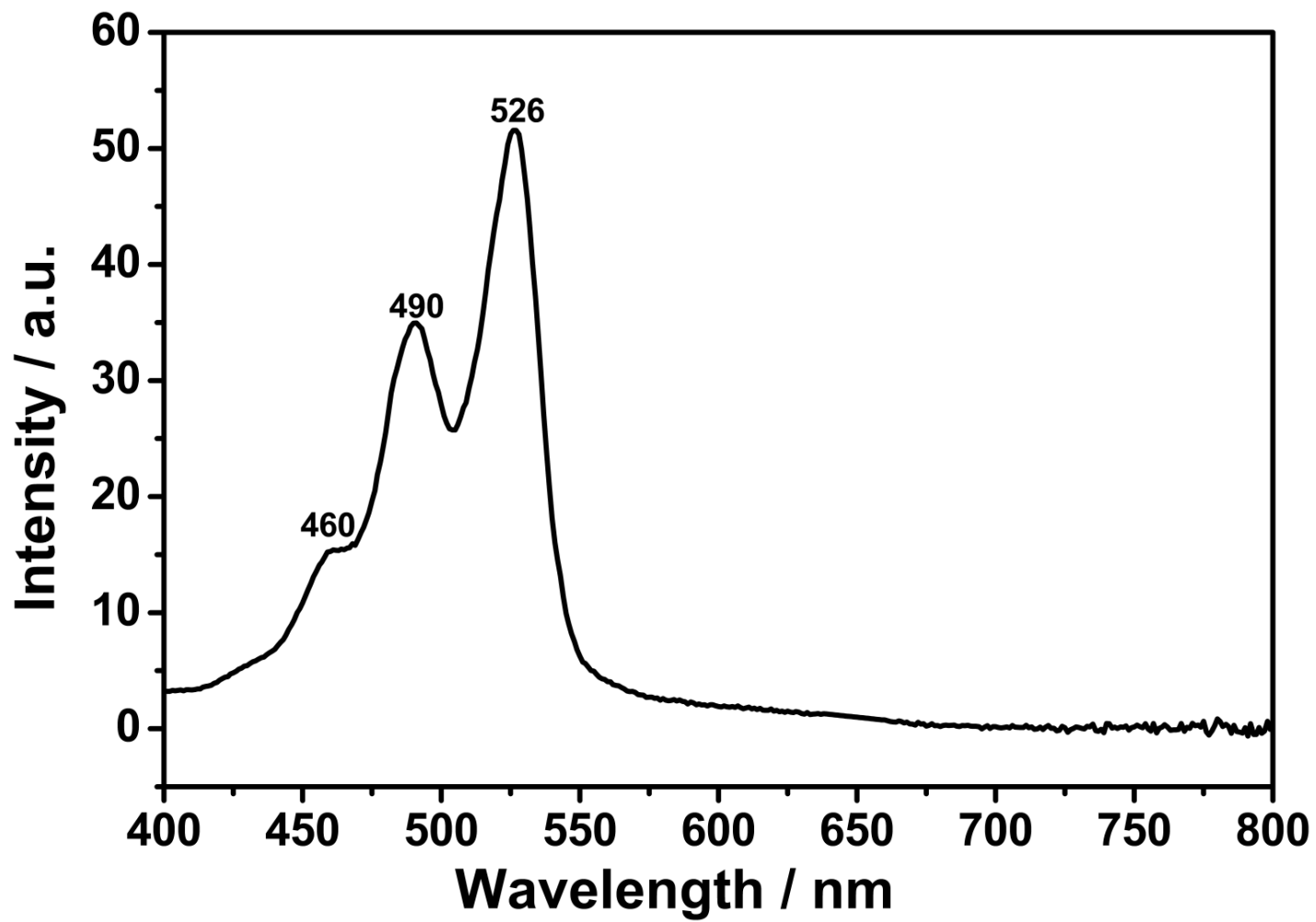
Figure 4.30: Excitation Spectrum of TAPPI in Pyridine (C = 1 $\times$ 10^{-5} M; λ_{em} = 650 nm)
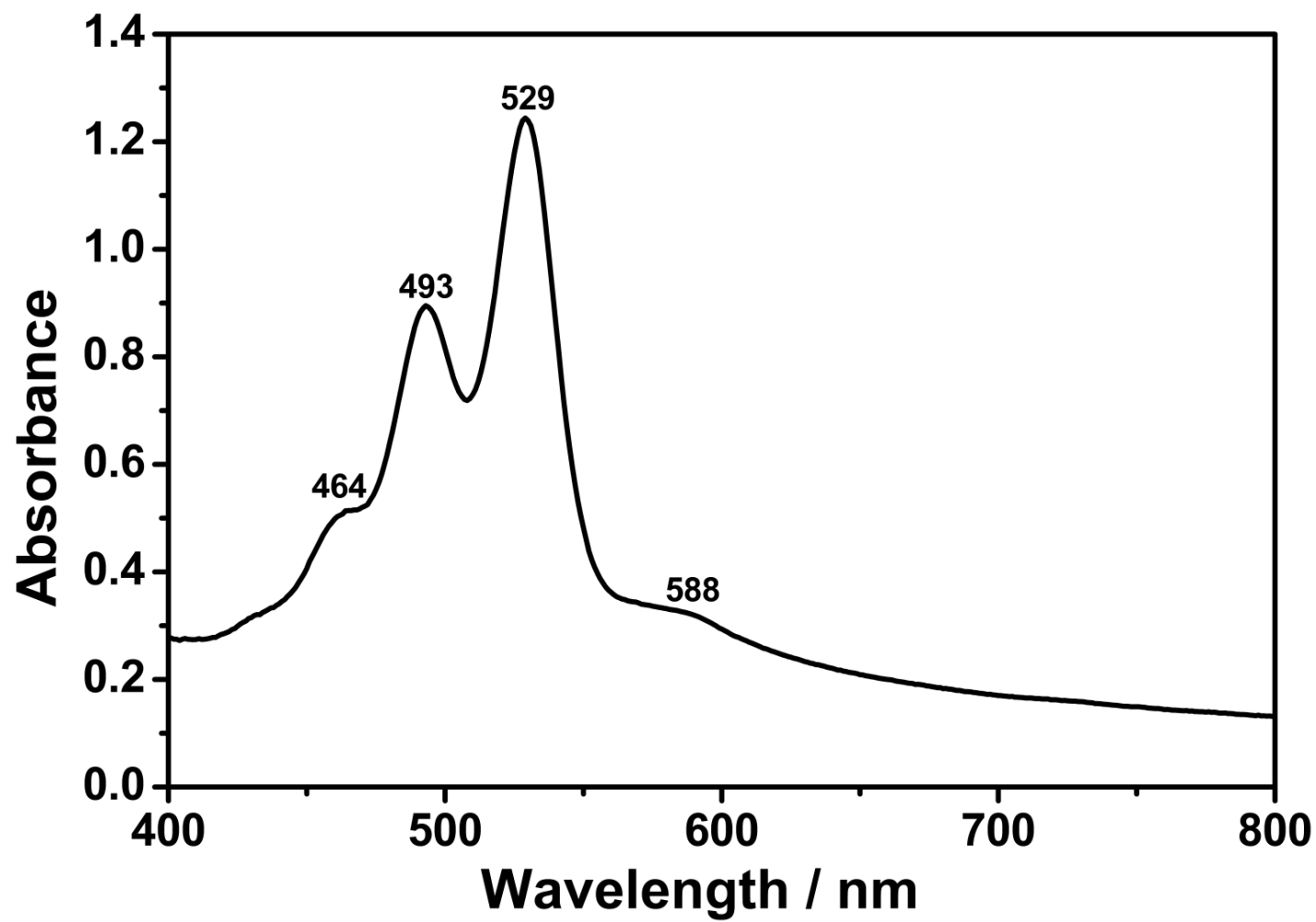
Figure 4.31: UV-Vis Absorption Spectrum of TAPPI in TFAc (C = 1 $\times$ 10^{-5} M)
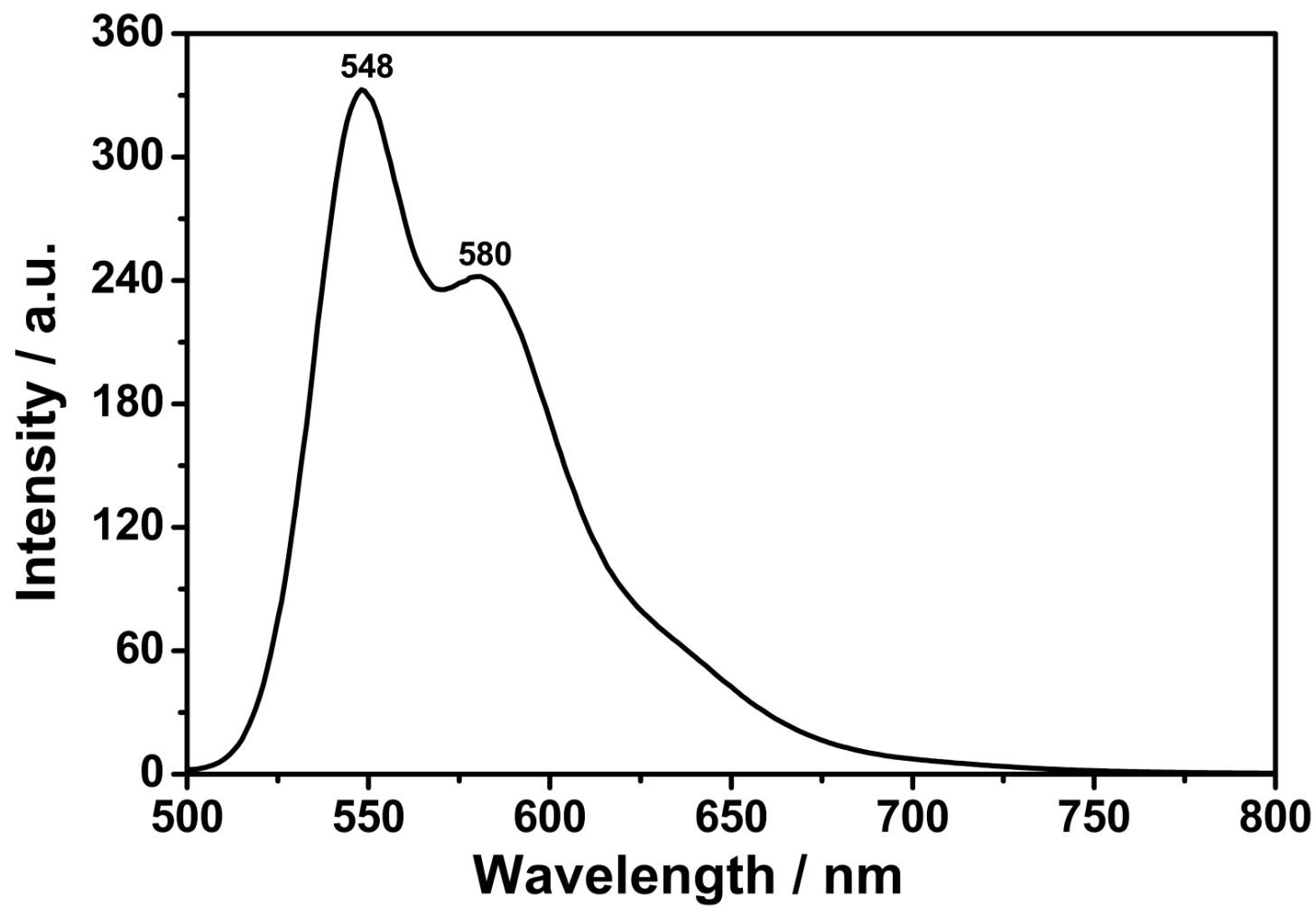
Figure 4.32: Emission Spectrum of TAPPI in TFAc (C = 1 $\times$ 10^{-5} M; λ_{exc} = 485 nm)
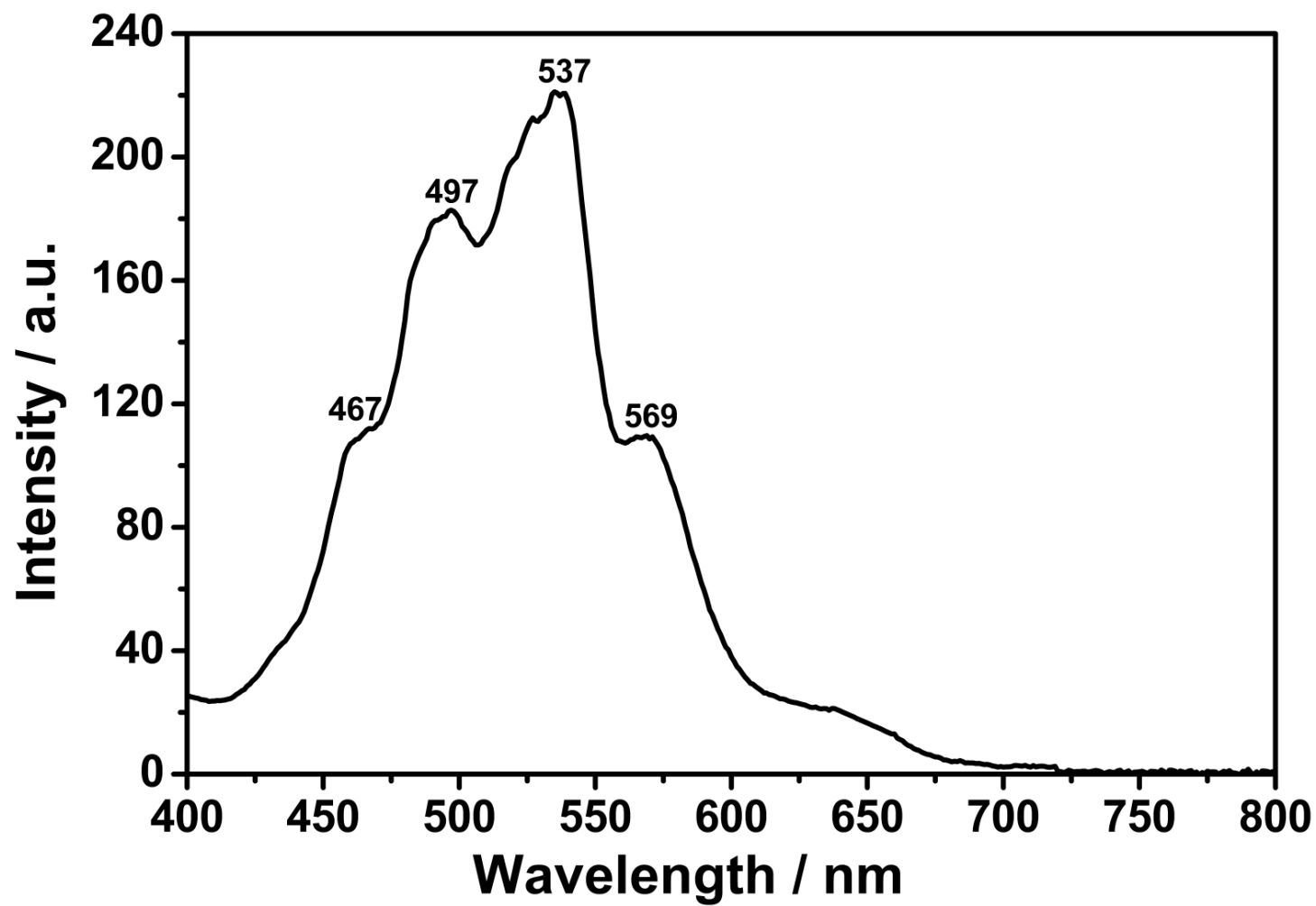
Figure 4.33: Excitation Spectrum of TAPPI in TFAc (C = 1 $\times$ 10^{-5} M; λ_{em} = 650 nm)
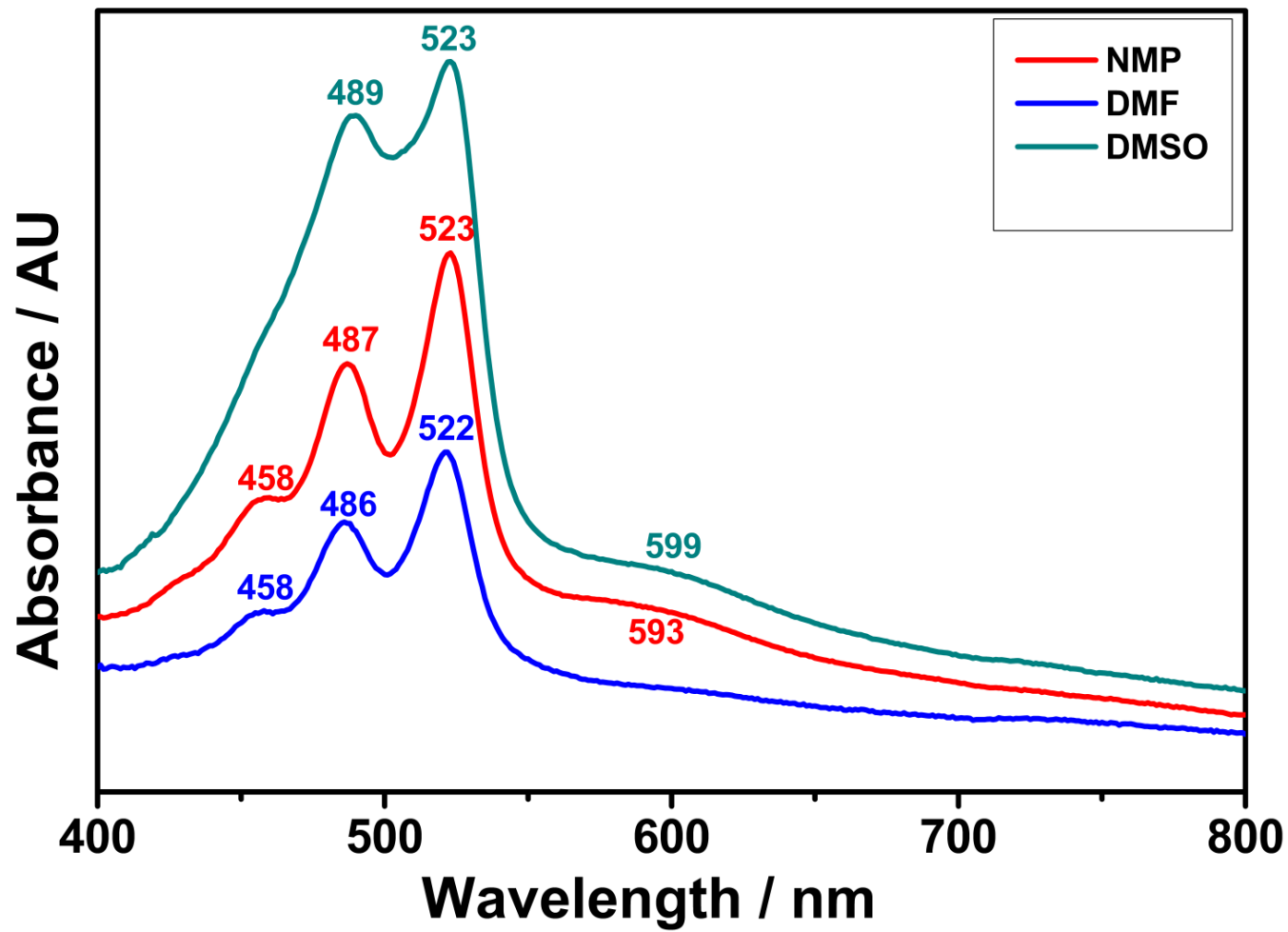
Figure 4.34: UV-Vis Absorption Spectrum of TAPPI in NMP, DMF, and DMSO (C = 1 $\times$ 10^{-5} M)
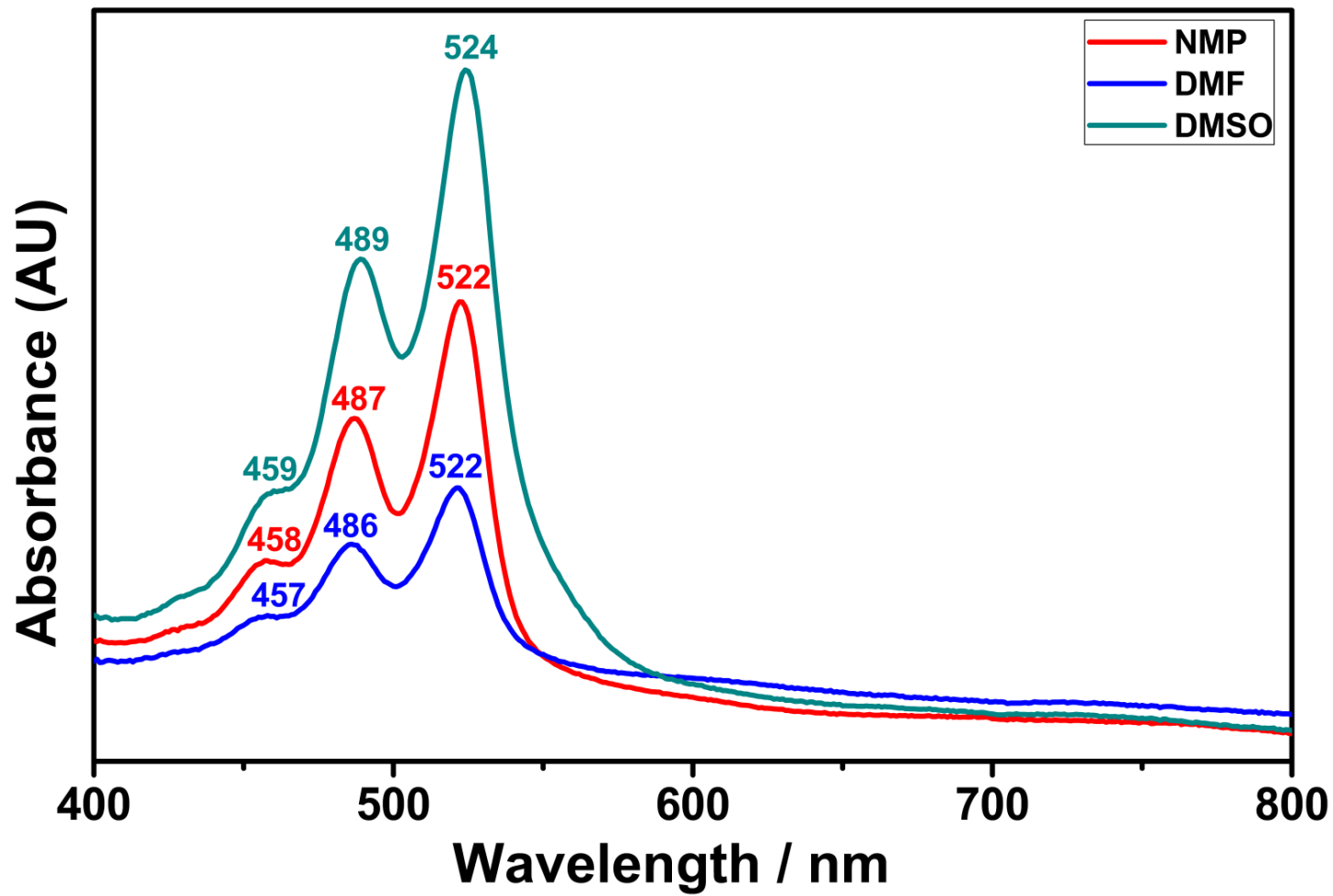
Figure 4.35: UV-Vis Absorption Spectrum of TAPPI in NMP, DMF, and DMSO (Microfiltered)
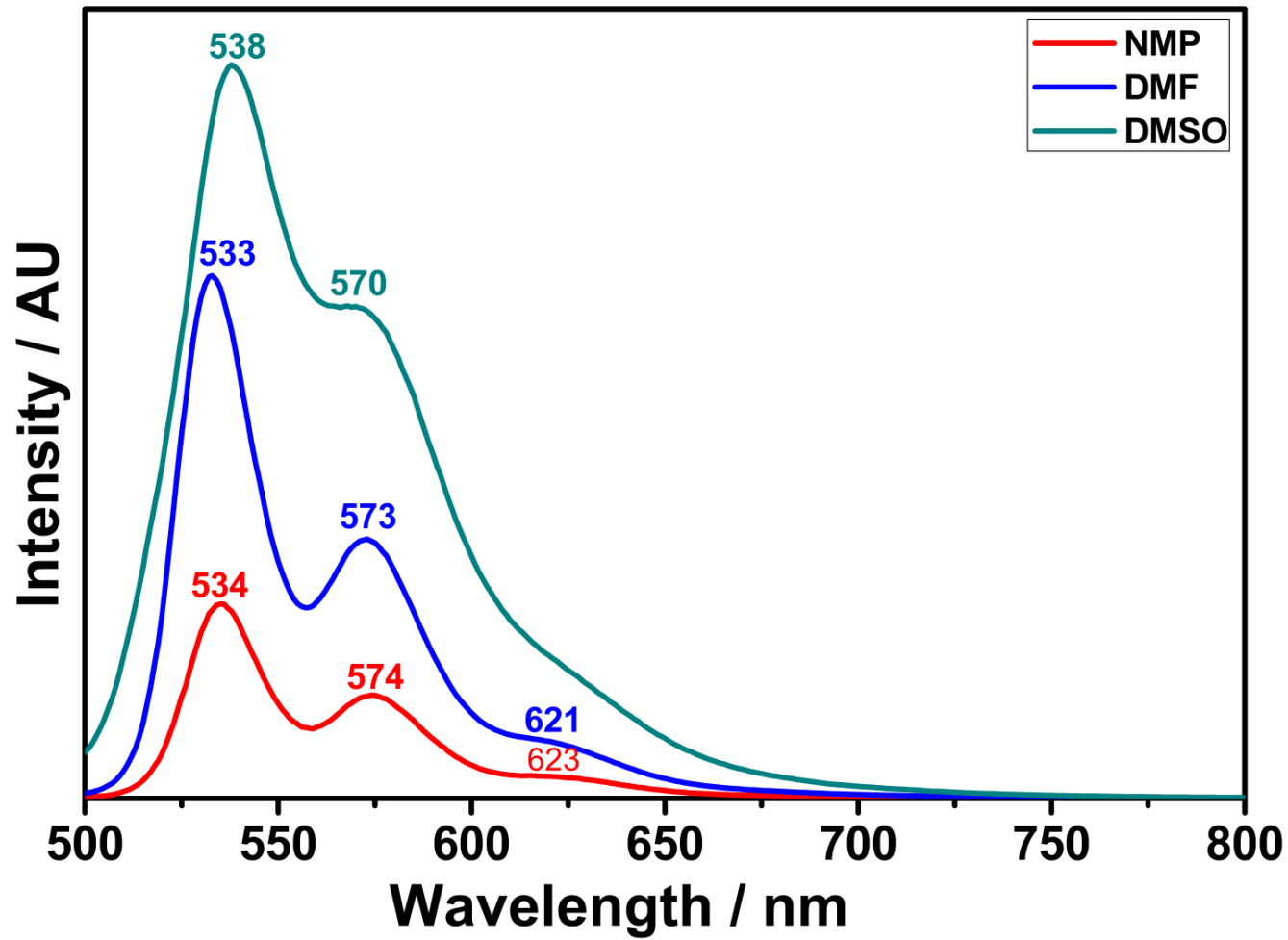
Figure 4.36: Emission Spectrum of TAPPI in NMP, DMF, and DMSO (C = 1 $\times$ 10^{-5} M)
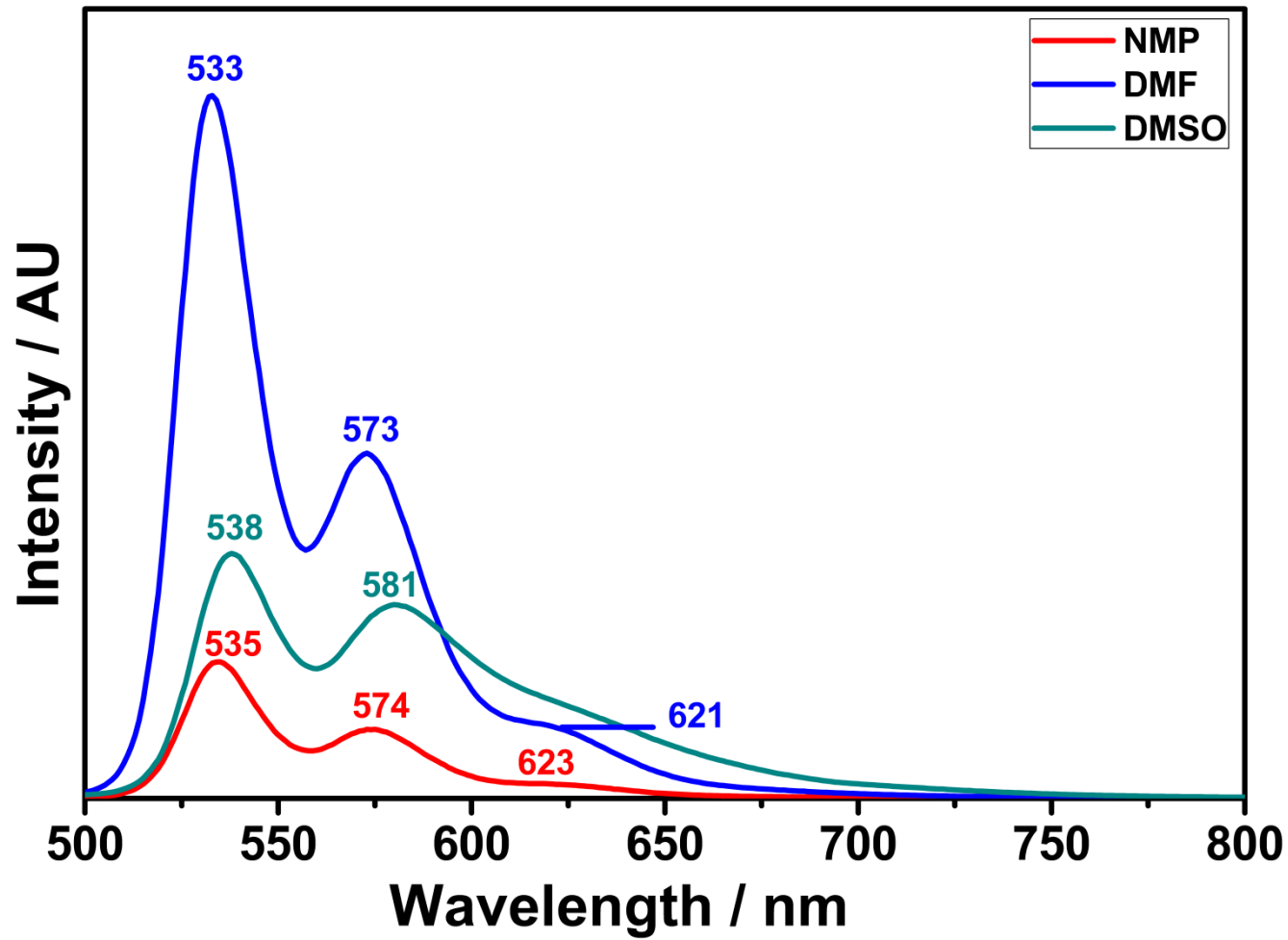
Figure 4.37: Emission Spectrum of TAPPI in NMP, DMF, and DMSO (Microfiltered)
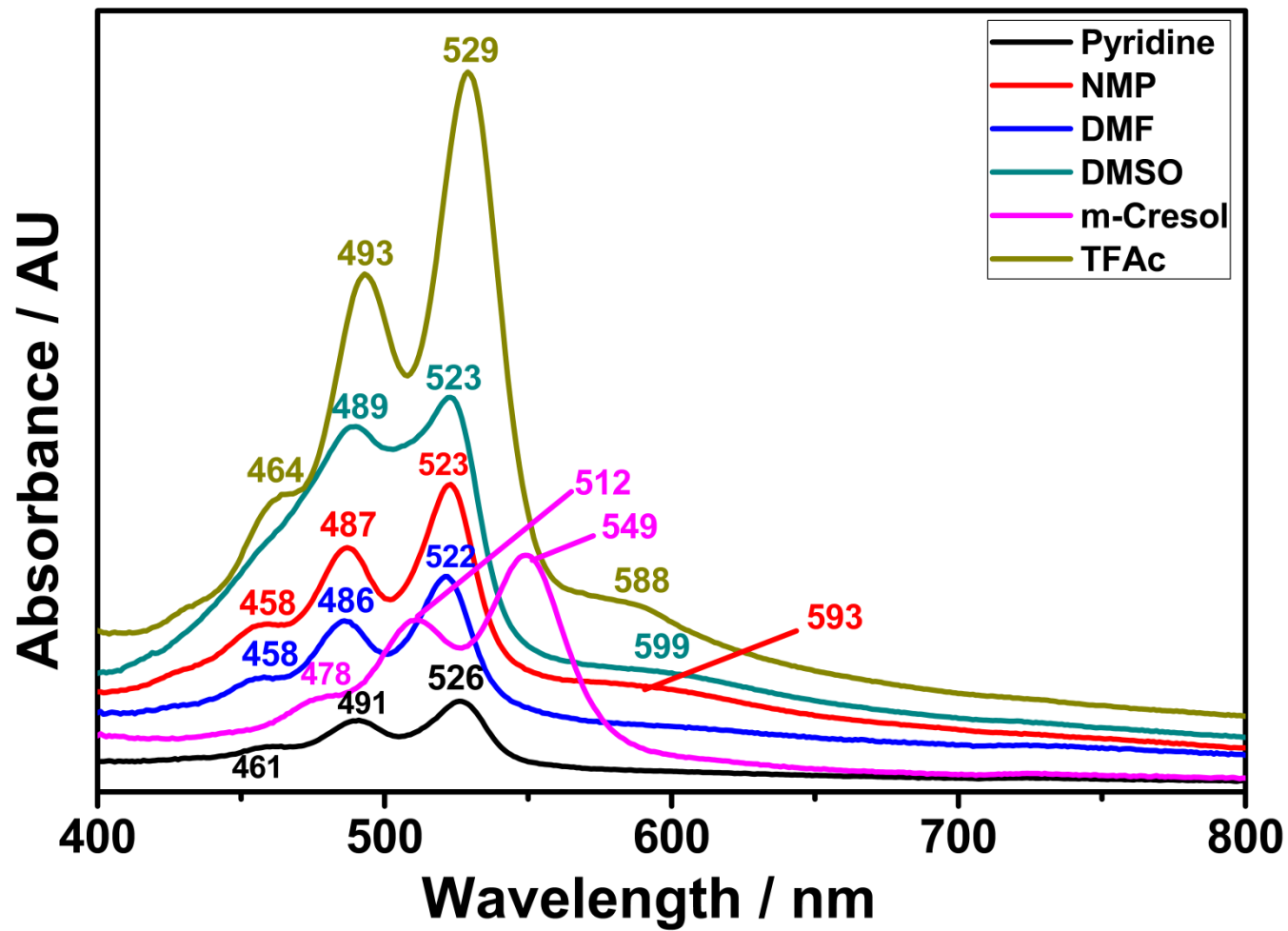
Figure 4.38: UV-Vis Absoption Spectrum of TAPPI in Pyridine, NMP, DMF, DMSO, m-Cresol and TFAc (C = 1 $\times$ 10^{-5} M)
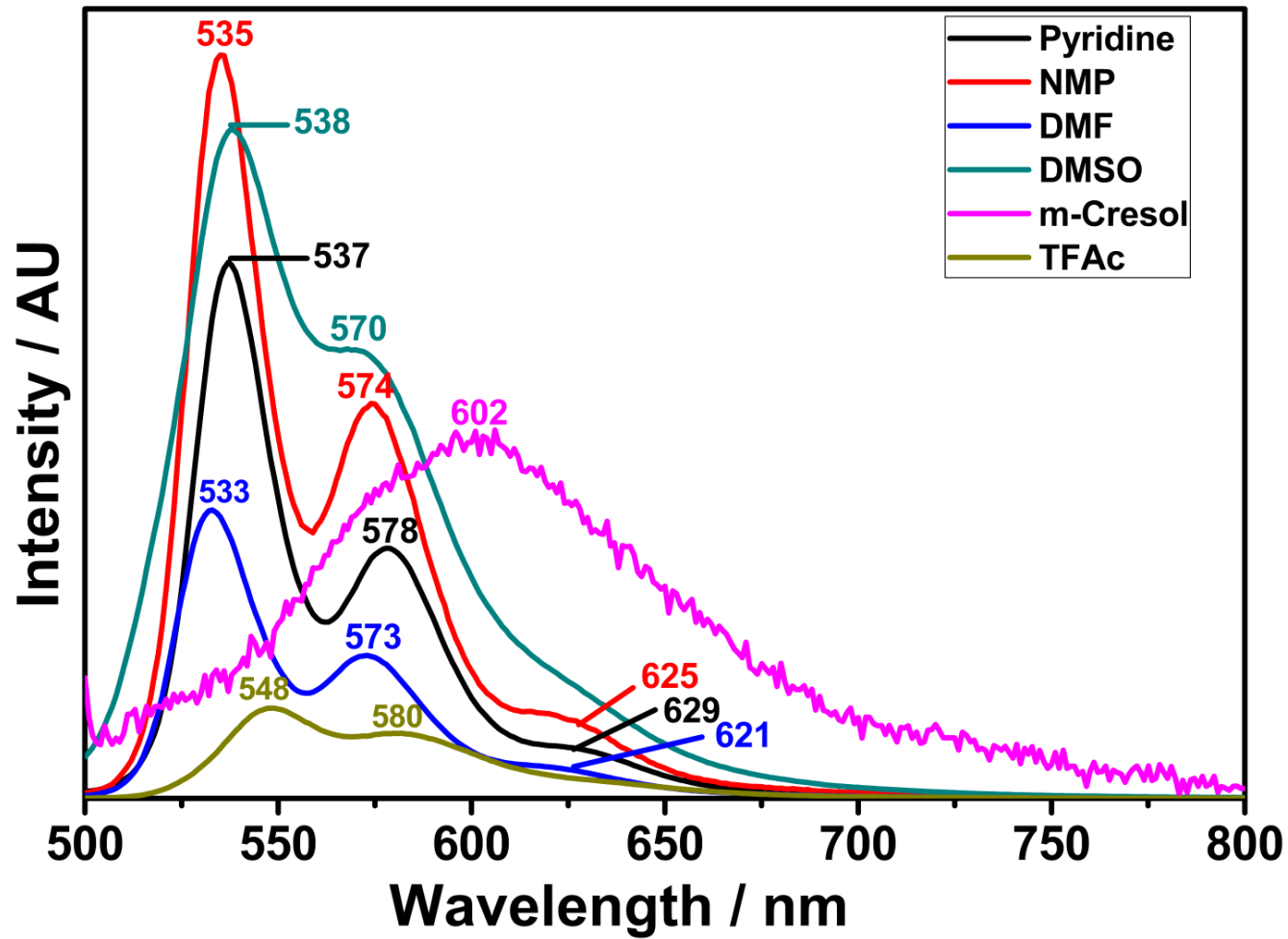
Figure 4.39: Emisson Spectrum of TAPPI in Pyridine, NMP, DMF, DMSO, m-Cresol and TFAc (C = 1 $\times$ 10^{-5} M)

Chapter 5

RESULTS AND DISCUSSIONS

5.1 Synthesis of the Compound TAPPI

The synthetic route of TAPPI compound is shown in Scheme 3.1. TAPPI was synthesized by condensation of perylene-3,4,9,10-tetracarboxylic dianhydride (PDA) with 2,4-diamino-6-phenyl-1,3,5-triazine in isoquinoline / m-cresol solvent mixture under argon atmosphere. The synthesized product was characterized through the data from IR, UV-vis and elemental analysis. These characterizations confirmed the formation of a new polymer as major product (Schemes 3.1).

5.2 Solubility of TAPPI

The solubility of the product was studied in detail. The product TAPPI is soluble mainly in polar solvents such as pyridine, NMP, DMF, DMSO, m-cresol and TFAc in pink or purple colour (Table 5.1).

Table 5.1: Solubility test.

Solubility / color	
Solvent	**TAPPI**
Pyridine	(− +) / purple
NMP	(+ +) / dark purple
DMF	(+ +) / dark puple
DMSO	(+ +) / dark purple
m-Cresol	(− +) / purple
TFAc	(+ −) / pink

(+ +) is soluble at room tempreture, (+ −) is patially soluble at room tempreture, (− +) is soluble on heating at 60 °C.

5.3 Analysis of FTIR Spectra

The IR spectrum of TAPPI was consistent with its chemical structure. As shown in Fig. 4.3, the IR spectrum of TAPPI exhibited characteristic absorption bands at 3385 (N−H stretch); 3160, 3049 (aromatic C−H stretch); 2927, 2853(aromatic C−H stretch); 1682 (imide C=O stretch); 1676 (imide N−C=O stretch); 1592 (conjugated C=C stretch); 1517 (N−H bending); 1434 (C=N triazine); 1396 (C-N stretch); 1360 (CN) stretch; 1277 (CN stretch); 1186, 1106 (CNC stretch); 887, 812 and 662 (C−H bend) cm^{-1}. Result of elemental analysis of compound is in a good agreement with the calculated value.

5.4 Optical Properties

Figure 4.4, 4.5 and 4.6 shows that the shape of the absorption bands of TAPPI in DMSO before (λ_{max}= 489, 523 nm) and after microfiltration ((λ_{max}= 459, 489, 524 nm) are different (all concentrations before microfiltration were 10^{-5} M, pore size of micro filter; 0.2 μm SPR). The rather broad peaks observed in Figure 4.4 indicate the presence of aggregation (Figures 4.6). In the fluorescence spectra of TAPPI taken at λ_{exc}= 485 nm, two broad excimer-like peaks observed before (538 and 570) and after microfiltration (538 and 581) in DMSO (Figure 4.7, 4.8 and 4.9) with 14 nm Stoke shift. Respective excitation spectrum has shown broad and red shifted two different bands (Figure 4.10, λ_{em}= 650 nm).

On the other hand, 3 characteristic absorption peaks at 458, 586 and 522 nm in DMF observed both before and after microfiltration (Figure 4.11, 4.12 and 4.13) without aggregation. In fluorescence spectra measured in DMF, 3 characteristic emission peaks at 533, 573 and 621 nm with 11 nm Stoke shift (Figure 4.14, 4.15 and 4.16).

Respective excitation spectrum has shown blue shifted three well separated bands (458, 483 and 520 nm, Figure 4.17, $\lambda_{em} = 650$ nm).

The UV-vis absorption spectra taken in NMP have shown similar absorption bands before and after microfiltration (458, 487 and 523 nm; Figure 4.18, 4.19 and 4.20). The fluorescence spectra of TAPPI taken at $\lambda_{exc} = 485$ nm in NMP showed mirror images of their absorption spectra with 12 nm Stokes shifts and the absence of excimer emission before and after microfiltration (535, 574 and 623 nm; Figure 4.21, 4.22 and 4.23). Respective excitation spectrum was similar to the UV-vis absorption spectra (459, 487 and 523 nm, Figure 4.24, $\lambda_{em} = 650$ nm).

In the absorption spectra taken in m-cresol, 3 red-shifted absorption peaks at 478, 512 and 549 nm were observed (Figure 4.25). Interestingly, the fluorescence spectra taken in m-cresol have shown one excimer-like and quenched emission (Figure 4.26). Respective excitation spectrum has shown a broad charge transfer style peak at 538 nm (Figure 4.27, $\lambda_{em} = 650$ nm).

In the absorption spectra of TAPPI taken in pyridine, three well separated absorbance bands were observed ($\lambda_{max} = 461$, 491 and 526 nm, Figure 4.28). Notably, the fluorescence spectrum exhibited mirror symmetry for all the absorption bands (537, 578 and 629 nm, Figure 4.29) with a 13 nm Stoke shift (537, 578 and 629 nm, Figure 4.29, $\lambda_{exc} = 485$ nm). Expectedly, the excitation spectrum was similar to the absorption spectrum ($\lambda_{max} = 460$, 490 and 526 nm, Figure 4.30, $\lambda_{em} = 650$ nm).

In trifluoroacetic acid, TAPPI showed 3 characteristic peaks at 464, 493 and 529 nm which are assigned to vibronic 0→0, 0→1 and 0→2 progressions of the electronic $S_0 \rightarrow S_1$ transition respectively (shoulder peak; 588 nm, Figure 4.31). In fluorescence spectra of the compound in trifluoroacetic acid, two broader excimer-like peaks were observed at 548 and 580 nm with a 19 nm Stoke shift (Figure 4.32, λ_{exc}= 485 nm). Respective excitation spectrum was not similar to the UV-vis absorption spectra with red shifted and broader 3 peaks and one shoulder (467, 497, 537 and 569 nm, Figure 4.33, λ_{em} = 650 nm). It is important to note that, different absorption and emission properties have been observed due to different intermolecular interactions as can be observed in Figures from 4.34 to 4.39.

The emission spectra of TAPPI was taken at λ_{exc} = 485 nm and the relative fluorescence quantum yields were determined in NMP, DMF and DMSO using *N,N´-*didodecyl-3,4,9,10-perylenebis(dicarboximide) in chloroform as standard. The lower fluorescence quantum yield of the product could be attributed to conformational changes, torsional movement, or other non-radiative decays (NMP: 70%, DMF: 60% and DMSO: 30%).

Table 5.2: Stokes shifts of TAPPI ($C = 1 \times 10^{-5}$) in different solvents.

Solvent	UV-Vis Absorption	Emission	Stokes Shift (nm)	Stokes Shift (cm)
	λ_{max}	λ_{max}		
Pyridine	526	537	11	1.1×10^{-6}
NMP	523	535	12	1.2×10^{-6}
DMF	522	533	11	1.1×10^{-6}
DMSO	523	538	15	1.5×10^{-6}
m-Cresol	549	602	53	5.3×10^{-6}
TFA	529	548	19	1.9×10^{-6}

Table 5.3: Stokes shifts of TAPPI (microfiltered) in different solvents.

Solvent	UV-Vis Absorption	Emission	Stokes Shift (nm)	Stokes Shift (cm)
	λ_{max}	λ_{max}		
NMP	522	534	12	1.2×10^{-6}
DMF	522	533	11	1.1×10^{-6}
DMSO	524	538	14	1.4×10^{-6}

Table 5.4: Maximum absorption wavelengths λ_{max} (nm), molar absorption coefficients ε_{max} (L . mol^{-1} . cm^{-1}), fluorescence quantum yields Φf, radiative lifetimes τ_0 (ns), fluorescence lifetimes τ_f (ns), fluorescence rate constants k_f (10^7 s^{-1}), radiationless deactivation rate constants k_d (10^7 s^{-1}), oscillator strengths (f), and singlet energies E_s (kcal . mol^{-1}) data of TAPPI in different solvents.

Solvent	λ_{max}	ε_{max}	Φf	$\Delta\bar{v}_{1/2}$	τ_0	τ_f	k_f	k_d	f	E_s
NMP	523	33000	0.70	1350.32	21.5	15.05	4.65	1.99	0.19	54.68
DMF	522	24000	0.60	1357.34	29.3	17.58	3.41	2.27	0.14	54.79
DMSO	523	28000	0.30	1319.80	25.9	7.77	3.86	9.01	0.16	54.68

Chapter 6

CONCLUSION

A new chromogenic polymer (TAPPI) was synthesized by polycondensation of perylene-3,4,9,10-tetracarboxylic dianhydride (PDA) with hindered aromatic diamine, 2,4-diamino-6-phenyl-1,3,5-triazine successfully. The synthesized product purity was confirmed using elemental analysis, IR and UV-vis spectroscopy.

The polymer, TAPDI is soluble mainly in polar solvents such as pyridine, NMP, DMF, DMSO, m-cresol in purple and TFAc pink colours.

Interestingly, different absorption and emission characteristics were observed in different solvents due to different intermolecular interactions.

The emission spectra of TAPDI was taken at $\lambda_{exc} = 485$ nm and the relative fluorescence quantum yields were determined in NMP, DMF and DMSO using *N,N´*-didodecyl-3,4,9,10-perylenebis(dicarboximide) in chloroform as standard. The lower fluorescence quantum yield of the product could be attributed to conformational changes, torsional movement, or other non-radiative decays (NMP: 70%, DMF: 60% and DMSO: 30%).

Complete characterisation of the polymer and its photophysical, photochemical and electrochemical properties will be explored in future studies.

REFERENCES

[1] Kardos M. PhD Thesis (1913). University of Berlin.

[2] Langhals, H. (1995). Cyclic Carboxylic Imide Structures as Structure Elements of High Stability. Novel Developments in Perylene Dye Chemistry. *Heterocycles.* 40, 477-500.

[3] Langhals, H., Sprenger, S., & Brandherm M. T. (1995). Perylenamidine-Imide Dyes. *Liebigs Annalen der Chemie*. 481-486.

[4] Demmig, S., Langhals, H., & Leichtlösliche (1988). Very Soluble and Photostable Perylene Fluorescent Dyes. *Chemische Berichte.* 121: 225-230.

[5] İcil, H., Uzun D., & Paşaoğulları N. (1998). Synthesis of a New Thermal and Photostable Refence Probe for Qf Measurement in Aqua: Water Soluble N,N'-Bis-(2-Hydroxy-4-Benziocacid)-3,4,9,10-Perylenebis(dicarboximide), *Spectroscopy Letters.* 31 (3), 667-671.

[6] Ahrens, M. J., Fuller, M. J., & Wasielewski, M. R. (2003). Cyanated Perylene-3,4-Dicarboximides and Perylene-3,4 : 9,10-Bis(Dicarboximide): Facile Chromophoric Oxidants for Organic Photonics And Electronics. *Chemistry of Materials.* 15, 2684-2686.

[7] Lindner, S. M., Kaufmann, N., & Thelakkat, M. (2007). Nanostructured Semiconductor Block Copolymers: Pi-Pi Stacking, Optical and Electrochemical Properties. *Organic Electronics*. 8, 69-75.

[8] Kazmaier, P. M., & Hoffmann, R. J. (1994). A Theoretical-Study of Crystallochromy − Quantum Interference Effects in the Spectra of Perylene Pigments. *Journal of the American Chemical Society*. 116, 9684-9691.

[9] Sadrai, M., & Bird, G. R. (1984). A New Laser-Dye With Potential for High-Stability and a Broad-Band of Lasing Action - Perylene-3,4,9,10-Tetracarboxylic Acid-Bis-N,N'(2',6'xylidyl)Diimide. *Optics Communications*. 51, 62-64.

[10] Ford, W. E., & Kamat, P. V. J. (1987). Photochemistry of 3,4,9,10-Perylenetetracarboxylic Dianhydride Dyes .3. Singlet and Triplet Excited-State Properties of the Bis(2,5-Di-Tert-Butylphenyl)Imide Derivative. *Journal of Physical Chemistry*. 91, 6373-6380.

[11] Zhan, X., Tan, Z. A.; Domercq, B., An, Z., Zhang, X., Barlow, S., Li, Y., Zhu, D. Kippelen, B., & Marder, S. R. (2007). Effects of Adding over Spray Powder on Microstructures and Mechanical Properties of Spray Deposited 8009 Aluminium Alloy. *Journal of the American Chemical Society*. 129, 7246-7247.

[12] Tan, Z. A., Zhou, E., Zhan, X., Wang, X., Li, Y., Barlow, S., & Marder, S. R. (2008). Efficient All-Polymer Solar Cells Based on Blend of

Tris(Thienylenevinylene)-Substituted Polythiophene and Poly[Perylene Diimide-Alt-Bis(Dithienothiophene)]. *Applied Physics Letters*. 93, 073309.

[13] Suzuki, H., & Hoshino, S. J. (1996). Effects of Doping Dyes on the Electroluminescent Characteristics of Multilayer Organic Light-Emitting-Diodes. *Journal of Applied Physics*. 79, 8816–8822.

[14] Roncali, J. & Garnier, F. (1984). Proton-Transport Properties of Luminescent Solar Concentrators-Analysis and Optimization. *Applied Optics*. 23, 2809–2817.

[15] Feng J., Zhang Y., Zhao C., Li R., Xu W., Li X., & Jiang J. (2008). Cyclophanes of Perylene Tetracarboxilic Diimide with Different Substituents at Bay Positions. *Chemistry of a European Journal.* 14, 7000-7010.

[16] Weibel, D., Gevorgyan V., & Yamamoto Y. (1997). Synthesis of Polyether Exomethylene Paracyclophanes via an Intramolecular Pd-Catalyzed Bis-Enyne Benzannulation Protocol. *Journal of Organic Chemistry*. 63, 1217-1220.

[17] Zhang, P., Yang B., Fang X., Cheng Z., & Yang, P. (2012). Synthesis, Crystal Structure and Biological Activity of Novel Diester Cyclophanes. *Journal of the Brazilian Chemical Society.* 23, 1771-1775.

[18] Bartholomew, G. P., & Bazan, G. C. (2001). Bichromophoric Paracyclophanes: Models for Interchromophore Delocalization. *Accounts of Chemical Research.* 34, 30-39.

[19] Pelter, A., Mootoo, B., Maxwell, A., & Reid, A. (2001). The Synthesis of Homo Chrial Ligands based on [2,2] Paracyclophane. *Tetrahedron Letters*. 42, 8391-8394.

[20] Hopf, H., Raulfs, F.-W., & Schomburg, D. (1986). Cyclophanes .25. [2,2] Indenophanes- Potential Building Blocks for Oligomeric Ferrocenophanes. *Tetrahedron*. 42, 1655-1663.

[21] Hopf, H. (2008). [2,2] Paracyclophane in Polymer Chemistry and Materials Science. *Angewandte Chemie- International Edition*. 47, 9808-9812.

[22] Morisaki, Y., Hifumi, R., Lin, L., Inoshita, K., & Chujo, Y. (2012). Through-Space Conjugated Polymers Consisting of Planar Chrial Pseudo-Ortho-Linked [2,2] Paracyclophane. *Polymer Chemistry*. 3, 2727-2730.

[23] Taylor, J. S., & Cohrs, M. P. J. (1987). DNA, Light, and Dewar Pyrimidinones - the Structure and Biological Significance of TPT3. *Journal of the American Chemical Society*. 109, 2834–2835.

[24] Ozser, M. E., Uzun, D., Elci, I., Icil, H., & Demuth, M. (2003). Novel Naphthalene Diimides And A Cyclophane Thereof: Synthesis, Characterization, Photopysical and Electrochemical Properties. *Photochemical and Photobiological Sciences*. 2, 218-223.

[25] Jones, B. A., Ahrens, M. J., Yoon, M.-H., Facchetti, A., Marks, T. J., & Wasielewski, M. R. (2004). High-Mobility Air-Stable N-Type Semiconductors

with Processing Versatility: Dicyanoperylene-3,4 : 9,10-Bis(Dicarboximides). *Angewandte Chemie - International Edition.* 43, 6363-6366.

[26] Hadicke, E., & Graser, F. (1986). Structures of three Perylene-3,4-9,10 Bis(Dicarboximide) Pigments. *Acta Crystallographica Section C.* 42, 195-198.

[27] Nagao, Y. (1997). Synthesis and Properties of Perylene Pigments. *Progress in Organic Coatings.* 31, 43-49.

[28] Bao, Z., & Locklin, J. (2006). Effect of Morphology on Organic Thin Film Transistor Sensors. *Analitical Bioanalitical Chemistry Reviews.* 384, 336-342.

[29] Zhang, X.-H. Ph.D thesis (2009). Georgia Institute of Technology.

[30] Arias, A. C., MacKenzie, J. D., McCulloch, I.; Rivnay, J., & Salleo, A. (2010). Materials and Applications for Large Area Electronics: Solution-Based Approaches. *Chemical Rev*iews. 110, 3-24.

[31] Gelinck, G. H., Huitema, H. E. A., Van Veenendaal, E., Cantatore, E., Schrijnemakers, L., Van der Putten, J., Geuns, T. C. T., Beenhakkers, M., Giesbers, J. B., Huisman, B. H., Meijer, E. J., Benito, E. M., Touwslager, F. J., Marsman, A. W., Van Rens, B. J. E., & De Leeuw, D. M. (2004). Flexible Active Matrix Displays and Shift Registers based on Solution- Processed Organic Transistors. *Nature Materials.* 3, 106-110.

[32] Lehn, J. M. (2002). Toward Complex Matter: Supramolecular Chemistry and Self-Organization. *Proceedings of the National. Academy of the Sciences of the USA*. 99, 4763–4768.

[33] Tang, C. W. (1986). Two Layer Organic Photovoltaic Cell). *Applied Physics Letter*. 48,183-185.

[34] Paşaoğulları, N. PhD Thesis (2005). Eastern Mediterranean Universitiy.

[35] Vayá I., Bonancía P., Jiménez, M. C., Markovitsi D., Gustavsson, T., & Miranda, M. A. (2013). Excited State Interactions between Flurbiprofen and Tryptophan in Drug–protein Complexes and in Model Dyads. Fluorescence Studies from the Femtosecond to the Nanosecond Time Domains. *Phisical Chemistry Chemical Physics*. 15, 4727-4734.

[36] Yeganeh, S., & Voorhis, T. V. (2010). Triplet Excitation Energy Transfer with Constrained Density Functional Theory. *The Journal of Physical Chemistry*. 114.48, 20756-20763.

[37] Liddell, P. A., Kodis, G., Kuciauskas, D., Andre´asson, J., Moore, A. L., Moore, T. A., & Gust, D. (2004). Photoinduced Electron Transfer in a Symmetrical Diporphyrin − Fullerene Triad. *Physical Chemistry Chemical Physics*. 6(24), 5509-5515.

[38] Marcus, R. A. (1993). Electron-Transfer Reactions in Chemistry - Theory and Experiment (Nobel Lecture). *Angewandte Chemie - International Edition*. 32, 1111-1121.

[39] Marcus, R. A. (1993). Electron-Transfer Reactions in Chemistry - Theory and Experiment. *Reviews of Modern Physics*. 65, 599-610.

[40] Ziener, U., Lehn, J.M., Mourran, A., & Möller, M. (2002). Supramolecular Assemblies of A Bis(Terpyridine) Ligand and of Its [2x2] Grid-Type Zn-ii and Co-ii Complexes on Highly Ordered Pyrolytic Graphite. *Chemistry European Journal*. 8, 951-957.

[41] Rebek, J. (2000). Host-Guest Chemistry of Calixarene Capsules. *Chemical Communications.* 8, 637-643.

[42] Philip, D., & Stoddart, J. F. (1996). Self-Assembly in Natural And Unnatural Systems. *Angewandte Chemie International Edition.* 35, 1155-1196.

[43] Lehn, J.M., & Ball, P. (1995). The New Chemistry. *Cambridge Univ. Press: Cambridge.* 300–351.

[44] Slone, R.V., Benkstein, K.D., Belanger, S., Hupp, J.T., Guzei, I.A., & Rheingold, A. L. (1998). Luminescent Transition-Metal-Containing Cyclophanes ("Molecular Squares"): Covalent Self-Assembly, Host-Guest Studies and Preliminary Nanoporous Materials Applications. *Coordination Chemistry Rev*iew. 171, 221–243.

[45] Manez, R.M., & Sancenon, F. (2003). Fluorogenic and Choromogenic Chemosensors and Reagents for Anions. *Chemistry Review.* 103, 4419–4476.

[46] Sugou, K., Sasaki, K., Kitajima, K., Iwaki, T., & Kuroda, Y. J. (2002). Light-Harvesting Heptadecomeric Porphyrin Assemblies. *Journal of the American Chemical Society.* 124, 1182-1183.

[47] McQuade, D. T., Hegedus, A. H., & Swager, *T. M.* (2000). Signal Amplification of a "Turn-On" Sensor: Harvesting the Light Captured by a Conjugated Polymer. *Journal of the American Chemical Society.* 122, 12389-12390.

[48] Pischel, U. (2007). Chemical Approaches to Molecular Logic Elements for Addition and Subtraction. *Angewandte Chemie - International Edition.* 46, 4026-4040.

[49] Credi, A. (2007). Molecules that Make Decisions. *Angewandte Chemie - International Edition.* 46, 5472-5475.

[50] Nijhuis, C. A., Huskens, J., & Reinhoudt, D. N. (2004). Binding Control and Stoichiometry of Ferrocenyl Dendrimers at a Molecular Print Board. *Journal of the American Chemical Society.* 126, 12266-12267.

[51] Credo, G. M., Boal, A. K., Das, K., Galow, T. H., Rotello, V. M. ,Feldheim, D. L., Gorman, C. B. (2002). Supramolecular Assembly on Surfaces. Manipulating Conductance in Noncovalently Modified Mesoscale Structures. *Journal of the American Chemical Society.* 124, 9036-9037.

[52] Steed, J. W., Turner, D. R., & Wallace, K. J. (2007). Core Concepts in Supramolecular Chemistry and Nanochemistry. *Wiley: Chichester.*107-170.

[53] Ma, J. C., & Dougherty, D. A. (1997). The Cation–Pi Interaction. *Chemical Rev*iews. 97, 1303–1324.

[54] Hunter, C. A., Lawson, K. R., Perkins, J., & Urch, C. J. (2001). Aromatic Interactions. *Journal of Chemical Society-Perkin Transactions.* 2, 651–669.

[55] Perrin, D. D., & Armarego, W. L. F. (1980). Purification of Laboratory Chemicals.

[56] Williams, A. T. R., Winfield S. A., & Miller, J. N. (1983). Relative fluorescence quantum yields using a computer controlled luminescence spectrometer. *Analyst*. 108, 1067.

[57] Scaiano, J. C. (1989) (Ed.) Handbook of Organic Photochemistry, CRC press.

[58] Icil, H., & Icli S. (1997). Synthesis and Properties of a New Photostable Polymer: Perylene- 3,4,9,10-Tetracarboxylic Acid-Bis-(N,N'-Dodecylpolyimide). *Journal of Polymer Sciences A: Polymer Chemistry*. 35, 2137-2142.

[59] Turro, N. J. (1965). Molecular Photochemistry, Benjamin, London, 44-64.

APPENDIX

Appendix A: Curriculum Vitae

Personal Information

Name	Meltem
Surname	Dinleyici
Adress	Anadolu Sok. No:5 Korkuteli Famagusta-TRNC Mersin 10 Turkey
Phone	Office:+90 0392 630 13 71/ Mobile: 0548 876 75 34
e-mail	meltemdinleyici@hotmail.com
Date of Birth	09/10/1991
Citizenship	TRNC
Marital Status	Single

Education

1997-2002	Dörtyol İlkokulu, Famagusta, Cycprus
2002-2005	Çanakkale Ortaokulu, Famagusta, Cyprus
2005-2009	20 Temmuz Fen Lisesi, Nicosia, Cyprus
2009-2013	Cukurova University Faculty of Arts & Sciences
	Depertmant of Chemistry (BS)
2013-present	Eastern Mediterranean University Faculty of Arts & Sciences
	Department of Chemistry Organic Chemistry (MS)

Work Experience

2013-present	EASTERN MEDITERRANEAN UNIVERSITY,
	Department of Chemistry (Research Assistant)

2012	Dr. Burhan Nalbantoğlu Devlet Hastanesi, Biochemistry Laboratory (Summer Intern)
Teaching Experience	Attended to KİMY 103/ 107/ 109, General Chemistry lab and tutorial sessions (2013-2015).

Skills

Language	Turkish, English
Computer	Microsoft Applications